



UNIVERSIDADE ESTADUAL DE CAMPINAS
INSTITUTO DE BIOLOGIA

NADIA RASHEED

**“STRUCTURAL AND FUNCTIONAL CHARACTERIZATION OF THE SUBUNITS
OF RAGULATOR COMPLEX, A REGULATOR OF AMINO ACID SENSING IN
mTORC1 PATHWAY”**

**“CARACTERIZAÇÃO ESTRUTURAL E FUNCIONAL DE SUBUNIDADES DO
COMPLEXO RAGULATOR, UM REGULADOR DA SINALIZAÇÃO POR
AMINOÁCIDOS NA VIA mTORC1”**

CAMPINAS

2017

NADIA RASHEED

**“STRUCTURAL AND FUNCTIONAL CHARACTERIZATION OF THE SUBUNITS
OF RAGULATOR COMPLEX, A REGULATOR OF AMINO ACID SENSING IN
mTORC1 PATHWAY”**

**“CARACTERIZAÇÃO ESTRUTURAL E FUNCIONAL DE SUBUNIDADES DO
COMPLEXO RAGULATOR, UM REGULADOR DA SINALIZAÇÃO POR
AMINOÁCIDOS NA VIA mTORC1”**

Thesis presented to the Institute of Biology the University of Campinas in partial fulfillment of the requirements for the degree of Doctor Genetics and Molecular Biology, in the area of Animal Genetics and Evolution.

Tese apresentada ao Instituto de Biologia da Universidade Estadual de Campinas como parte dos requisitos exigidos para a obtenção do título de Doutora em Genética e Biologia Molecular, na área de Genética Animal e Evolução.

Orientador/Supervisor: DRA. JULIANA HELENA COSTA SMETANA

ESTE ARQUIVO DIGITAL CORRESPONDE
À VERSÃO FINAL DA TESE DEFENDIDA
PELA ALUNA NADIA RASHEED E
ORIENTADA PELA DRA. JULIANA
HELENA COSTA SMETANA.

CAMPINAS
2017

Agência(s) de fomento e n°(s) de processo(s): CNPq, 190174/2012-9; FAPESP, 2014/12445-0

Ficha catalográfica
Universidade Estadual de Campinas
Biblioteca do Instituto de Biologia
Mara Janaina de Oliveira - CRB 8/6972

R183s Rasheed, Nadia, 1985-
Structural and functional characterization of the subunits of Ragulator complex, a regulator of amino acid sensing in mTORC1 pathway / Nadia Rasheed. – Campinas, SP : [s.n.], 2017.

Orientador: Juliana Helena Costa Smetana.
Tese (doutorado) – Universidade Estadual de Campinas, Instituto de Biologia.

1. Complexo Ragulator. 2. Fatores de troca do nucleotídeo guanina. 3. mTORC1. 4. Proteína quinase A. I. Smetana, Juliana Helena Costa. II. Universidade Estadual de Campinas. Instituto de Biologia. III. Título.

Informações para Biblioteca Digital

Título em outro idioma: Caracterização estrutural e funcional de subunidades do complexo Ragulator, um regulador da sinalização por aminoácidos na via mTORC1.

Palavras-chave em inglês:

Ragulator complex
Guanine nucleotide exchange factors
mTORC1
Protein kinase A

Área de concentração: Genética Animal e Evolução

Titulação: Doutora em Genética e Biologia Molecular

Banca examinadora:

Juliana Helena Costa Smetana [Orientador]
Celso Eduardo Benedetti
Jörg Kobarg

Marcio Chaim Bajgelman

Daniel Maragno Trindade

Data de defesa: 25-04-2017

Programa de Pós-Graduação: Genética e Biologia Molecular

Campinas, 25 de Abril de 2017

COMISSÃO EXAMINADORA/EXAMINATION COMMITTEE

Dr. Juliana Helena Costa Smetana (supervisor/orientadora)

Prof. Dr. Celso Eduardo Benedetti

Prof. Dr. Jörg Kobarg

Prof. Dr. Marcio Chaim Bajgelman

Dr. Daniel Maragno Trindade

Os membros da Comissão Examinadora acima assinaram a Ata de Defesa, que se encontra no processo de vida acadêmica do aluno.

DEDICATION

Dedicated to my parents and my siblings

ACKNOWLEDGEMENTS

Alhamdulillah. This PhD study presented me a unique and amazing opportunity to meet, work and learn with so many great academics including researchers, colleagues and friends. First, I would like to thank my supervisor Dr. Juliana Helena Costa Smetana for all the guidance and devotion she showed throughout my PhD. I have not only started to learn to do research from her but she also subconsciously instilled in me the professional drive, and appreciation for science and research. I would love to cherish all those moments that occurred during formal or informal meetings when we were in awe of either a recently published paper unveiling an important piece of information or our own results. Juliana, I am indeed grateful for your supervision and support throughout these four years. I owe every word of this thesis to you. This project would not be possible without the support of our collaborators starting with Dr. Ricardo Aparicio who performed the analysis of SAXS and crystallography data. I am grateful to Dr. Andrey F. Z. Nascimento to assist Dr. Ricardo in solving the crystal structure. I am personally thankful to Dr. Ricardo for not only helping me to get the PhD fellowship but also for introducing me to Juliana. I deeply appreciate the efforts of Dr. Fabio Gozzo and his group especially Tatiani B. Lima for handling crosslink and HDX experiments. I also look forward for more collaborations with both Dr. Ricardo and Dr. Fabio for future endeavours. I would also like to take an opportunity to thank Dr. Sabatini and Dr. M. Cygler for sending us the plasmids. I also want to acknowledge the efforts of Edmarcia, Silvio and Marilia for helping me with confocal microscopy experiments.

Four years back, I came from Pakistan to a country with a different language, food and cultural background. After four years of staying and studying in Brazil, *tento falar em português, agradeço pessoas pela ajuda e gostei de comida brasileira também*. This would not have been possible without the affection I felt from my colleagues and friends at LNBio-CNPEN. You not only supported me throughout these four challenging years but also turned these years into an amicable and cherishable memory. I owe words of gratitude to all the members of my group including Ana Luiza and Germanna whom I worked in the first and half years of my PhD and also current members; Ana, Mariana, Tatiani and Valeria for their help and support.

I am being lucky to share this experience with helping hands who work at LNBio as technicians, students, researchers, internees and other people from administration for paving the path on which I am about to lay the first foundation of my career. There is no way that I can return the favour that could compensate the care and help, I received from you. I am grateful to

Dr. Daniel Maragno Trindade for answering my research related questions and clearing doubts during informal interactions in the Lab. On a personal note; Thanks for being there as an elder brother with great research ethics and not letting me mess up in stressful situations. I feel blessed to become friends with Soledad, Rhubia, Mayara, Jhenifer and Amanda. I am thankful to everyone at CNPEM for showing affection and being supportive in the best possible way.

My family is the vital source of my well-being. I feel speechless at what my parents have endured for me. I dedicate this thesis to the loving memory of my father “Rasheed Ahmed Salis” (who would have loved to read this thesis even though he was not a biologist), my recently deceased uncle “Abdul Mateen” and every loving soul that I lost. My mother “Waqar un Nisa” and my sisters: Sadia, Sana, Hafsa, Warda and Manahil; I love you all with all my heart. You are the reason for all the good things that happen to me. JAZAKALLAH KHAIR to my entire family, friends and colleagues for showing warmth, love and for being always supportive.

RESUMO

A proteína mTOR (mammalian target of rapamycin) é uma proteína quinase de serina e treonina, que funciona como um integrador celular para o crescimento e atividades metabólicas. mTOR existe em dois complexos: mTORC1 e mTORC2. mTORC1 responde a uma variedade de sinais, incluindo fatores de crescimento, hormônios, citocinas, glicose, energia e aminoácidos. A sinalização de aminoácidos através de mTORC1 depende de uma família de proteínas pequenas GTPases. As GTPases Rag são ativadas por um complexo pentamérico denominado Ragulator. O complexo Ragulator foi recentemente identificado como fator de troca de nucleotídeo de guanina (GEF) para as GTPases Rag. Vários estudos indicaram a importância do complexo Ragulator para a ativação de mTORC1 na sinalização mediada por aminoácidos. O complexo consiste em MP1, p14, p18, HBXIP e C7orf59. Aqui apresentamos a estrutura cristalográfica de C7orf59-HBXIP que exibe o domínio *roadblock* assim como MP1 p14. Surpreendentemente, a região N-terminal de C7orf59 apareceu como um *loop* não estruturado, o que é uma informação completamente nova. A presença do N-terminal flexível lembra a subunidade Ego2 do complexo Ego em levedura. Os resultados da mutagenese nos levaram a desvendar os achados iniciais de um possível mecanismo regulador para a ativação de mTORC1 envolvendo a quinase PKA e subunidades do Ragulator. Após tratamento com moduladores de PKA, existe uma alteração clara no padrão de ligação de p18 e HBXIP com C7orf59. Tais descobertas abriram novas possibilidades de controlar a atividade mTORC1 especialmente em condições patológicas. Propusemos também uma interface potencial de p18 com C7orf59 e MP1-p14 através de mutantes de terminação prematura e dados de ligação cruzada e espectrometria de massas. Os dados revelaram muita informação que seria útil para futuros estudos sobre o complexo Ragulator e sua caracterização como alvo potencial para controlar mTORC1 em várias condições patológicas.

Palavras-chaves: proteína quinase de serina, sinalização de aminoácidos, subunidades do complexo Ragulator, estrutura cristalográfica

ABSTRACT

The mammalian target of rapamycin (mTOR) is a serine/threonine protein kinase, which functions as a cellular hub for growth and metabolic activities. mTOR exists in two complexes mTORC1 and mTORC2. mTORC1 responds to a variety of signals including growth factors, hormones, cytokines, glucose, energy and amino acids. Amino acids signaling through mTORC1 depends on a family of small Ras-related GTP-binding protein. Rag GTPases are activated by a pentameric complex named Ragulator. Ragulator complex has recently been identified as guanine exchange factor (GEF) for the Rag GTPases. Several studies have indicated the importance of Ragulator complex for the activation of mTORC1 through amino acid signaling. The complex consists of MP1, p14, p18, HBXIP and C7orf59. Here we present the crystal structure of C7orf59-HBXIP that displays roadblock domain like MP1-p14. Surprisingly, the N-terminal region of C7orf59 appeared as an unstructured loop, which is a completely new information. The presence of flexible N-terminal reminds of the Ego2 subunit of Ego complex in yeast. Mutagenesis results led us to unveil the initial findings of a possible regulatory mechanism for mTORC1 activation involving PKA and Ragulator complex subunits. Upon treatment with PKA modulators, there is clear change in the binding pattern of p18 and HBXIP with C7orf59. Such findings have opened a new way of controlling mTORC1 activity especially in pathological conditions. We have also proposed a potential interface of p18 with C7orf59 and MP1-p14 through stop codon mutants and crosslink data. The observed data revealed a lot of information that would be useful for future studies on Ragulator complex and its characterization as potential target to control mTORC1 in various disease conditions.

Keywords: serine/threonine protein kinase, amino acids signaling, subunits of Ragulator complex, crystal structure

ABBREVIATIONS LIST

A.As - Amino Acids

AMPK - AMP-dependent kinase

ATF6 - Activating transcription factor 6

ATG13 - Autophagy-related gene 13

ATM - Ataxia telangiectasia mutated

ATP - Adenosine 5'-triphosphate

ATR - ATM related

BAD - Bcl-2-associated death promoter

BAK - Bcl2 homologous antagonist/killer

BCAAs - Branched chain amino acids

BCL-2 - B cell leukemia/lymphoma 2

bFGF - Basic fibroblast growth factor

BNIP3 - BCL2/ adenovirus E1B 19 kDa protein-interacting protein3

CAD2 - Carbamoyl-phosphate synthetase 2

CASTOR1 - Cellular Arginine Sensor for mTORC1

CBP80 - 80 kDa nuclear cap-binding protein

Cryo-EM - Cryo-electron microscopy

CR - Caloric restriction

CS - Cowden syndrome

DEPTOR - DEP domain containing mTOR interacting protein

Dmax - Maximum distance

DNA-PK - DNA-dependent protein kinase

DNA-PKcs - DNA-dependent protein kinase, catalytic subunit

4E-BP1 - 4E-binding protein 1

eEF2K - Eukaryotic elongation factor 2 kinase

eIF2 α - Eukaryotic Initiation Factor 2 α

eIF3 - eukaryotic initiation factor 3

eIF4B - Eukaryotic translation initiation factor 4B

eIF4E - Eukaryotic translation initiation factor 4E

EGOC - Ego complex

ER - Endoplasmic reticulum

ERK1/2 - MAP kinase signaling through Extracellular-signal-regulated kinase 1/2
FAT domain - (FRAP)–ATM–(TRRAP)
FATKIN - FAT and Kinase domains of mTOR
FDA - Food and Drug Administration
FIP200 - Focal adhesion kinase family-interacting protein of 200 kDa
FOXO1/3a - Forkhead class O transcription factors 1/3a
FRAP1 - FK506 binding protein 12-rapamycin associated protein 1 (mTOR)
FRB - FKBP rapamycin binding domain
GADD34 - Growth arrest and DNA damage-inducible protein
GAP - GTPase Activating Protein
GATOR - GAP activity towards the Rags
GEF - Guanine nucleotide exchange factor
GDIs - Guanine dissociation inhibitors
GDI1 - GDP dissociation inhibitor 1
GSK3 - Glycogen synthase kinase 3
HBXIP - Hepatitis B virus X-interacting protein
HDX - Hydrogen/deuterium exchange
HEAT - Huntingtin, elongation factor 3 (EF3), protein phosphatase 2A (PP2A), TOR1
HIF1 α - Hypoxia-inducible factor I alpha
HRD - HEAT-repeat domain
IKK β - I κ B kinase β
IRE1 - Inositol-requiring protein 1
IRS1 - Insulin receptor substrate-1
JNK - Jun N-terminal kinase
LD - Longin domain
LKB1 - Liver kinase B1
LRS - Leucyl t-RNA synthetase
MDM2 - Mouse double minute 2 homolog
MEFs - Mouse embryonic fibroblasts
mLST8 - Mammalian Lethal with sec-13 protein 8
mSin1 - Mammalian stress-activated map kinase-interacting protein 1
mTOR - Mammalian target of rapamycin or mechanistic target of rapamycin
mTORC1 - mTOR complex 1
mTORC2 - mTOR complex 2

mTORKi - mTOR Kinase inhibitor
PDCD4 - Programmed cell death 4
PDK1 - Phosphoinositide-dependent kinase 1
PERK - Protein kinase R- like endoplasmic reticulum kinase
PI3K - Phosphatidylinositol 3-kinase
PIKKs- Phosphoinositide 3-kinase related kinases
PIP2 - Phosphatidylinositol 4, 5-bisphosphate
PIP3 - Phosphatidylinositol 3, 4, 5 trisphosphate
PJS - Peutz-Jeghers syndrome
PKC - Protein kinase C
PKC β - Protein kinase C β
PKR - Protein kinase R
PML - Myelocytic leukaemia tumor suppressor
PPAR- γ - Peroxisome proliferator-activated receptor γ
PRAS40 - Proline rich Akt substrate 40kDa
PPP - Pentose phosphate pathway
PTEN - Phosphatase and Tensin Homologue deleted from chromosome 10
Raptor - Regulatory-associated protein of mTOR
REDD1 - DNA damage response 1
RD - Roadblock domain
Rg - Radius of gyration
Rheb - Ras homologue enriched in brain
Rictor - Rapamycin-insensitive companion of mTOR
RNC - Raptor N-terminal Conserved
RPS6 - 40s ribosomal subunit protein 6
RRAGs - Ras-related GTP-binding protein
RTK - Receptor tyrosine kinase
SAXS - Small angle X-ray scattering
SEAC - Seh1-associated SEA complex
Sesn - Sestrins
SDS-PAGE - Sodium dodecyl sulfate-Polyacrylamide gel electrophoresis
SGK1 - Serum/glucocorticoid-regulated kinase 1
SH3BP4 - SH3 domain-binding protein 4
SKAR - S6K1 Aly/REF-like substrate

SLC - Solute carrier
SMG-1 - Suppressor of morphogenesis in genitalia-1
SREBP - Sterol-regulatory-element-binding protein
TOP - Terminal oligopyrimidine
TOR - Target of Rapamycin
TRAF2 - Tumor necrosis factor receptor associated factor 2
TRAPP - Transformation/Transcription Domain Associated Protein
TRD1/2/3 - Tetratricopeptide repeat domain1/2/3
TSC1/2 - Tuberous sclerosis complex protein 1/2
TSCS - Tuberous sclerosis complex syndrome
ULK1 - Unc 51 like kinase 1
UPR - unfolded protein response
VEGF - Vascular endothelial growth factor
VPS39 - Vacuolar Protein Sorting 39
XBP1 - X-box binding protein 1
XIAP - X-linked inhibitor of apoptosis
XPOF - referred to the heterodimer of C7orf59-HBXIP for simplicity
YY1 - Yin-yang 1

TABLE OF CONTENTS

CHAPTER 1	17
1. INTRODUCTION	17
1.1 <i>The Target of Rapamycin kinase: structure and function</i>	17
1.1.1 The architecture of two complexes: mTORC1 and mTORC2	18
1.1.2 A detailed view of mTORC1 structure	19
1.2 <i>Biological function and substrates of mTOR complexes</i>	22
1.3 <i>Downstream effects of mTORC1</i>	24
1.3.1 Lipid synthesis	24
1.3.2 Protein synthesis and ribosome biogenesis	24
1.3.3 Cellular energy levels and mitochondrial biogenesis	25
1.3.4 Autophagy	25
1.4 <i>mTOR pathway and Cancer</i>	26
1.5 <i>mTOR inhibitors and their significance</i>	30
1.5.1 Rapamycin and rapalogues	30
1.5.2 Catalytic Inhibitors.....	31
1.5.3 Rapalink: a third-generation mTOR inhibitor	31
1.5.4 mTOR as a drug target: an open debate	32
1.6 <i>Influx and signal integration upstream of mTORC1</i>	34
1.6.1 Signal convergence through the TSC/Rheb-GTPase axis	34
1.6.2 TSC-independent, Rag-mediated amino acid sensing	35
1.7 <i>Amino acid signaling to mTORC1</i>	36
1.7.1 Regulation of mTORC1 at the Lysosome by Ragulator, V-ATPase and SLC38A9	37
1.7.2 Regulation of mTORC1 at cytosol–lysosome interface by GATOR, Sestrins and CASTOR.....	38
1.7.3 Other proteins involved in nutrient sensing via mTORC1	40
1.7.4 Amino acid signaling through evolution	41
1.7.5 Structural features of Ragulator/Ego complex	42
1.7.6 Amino acid signaling: a target for therapeutic intervention	44
2. JUSTIFICATION	47
 CHAPTER 2	 48
CRYSTAL STRUCTURE OF C7ORF59-HBXIP AND INSIGHTS INTO RAGULATOR ASSEMBLY*	
.....	48
<i>Summary</i>	48
<i>Introduction</i>	50
<i>Results</i>	52
Structure and dynamics of the XPOF dimer	52
Purification of a XPOF–p18 complex	58

Different regions of p18 are required to bind XPOF and MP1-p14 dimers	60
PKA activation induces dissociation of the Ragulator complex.....	63
<i>Discussion</i>	65
<i>Methods</i>	67
Plasmids.....	67
Purification and crystallization of XPOF	67
<i>In silico</i> model building of C7orf59-HBXIP heterodimer.....	67
Data collection and structure solution	67
ConSurf analysis of evolutionary conservation	69
Pull-down assays	69
Cell culture, transfection and coimmunoprecipitation and localization	69
Hydrogen-deuterium exchange.....	70
Chemical crosslinking/ Mass spectrometry analysis	70
Small angle X-ray scattering	71
SUPPLEMENTAL DATA.....	74
<i>SUPPLEMENTAL METHODS</i>	74
Plasmid construction and mutagenesis.....	74
Expression of His-C7orf59-HBXIP	74
Affinity purification	75
Size exclusion chromatography.....	75
Chemical crosslinking/Mass spectrometry analysis	75
Small angle X-ray scattering	76
<i>SUPPLEMENTAL FIGURES</i>	79
<i>References</i>	85
<i>Additional Supplemental Figures</i>	89
CHAPTER 3	91
ADDITIONAL DATA ON RAGULATOR COMPLEX AND ITS SUBUNITS	91
<i>INTRODUCTION</i>	91
<i>Materials and Methods</i>	91
Expression vectors.....	91
Protein purification	92
Crosslinking, SAXS, mutagenesis and pull down analysis of the pentamer.....	92
<i>Results and Discussion</i>	92
Strategy for complex assembly	92
Large Scale purification of GST-p18 Δ N-C7orf59-HBXIP trimer.....	93
GST-p18 Δ N LAKTA_AAAAA mutant does not interact with MP1-p14.....	93
SAXS data analysis	94
Crosslinking evidence	94
<i>Tables</i>	96
<i>Figures</i>	97

Chapter 4	102
CONCLUSION AND FUTURE DIRECTIONS	102
<i>Figures</i>	106
REFERENCES	109
ANNEXES	126

Chapter 1

1. INTRODUCTION

The organizational and functional complexity endorsed by all the eukaryotic organisms deeply relies upon the balancing act between the anabolic and catabolic cellular activities in mutable environmental conditions. The execution of growth related processes requires the detection and coordination of favorable conditions such as nutrients, growth factors and high energy levels. Conversely, lack of growth stimulating signals hinders cell growth and promotes catabolic activities. Most eukaryotic organisms have a conserved signaling pathway controlled by the protein kinase TOR (Target of Rapamycin) which enables them to survive in nutrient insufficient/deprived conditions.

1.1 THE TARGET OF RAPAMYCIN KINASE: STRUCTURE AND FUNCTION

The mammalian target of rapamycin (mTOR) is a serine/threonine protein kinase that belongs to phosphatidylinositol 3-kinase-related kinase protein family and is also known as mechanistic target of rapamycin or FK506 binding protein 12-rapamycin associated protein 1 (FRAP1) (Brown et al., 1994; Chiu et al., 1994; Sabatini et al., 1994; Sabers et al., 1995). The TOR proteins were first identified in yeast as mediator of rapamycin toxic effects (Cafferkey et al., 1993; Kunz et al., 1993). Over the last decades, rapamycin has been well characterized as an anti-fungal, immunosuppressive and anti-cancer drug. It was isolated from a bacterial strain *Streptomyces hygroscopicus* from the island of Rapa Nui. Initial screening showed that the compound seemingly did not have any effect on the bacterial cells while its uptake by yeast and mammalian cells led to significant growth arrest. Later on, several studies based on mammalian cells confirmed TOR as the target of Rapamycin (Brown et al., 1994; Sabatini et al., 1994; Sabers et al., 1995). In mammalian cells, mTOR interacts with different proteins to form two complexes, mTORC1 and mTORC2, depending upon its distinct interaction with the accessory protein Raptor (regulatory-associated protein of mTOR) and with Rictor (rapamycin-insensitive companion of mTOR), respectively (Hara et al., 2002; Jacinto et al., 2004; Kim et al., 2002; Loewith et al., 2002; Sarbassov et al., 2004). The discovery of these two complexes added significant complexity to mTOR signaling as mTORC1 was found to be the real target of rapamycin inhibition while mTORC2 was initially considered rapamycin-insensitive (Jacinto et al., 2004; Sarbassov et al., 2004). However, mTORC2 is only insensitive to an acute dose of

rapamycin, exposure to chronic treatment can lead to disruption of its structure (Sarbasov et al., 2006).

1.1.1 The architecture of two complexes: mTORC1 and mTORC2

Figure 1.1 illustrates the components of mTORC1 and mTORC2. On the structural basis, both mTORC1 and mTORC2 complexes share a structural core composed of the catalytic subunit mTOR and a β -propeller protein named G β L or Mammalian Lethal with sec-13 protein 8 (mLST8) (Kim et al., 2003). These two complexes are defined by the presence of mutually exclusive subunits Raptor (regulatory associated protein of mTOR) in mTORC1 (Hara et al., 2002; Kim et al., 2002) or Rictor (rapamycin insensitive companion of mTOR) in mTORC2 (Jacinto et al., 2004; Sarbasov et al., 2004). Additionally, a negative regulator called DEP domain containing mTOR interacting protein (DEPTOR) (Peterson et al., 2009) and the Tti1/Tel2 scaffold protein complex (Kaizuka et al., 2010) are associated both with mTORC1 and mTORC2. On the other hand, proline rich Akt substrate 40kDa (PRAS40), which negatively regulates the pathway, is an exclusive subunit of mTORC1 (Sancak et al., 2007; Thedieck et al., 2007), while mammalian stress-activated map kinase-interacting protein 1 (mSin1) (Frias et al., 2006; Jacinto et al., 2006) and protein observed with Rictor 1 and 2 (protor1/2) (Pearce et al., 2007; Thedieck et al., 2007) are specific to mTORC2. mTORC2 can be found in three variants, depending upon which of the three different isoforms of the mSin1 is bound to the Rictor at the time of mTORC2 assembly. The existence of three mTORC2 variants has been associated to varying level of insulin input (Frias et al., 2006). The diversity in the architectural assembly of both mTOR complexes is the basis of their different regulatory mechanisms and unique downstream effects mediated by distinct substrates.

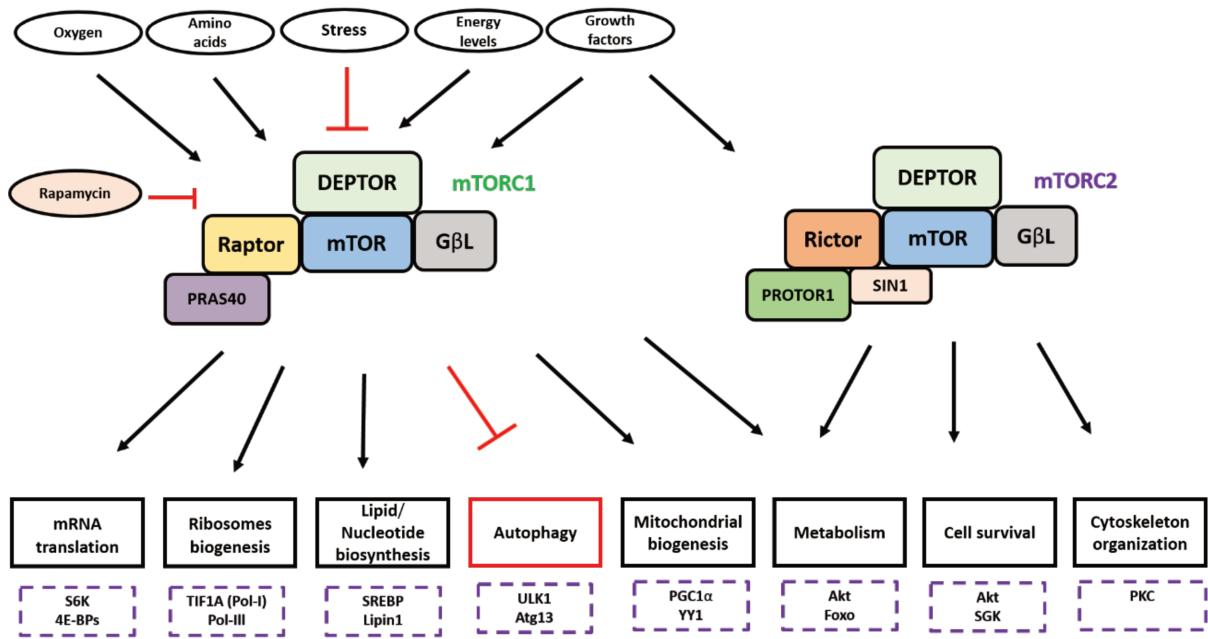


Figure 1.1. Composition, function and known substrates of mTOR complexes; mTORC1 and mTORC2 (Inspired by Laplante and Sabatini, 2012).

1.1.2 A detailed view of mTORC1 structure

mTOR belongs to the family of phosphoinositide 3-kinase related kinases (PIKKs) which also includes Ataxia telangiectasia mutated (ATM), ATR (ATM related), Suppressor of morphogenesis in genitalia-1 (SMG-1), DNA-dependent protein kinase, catalytic subunit (DNA-PKcs) and Transformation/Transcription Domain Associated Protein (TRRAP). A catalytic core consisting of a kinase domain flanked by an N-terminal helical FAT domain (named after FKBP12 Rapamycin Associated Protein (FRAP)–ATM–TRRAP) and a C-terminal short FAT-C domain is a common structural feature of PIKKs. FAT region further consists of four domains, three tetratricopeptide repeat domains (TRD1, TRD2 and TRD3) and a HEAT-repeat domain (HRD). Unlike the N-terminal region of other members of PIKKs, mTOR kinase domain has a 100-residue insertion in its N-lobe known as the FRB (FKBP12-rapamycin binding). The FRB is responsible for substrate recruitment and rapamycin inhibits mTOR by binding to this region. The FAT and Kinase domain are collectively referred as FATKIN domain. The vast N-terminal regions of PIKKs consist of helical solenoids. The helical solenoids are composed of HEAT repeats that form interactions with other proteins and define the enzymatic activity of the formed complex. In mTORC1, HEAT repeats interact with Raptor component. Hsp90-TTT-R2TP is a chaperon supercomplex that regulates the stability of PIKKs. The chaperon Hsp90-TTT-R2TP binds to the N-terminal α -solenoid of PIKKs

through its component Tel2. Until year mid-2015, only low-resolution structure of full length Tor and mTOR were available. Baretić and colleagues have determined a 6Å resolution structure of the full-length Tor–Lst8 complex from the thermotolerant yeast *Kluyveromyces marxianus* (KmTor) (Baretić et al., 2016). The structure showed a dimer interface of two KmTor subunits distinct from the previously described interface in the low-resolution structure of human mTORC1.

A recent Cryo-EM structure of mTORC1 has revealed useful insight about subunit interactions and N-terminus HEAT repeats (Aylett et al., 2016). This structure, shown in **Figure 1.2**, reveals that mTORC1 dimer adopts a hollow lozenge shape, in which kinase domains of mTOR come close to each other and reside near the center of the assembly without making any contact. The peripheral regions of the complex are occupied by Raptor and mLST8. For better visual understanding, the structure was viewed from an angle perpendicular to the symmetry axis. mTOR kinase domains and mLST8 subunits with outwardly open active site clefts can be observed from one side of the complex. The other side revealed N-terminal HEAT repeat domains of mTOR forming two superhelical α solenoids. The two superhelical α solenoids can be differentiated into a large and small α solenoids. The seven repeats of larger one forms a highly curved superhelix, while the remaining repeats which are poorly resolved in the structure. The small section with seven HEAT repeats assumes a relatively linear arrangement and appears like a helical linkage to a more compact large α solenoids. The compact (large) and linear (small) superhelical α solenoids have been named as “horn” and “bridge” by the authors respectively. The horn and bridge are linked to each other while the HEAT repeats of two individual mTORC1 do not interact each other within the mTORC1 dimer. The first HEAT repeat of the mTOR horn region is buried in the base of the adjacent mTOR FAT domain, thus forming a solid foundation of mTORC1 dimer assembly. This new structure differs from the old monomeric crystal structure due to changes in the conformation of FAT domain triggered by dimerization (Aylett et al., 2016).

The Cryo-EM structure has revealed that the FRB domain and mLST8 prevents mTORC1 activity toward noncognate substrates by limiting the access to the adenosine5'-triphosphate (ATP)–binding groove. The active site cleft not only appeared to be constricted by the FRB domain and mLST8, the RNC (Raptor N-terminal Conserved) domain of Raptor also restricts the active site from being accessed through solvent-exposed surface. The new mTORC1 structure dismisses the notion that rapamycin binding to mTORC1 destabilizes Raptor binding by steric hindrance (Yip et al., 2010). FKBP rapamycin binding domain (FRB)

is away from the dimerization interface and does not make any contact the RNC domain of Raptor (Aylett et al., 2016).

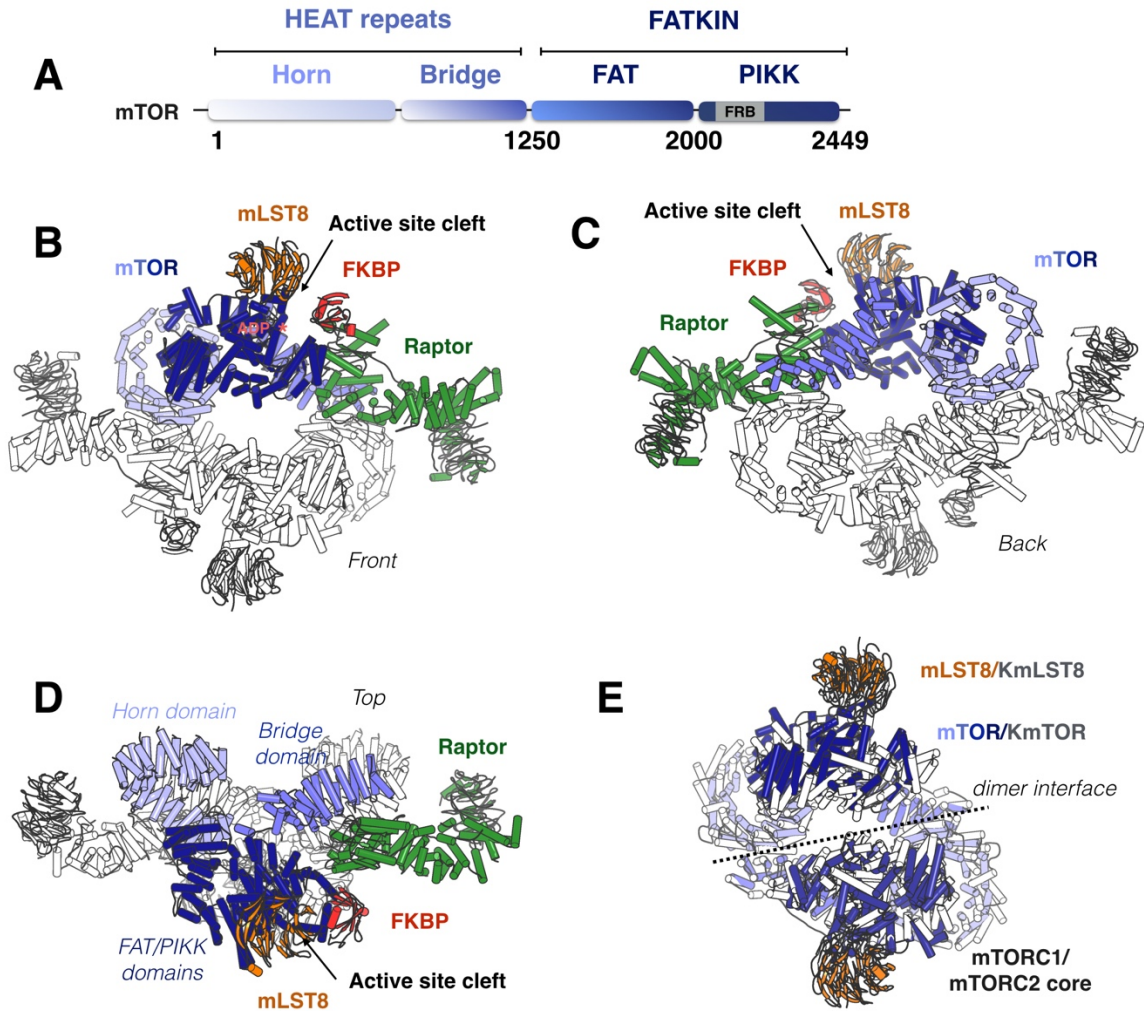


Figure 1.2. High-resolution structure of mTORC1 and core structure of TORC1/TORC2 **A:** Schematic representation of the primary structure and domain organization of mTOR kinase. The Cryo-EM structure of mTORC1/FKBP complex (PDB: 5FLC) is shown in cartoon representation in different orientations: “front” (**B**), “back” (**C**) and “top” (**D**). The mTOR subunit is colored in blue shades from light (N-terminus) to dark (C-terminus). Raptor is colored green, mLST8 is orange and FKBP is red. The symmetry related subunits of the dimeric complex are colored in white. **E:** Superposition of the core mTORC1/mTORC2 and TORC1/2 complexes from human and yeast, respectively. The mTOR/mLST8 subunits (PDB: 5FLC) were superposed to the Cryo-EM structure of TOR/LST8 complex from the thermophilic yeast *Kluyveromyces marxianus* (PDB: 5FVM). The human complex is shown in blue/orange as indicated and the yeast complex is colored white. Figures were prepared with PyMol.

1.2 BIOLOGICAL FUNCTION AND SUBSTRATES OF mTOR COMPLEXES

Despite the widespread efforts to characterize the downstream effectors of mTOR pathway, there are relatively few validated substrates of mTORC1 and mTORC2, partially because unlike other kinases, mTOR lacks a clear linear consensus motif. An updated list of mTORC1 substrates includes 4E-BP, S6K, ULK1, Lipin1, TFEB, Grb10 (Yu et al., 2011), PRAS40, Maf1 (Kantidakis et al., 2010), and mTOR itself. These substrates differ in their rapamycin sensitivity, and mTORC1 rapamycin-sensitive and rapamycin-insensitive sites may even coexist in a single protein substrate (Kang et al., 2013).

mTORC1 regulates mRNA translation through its substrates 4E-BP1 (4E-binding protein 1) and S6 Kinase 1 (S6K), which were the first substrates to be identified and still are the most widely studied. When activated by the presence of nutrients and growth factors, mTORC1 inhibits 4E-BP1 and activates S6K1 through phosphorylation.

4E-BP1 is a translation initiation repressor which binds and sequesters the translation initiation factor eIF4E (Eukaryotic translation initiation factor 4E), and upon phosphorylation by mTORC1, 4E-BP1 can no longer repress the translation initiation process (Gingras et al., 1998). The mTORC1 phosphorylation sites on 4E-BP1 are Ser65 (rapamycin sensitive), Thr37 and Thr46 (both rapamycin insensitive). The rapamycin sensitivity of 4E-BP1 phosphorylation is cell type-dependent and it is frequently rephosphorylated after long rapamycin exposure (Choo et al., 2008). 4E-BP1 mediates mTORC1 effects on cell proliferation, but not cell growth, the latter is dependent on S6K (Dowling et al., 2010). 4E-BP1 phosphorylation and 4EBP1/eIF4E ratio seem to underlie, at least partially, the complex phenomenon of rapamycin resistance, in which a cell no longer responds to the cytotoxic effect of rapamycin (Alain et al., 2012; Yoon and Roux, 2013).

On the other side, S6K1 phosphorylation on Thr389 behaves as a typical rapamycin-sensitive site and its phosphorylation status is frequently used to monitor mTORC1 inhibition. The most known substrate of S6K1, which is also used as a proxy of mTORC1 activation, is the ribosomal protein RPS6 (component of 40S ribosome subunit). Although it has been thought that S6K exerts its effects on translation initiation by directly phosphorylating a ribosomal protein, recent findings indicate that RPS6 phosphorylation is not required for the downstream effects of S6K activation. The effects of S6K1 activation on translation initiation, ribosome biogenesis and increased cell size depend on its interaction or phosphorylation of some members of translation machinery including eIF4B (Eukaryotic translation initiation factor 4B), S6K1 Aly/REF-like substrate (SKAR), eukaryotic elongation factor 2 kinase (eEF2K),

eukaryotic initiation factor 3 (eIF3), 80 kDa nuclear cap-binding protein (CBP80) and programmed cell death 4 (PDCD4) (Magnuson et al., 2012; Zoncu et al., 2011b).

mTORC1 also controls the processing and nuclear localization of sterol-regulatory-element-binding protein (SREBP) through S6K1 and Lipin 1 (Peterson et al., 2011). In turn, active SREBP enhances the expression of genes involved in pentose phosphate pathway (PPP) and lipid synthesis pathways (Düvel et al., 2010; Horton et al., 2002). mTORC1 also mediates the biosynthesis of pyrimidines by activating Carbamoyl-phosphate synthetase 2 (CAD2) enzyme and thus upregulates pentose phosphate pathway (PPP) (Ben-Sahra et al., 2013). mTORC1 also plays an important role in the negative regulation of the initiation of autophagy by directly phosphorylating its two substrates ATG13 (Puente et al., 2016) and ULK1 in the ULK1/Atg13/FIP200 complex (Ganley et al., 2009; Hosokawa et al., 2009; Jung et al., 2009). The details of how each substrate influences the anabolic and catabolic activities of the cell is described in 'Downstream Effects of mTORC1' section.

One of the major functions ascribed to mTORC2 is the regulation of the actin cytoskeleton and migration. However, the underlying mechanism through which mTORC2 controls the assembly of actin fibers is still unknown. Although Ser2448 phosphorylation site is predominantly associated, yet it is not specific to mTOR catalytic subunit of mTORC1. On the other hand, in 2009 Copp et al. showed Ser2481 as mTORC2-specific phosphorylation site (Copp et al., 2009). Although active mTORC2 phosphorylates Akt (direct substrate) at Ser473 that resides in the hydrophobic motif, still Akt can remain largely active due to phosphorylation of Thr308 by phosphoinositide-dependent kinase 1 (PDK1, PI3K/PTEN pathway). Both sites can be independently phosphorylated and do not display any hierarchical phosphorylation pattern. However, mTORC2-mediated Akt phosphorylation determines substrate specificity for Akt. Akt substrates include glycogen synthase kinase 3 (GSK3), tuberous sclerosis complex protein 2 (TSC2), BAD (Bcl-2-associated death promoter) and the forkhead class O transcription factors 1/3a (FOXO1/3a). Phosphorylation of FOXO1/3a and to some extent of BAD by Akt is linked to its Ser473 phosphorylation whereas Thr308 phosphorylation is sufficient to phosphorylate GSK3 and TSC2. It is important to mention that GSK3 and FoxO1/3a can also be phosphorylated by kinases S6K and SGK1 (Serum/glucocorticoid-regulated kinase 1) respectively. Recently, SGK1 was identified as mTORC2 direct substrate. Various studies using different approaches have demonstrated that the effect of reduced mTORC2 activity on PKC (protein kinase C) protein levels and later PKC α and PKC ϵ were identified as additional substrates of mTORC2. Since the discovery of Akt and PKC as substrates of mTORC2, it is obvious that mTORC2 also controls a number of important aspects

of cell survival, metabolism and growth activities through poorly understood mechanisms. It is critical to comprehend how mTORC2 governs these activities for better functional characterization of the kinase.

The topics discussed in this section and the following section are illustrated in **Figure 1.3**.

1.3 DOWNSTREAM EFFECTS OF mTORC1

mTORC1 is considered as a cellular hub for growth and metabolic activities. Activated mTORC1 promotes anabolic process such as protein synthesis, lipogenesis, and energy metabolism (Zoncu et al., 2011) and inhibits autophagy and lysosome biogenesis whereas mTORC2 is activated by growth factors and regulates cytoskeletal organization and cell survival. mTORC1 has been better characterized over the last few years as compared to mTORC2. The remaining part of the introduction would be focused on mTORC1.

1.3.1 Lipid synthesis

Proliferating cells require lipids to form membranes, and mTORC1 regulates lipogenesis by controlling the expression of multiple genes involved in the biogenesis of fatty acids and cholesterol. Sterol regulatory element binding protein 1/2 (SREBP1/2) transcription factors are the key players in this mechanism. mTORC1 controls the levels and availability of SREBP1/2 through different ways such as by limiting Lipin-1 (a phosphatidic acid phosphatase) from entering into nucleus by phosphorylating it. Unphosphorylated Lipin-1, upon entering the nucleus, can suppress SREBP1/2 levels (Düvel et al., 2010; Li et al., 2011; Porstmann et al., 2008; Wang et al., 2011). mTORC1 also promotes adipogenesis by enhancing the expression of peroxisome proliferator-activated receptor γ (PPAR- γ) (Kim and Chen, 2004; Zhang et al., 2009).

1.3.2 Protein synthesis and ribosome biogenesis

Translation initiation/elongation factors and ribosomes biogenesis are the founding features of protein synthesis. Activated mTORC1 phosphorylates eukaryotic translation initiation factor 4E (eIF4E) binding protein 1(4E-BP1) and S6 kinase1 (S6K1). Upon mitogen stimulation, RPS6 (40s ribosomal subunit protein) has been observed to be phosphorylated by S6K1. mTORC1 activates S6K1 by phosphorylating it at a conserved threonine residue 389 (Thr 389). This S6K1 activation via mTORC1 embodies a substantial role in the regulation of

5' TOP (terminal oligopyrimidine) mediated translation which involves a specific subset of ribosomal protein mRNAs and elongation factors with pyrimidine-rich sequence at their 5' end, referred to as a 5' TOP (Jefferies et al., 1997; 1994; Ma and Blenis, 2009). mTORC1 also controls cell cycle progression at G1 stage. The cap-dependent translation of the Cyclin D1 (mRNA), one of the key regulators of G1 stage, is controlled by 4E-BP1. Cap-dependent translation heavily depends upon the attachment of initiation factor 4F (eIF4F) to the mRNA with extensive secondary structures. eIF4F is a complex of eIF4A, eIF4E, and eIF4G. In this complex, eIF4E is the cap-binding protein, which interacts with the 5' cap of mRNAs. Unphosphorylated 4E-BP1 binds eIF4E leading to the removal of eIF4F from the mRNA, which halts the cap-dependent translation. Upon phosphorylation, 4E-BP1 loses the interaction with eIF4E, and promotes translation initiation (Sonenberg and Hinnebusch, 2009).

1.3.3 Cellular energy levels and mitochondrial biogenesis

Mitochondrial membrane potential and function holds great importance in maintaining the energy hemostasis of the cell. Variations in the expression and translation of genes of the oxidative phosphorylation machinery directly reflects on the cellular ATP levels. As all anabolic activities require energy, the notion of potential involvement of mTORC1 in the regulation of mitochondrial biogenesis is indeed intriguing. A study based on the conditional deletion of Raptor in the skeletal muscle of mice demonstrated alterations in the mitochondrial phosphoproteome due to reduced expression of genes involved in the mitochondrial biogenesis (Bentzinger et al., 2008). The translocation of mTORC1 from cytoplasm to lysosomal surface has been well documented but the idea of mTORC1 shuttling in and out of the nucleus demands strong evidences. However, in 2007 Cunningham et al., showed that mTOR could directly influence the physical interaction and coactivation of the transcriptional factor yin-yang 1 (YY1) by a nuclear co factor called PPAR γ coactivator 1 (PGC-1 α) (Cunningham et al., 2007).

1.3.4 Autophagy

Autophagy is a catabolic cellular process involved in cellular recycling, which depends on various protein complexes. One of these conserved complexes, formed by the kinase ULK1 (unc 51 like kinase 1), ATG13 (autophagy-related gene 13) and FIP200 (focal adhesion kinase family-interacting protein of 200kDa) in mammals and the orthologues Atg1-Atg13-Atg17 in yeast, is the major target of TOR/mTORC1 regulation (Ganley et al., 2009; Hosokawa et al.,

2009; Jung et al., 2009; Kamada et al., 2000). These complexes initiate autophagy by forming the autophagosome. These autophagosomes grasp *intra* cellular components and deliver them to lysosomes for degradation. This degradation process becomes the source of energy and sustenance during starvation/low-nutrient condition for the cells. In addition to protein synthesis, mTORC1 also suppresses autophagy by either binding or phosphorylating the autophagosomes.

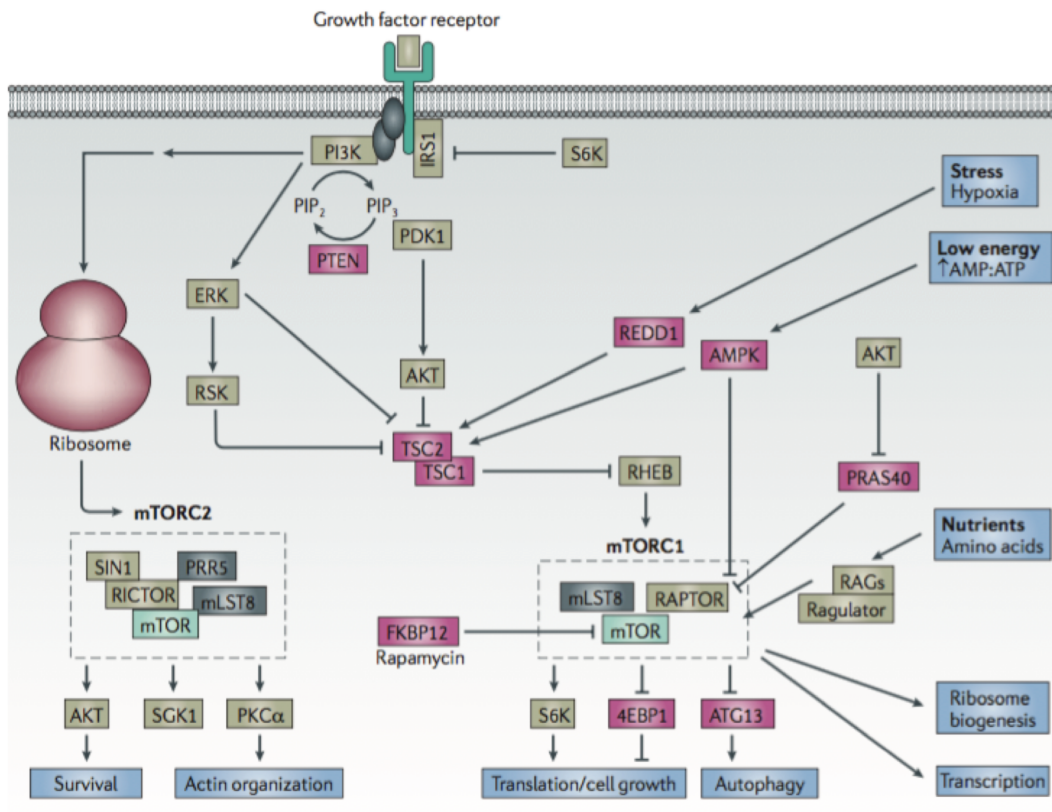


Figure 1.3. Upstream and downstream components of signaling through mTORC1 and mTORC2 (Benjamin et al., 2011).

1.4 mTOR PATHWAY AND CANCER

mTOR signaling allows G1-S phase cell cycle transit by promoting the synthesis of transit (G1-S phase) specific proteins. Mutations in TSC1 or TSC2, loss of PTEN phosphatase (Phosphatase and Tensin Homologue deleted from chromosome 10) or hyperactivation of Akt and loss of function mutations in LKB1 (liver kinase B1, a positive regulator of TSC2) are some of the examples that constitute the shift in the upstream regulation of the mTOR pathway in cancer. Well-vascularized hamartomas associated with Tuberous sclerosis syndrome are caused by mutations in TSC (Inoki et al., 2003). Although the disease related lesions are of benign

nature, yet the risk of renal cell carcinoma is increased (Kwiatkowski, 2003). LKB1 kinase inhibits the function of mTOR via AMP-dependent kinase pathway. Under low energy conditions, LKB1 activates AMPK, which in turn phosphorylates TSC2 that finally leads to inhibition of mTOR. Loss of function mutations in LKB1 and uncontrolled mTOR activity in low energy levels was observed in PeutzJeghers cancer prone syndrome (Shaw et al., 2004a, 2004b). Different types of tumors such as endometrial carcinomas, lung carcinoma, glioblastoma, hepatocellular carcinoma, melanoma and prostate cancer lack functional PTEN. Loss of function is either because of mutations, silencing or because of gene deletion. Since PTEN negatively regulates Akt activation by PIP3 (phosphatidylinositol 3,4,5 trisphosphate), loss of PTEN will result in the activation of Akt, which will later activate mTORC1 (Easton and Houghton, 2006). Active Akt also suppresses p53 activity by phosphorylating MDM2 (Mouse double minute 2 homolog, an E3 ubiquitin ligase). Phosphorylation by Akt results in the translocation of MDM2 to nucleus where it interacts with p53. MDM2 translocates p53 to cytosol for degradation (Hasty et al., 2013; Manning and Cantley, 2007).

In the early stage of tumorigenesis, the proliferating cells can outgrow their blood supply and suffer from oxygen deprivation. mTORC1 controls a diverse array of anabolic activities which makes it an oxygen sensitive pathway. The hypoxia negatively controls mTORC1 by inducing the expression of transcriptional regulation of DNA damage response 1 (REDD1), that results in the constitutive activation of TSC2 in a poorly understood fashion (DeYoung et al., 2008; Reiling and Hafen, 2004; Wouters and Koritzinsky, 2008). Under moderate hypoxic conditions, AMP-dependent kinase dependent TSC1-TSC2 activation leads to inhibition of mTORC1 (Arsham et al., 2003). The interaction between mTOR and Rheb (Ras homolog enriched in brain, a small GTPase) is also interfered during low oxygen levels. Hypoxia inducible proteins such as myelocytic leukaemia tumor suppressor (PML) and proapoptotic protein BCL2/ adenovirus E1B 19 kDa protein-interacting protein 3 (BNIP3) directly binds with mTOR and Rheb respectively and thus hinder the mTOR-Rheb interaction (Bernardi et al., 2006; Li et al., 2007). Cancer cells bypass hypoxia-mediated negative-regulation of mTORC1 by driving growth favouring mutations in the pathways regulated by hypoxia. Loss of PML is one of the ways through which tumorigenesis is promoted (Bernardi et al., 2006). In advanced cancers, where outgrowing tumor cells suffer through hypoxic stress, the O₂ dependency of mTORC1 regulation forces cancer cells to re-establish mTOR signaling for protein synthesis and other anabolic activities for cell survival. However, which pathway components drive this hypoxia tolerance in cancer cells is still not clearly understood (Wouters and Koritzinsky, 2008) **(Figure 1.4).**

Hypoxia can also induce unfolded protein response (UPR) in endoplasmic reticulum (ER) stress conditions. During ER stress, UPR signaling is activated by various other signals including secretory protein over load, redox state, glucose availability and calcium homeostasis. The general role of UPR signaling activation is to restore the ER homeostasis or in case of irreparable damage induce cell death. PKR-like ER kinase (PERK/ EIF2AK3), inositol-requiring protein 1 (IRE1) and ATF6 (Activating transcription factor 6) are ER integral membrane proteins that function as stress sensors. Hypoxia stimulates autophosphorylation of PERK (Protein kinase R (PKR)-like endoplasmic reticulum kinase) and phosphorylation of EIF2 α (Eukaryotic Initiation Factor 2 α), which is the main substrate of PERK. ATF6 negatively regulate the phosphorylation of EIF2 α by upregulating GADD34 (growth arrest and DNA damage-inducible protein) that is a substrate targeting subunit of protein phosphatase 1. Protein phosphatase 1 holds phosphatase activity against EIF2 α , as evidenced by the transient levels of phosphorylated EIF2 α (reviewed by Wouters and Koritzinsky, 2008). PERK-dependent phosphorylation of EIF2 α leads to overall inhibition of mRNA translation. Apart from controlling the ER stress, UPR signaling can also influence autophagy. In response to ER stress, autophagy happens to be mediated by either PERK or IRE1. IRE1 is another ER transmembrane stress sensor protein. It holds endonuclease activity. During ER based stress, IRE1 alters gene expression. Its splicing activity against X-box binding protein 1 (XBP1) pre-mRNA that leads to the activation of XBP1 is evident in hypoxia. The ratio of spliced to unspliced XBP1 is associated to poor disease free survival rate in breast cancer (Davies et al., 2008). A study showed an increase in the apoptosis rate and compromised tumor growth when IRE1 dependent arm of UPR was disrupted in XBP1 knock out cells (Romero-Ramirez et al., 2004).

UPR signaling also promotes apoptosis in case of prolonged ER stress. The pro-apoptotic family members BAX and Bcl2 homologous antagonist/killer (BAK) required for signaling the UPR transcriptional response are associated with XBP1 activation through IER1 (Hetz et al., 2006). IER1 influences mTOR activity by recruiting TRAF2 (tumor necrosis factor receptor associated factor 2), that leads to the inactivation of insulin receptor substrate 1 (IRS1) through Jun N-terminal kinase (JNK)-mediated phosphorylation. IRS1 is a positive regulator of mTOR (reviewed by Wouters and Koritzinsky, 2008). S6K1, substrate of mTORC1 also forms a negative loop by directly phosphorylating the insulin receptor substrate-1 (IRS1) which leads to IRS1 degradation and reduces the ability of growth factors to signal downstream of receptor tyrosine kinase (RTK). The presence of such negative loops further contributes to limited efficacy of drugs (reviewed by Laplante and Sabatini, 2012).

The importance of hypoxia in the regulation of mTOR is evident through its influence on autophagy and apoptosis. Oncogenic mutations in the regulatory components of the hypoxia mediated signaling pathways collaborate with mTOR to promote hypoxia tolerance. The interplay between mTOR and UPR pathways needs further exploration for better characterization of therapeutic targets for cancer treatment.

Deregulation of mTOR signaling through its downstream effectors has also been associated with tumor growth since its substrate eIF4E-binding protein (4E-BP1) is a major player in protein translation. Phosphorylated 4E-BP1 binds with eIF4E to form eIF4F complex, and this complex promotes protein translation therefore, amplified phosphorylation of 4E-BP1 by mTORC1 has been observed in various types of tumor. Irregular eIF4E-4E-BP1 axis is thought to fuel the translation of proteins involved in pro-oncogenesis and cell survival through an unknown mechanism (Laplane and Sabatini, 2012). Several types of late-stage carcinoma including head and neck carcinoma, breast (ductal cell) carcinoma and thyroid carcinoma reportedly show eIF4E gene amplification (Haydon et al., 2000; Wang et al., 2001). Elevated levels of eIF4E are also observed in some colon, breast and bladder carcinomas, however in case of breast and bladder carcinomas, high levels of vascular endothelial growth factor (VEGF) results in poor prognosis. In 2004 Wendel et al., showed how the cooperation of eIF4E with overexpressed c-myc promoted tumor formation in lymphomagenesis mouse model (Wendel et al., 2004). Down-regulation of eIF4E suppress the expression of angiogenic factors such as bFGF (Basic fibroblast growth factor) and VEGF and may possibly be therapeutically important in controlling the tumorigenicity. Considering the importance and frequency of overexpression of eIF4E in different types of cancer, in a 2006 review paper, Easton and Houghton pointed at the possibility that eIF4E may act as an oncogene under some conditions (Easton and Houghton, 2006).

In cancer-based studies, substantial amount of data has shown deregulation of pathways that lie upstream and downstream of mTOR whereas alterations in the expression or function related mutations in mTOR have not been reported. One can anticipate that cancer cells depend on mTOR pathway for continuous proliferation and care about the overall integrity of the kinase. Any variation within the kinase itself would not be favourable for the growing tumor to maintain the transformed phenotype. Apparently, tumor cell is not addicted to mTOR kinase; instead, aberrations in PI3K/AKT pathway are common in cancer.

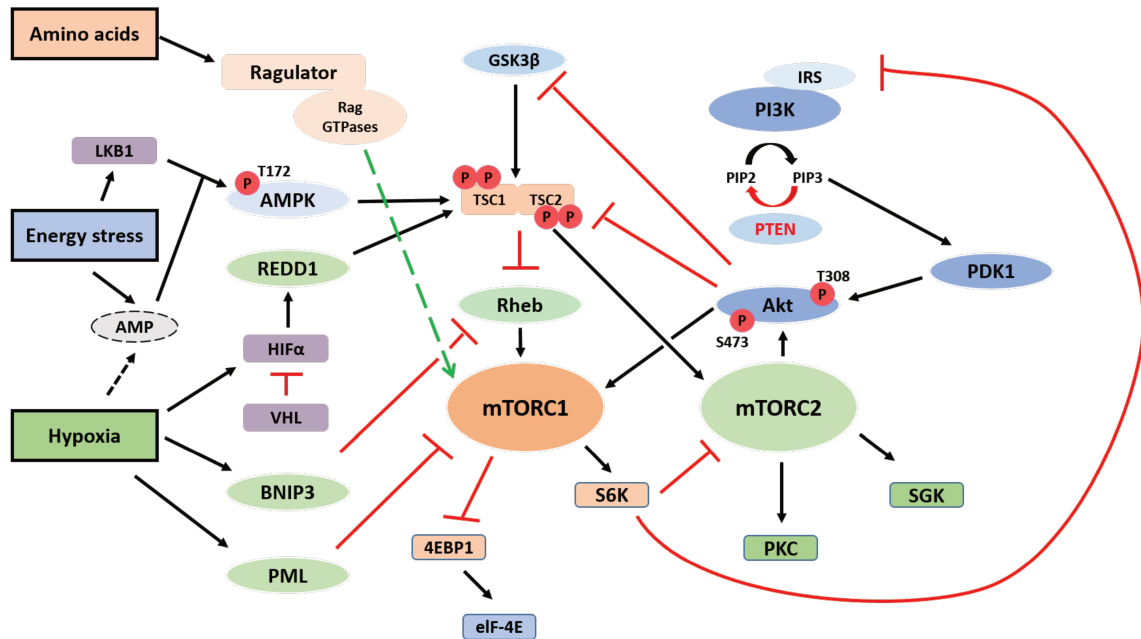


Figure 1.4. Illustration demonstrating the regulation of mTORC1 during hypoxia and energy stress, and how mTORC1 and mTORC2 crosstalk through their substrates (Inspired by Huang and Manning 2008; Sparks and Guertin 2010).

1.5 mTOR INHIBITORS AND THEIR SIGNIFICANCE

1.5.1 Rapamycin and rapalogues

Rapamycin is a highly selective allosteric inhibitor of mTORC1. The catalytic kinase activity of mTOR depends upon FKBP12-rapamycin binding domain (FRB) which is located upstream of the catalytic domain. Rapamycin in complex with FK506 binding protein (FKBP12) binds irreversibly to mTORC and impairs substrate recruitment. Ser2035 that exist within the FRB domain (residues 2025-2114) is associated with rapamycin binding. The mechanism through which rapamycin acts is not clear, however, it has been proposed that FKBP12 complex act as a physical obstruction between the mTOR catalytic domain and its substrates (Sarbasov et al., 2005). Although rapamycin is currently used as an anticancer drug, not all mTORC1 functions are blocked by rapamycin (Choo et al., 2008; Feldman et al., 2009; García-Martínez et al., 2009). Interestingly, rapamycin treatment may lead to Akt and MEK-ERK pathway activation due to its ability to block negative feedback loop that emanates from S6K1 to PI3K. Studies have shown that despite the high selectivity of rapamycin towards mTORC1, cells still may develop rapamycin resistance, which can be explained by various other Akt effectors. Apart from mTORC1, Akt also regulates various proteins involved in cell cycle progression such as cyclin D1, p27, GSK3 and FoxO. It also negatively controls MDM2,

caspase-9, IKK α and BAD to resist apoptosis (Manning and Cantley, 2007). Rapamycin can also indirectly activate PI3K-Akt independent effectors like PDK1. High levels of PDK1 have shown to be associated with sustaining tumor growth (Vasudevan et al., 2009). High concentration of rapamycin can also block mTORC2 activity but clinical applicability of such high levels of rapamycin demands thorough investigation (Shor et al., 2008). A series of structurally similar semi-synthetic derivatives of rapamycin have been developed. These derivatives namely Temsirolimus, Everolimus, Deforolimus, and Zotarolimus are collectively called Rapalogs (Benjamin et al., 2011). Rapalogs hold improved pharmacokinetic properties. They have the same mode of action as rapamycin and share similar side effects (Hartford and Ratain, 2007).

1.5.2 Catalytic Inhibitors

Several groups have simultaneously reported another class of mTORC1 inhibitor that blocks mTOR catalytic site. The catalytic inhibitors of mTOR includes Torin (Thoreen et al., 2009), PP242 and PP30 (Feldman et al., 2009), Ku-0063794 (García-Martínez et al., 2009) and WAY-600, WYE-687 and WYE-354 (Yu et al., 2009). Development of catalytic inhibitors presented another therapeutic advantage. These inhibitors not only inhibit all target activities of mTOR (both mTORC1 and mTORC2), they also obstruct Akt phosphorylation at Ser473. It would be interesting to determine if phosphorylation at Ser473 would affect Akt activity towards all its effectors or not, and if it does impair then to what extent. It is intuitive to think whether inhibition of all mTOR activities would cause potential toxicity. A study based on prostate cancer has shown that mTORC2 promotes tumor growth while lack of mTORC2 activity did not display any toxic effect on normal prostate (Yu et al., 2009).

1.5.3 Rapalink: a third-generation mTOR inhibitor

Rapalink was designed by linking a first-generation mTOR inhibitor, which binds to one part of the molecule, to a second-generation inhibitor, which targets a separate pocket in proximity. Resistance screening in MCF-7 cells revealed three somatic mutations within mTOR. Two mutations A2034V and F2108L in the FRB-FKBP12-rapamycin-binding-domain confer resistance to rapamycin while the third mutation at a position of M2327I within the kinase domain aggravates resistance against AZD8055 (ATP competitive inhibitor) (Rodrik-Outmezguine et al., 2016). The importance of these mutations concerning drug resistance came from the clinical data. A case report of a patient under treatment with everolimus (a rapalog),

after relapse acquired F2108L mTOR mutation (Wagle et al., 2014). Surprisingly, data from a different patient showed that hyperactive M2327I along with other kinase domain mutations were already present even before receiving any drug treatment (Grabiner et al., 2014). The recent elucidation of Cryo-EM structure of mTORC1 has also revealed that FRB and kinase domains exist in close proximity. The authors took a modeling approach to design a molecule that could bind both sites. Later, a bivalent molecule comprising rapamycin and MLN0128 (highly selective catalytic site inhibitor) joined by a chemical linker was developed and named as RapaLink. RapaLink effect was tested in cells expressing F2108L and M2327I mTOR mutants, as expected RapaLink showed inhibitory effects on both mutants and cells did develop resistance for a period of nine months. Further, the new drug was also tested on xenografts in mouse model, again RapaLink showed promising results (Rodrik-Outmezguine et al., 2016).

1.5.4 mTOR as a drug target: an open debate

mTOR pathway holds central role in various clinical pathologies such as diabetes, aging, neuro-degenerative diseases and more importantly cancer. Interestingly, mTOR pathway is rarely mutated in cancer but its activation is predominant in tumor growth, which has made it a popular target for the treatment of cancer. After the discovery of rapamycin inhibitory activity towards mTORC, both academics and pharmaceutical companies have made a lot of effort to manipulate the pathway that is so critical to cell growth and survival. Although rapalogs have shown promising anti-tumor effects, and some of them are also FDA (Food and Drug Administration) approved for use in chemotherapy. Temsirolimus and Everolimus are used in the treatment of renal cell carcinoma and kidney cancer respectively (Hartford and Ratain, 2007). Still, the effectiveness of the drugs is only limited to extended survival rate in cancer patients. It is also important to understand that oncogenic/gain of function mutations in the downstream effectors of mTORC1 may also contribute to cell resistance to rapamycin/catalytic inhibitors treatment. Downstream effectors such as S6K1 and 4E-BP1 are crucial for cell proliferation and cancer growth, but inhibition of these substrates is also not sufficient to control tumorigenesis. Contrary to general understanding of mTOR activity in growth, inhibition of mTOR pathway sometimes may result in more aggressive tumor growth such as in case of colorectal carcinoma (O'Reilly et al., 2006). This might be due to Akt activation as rapamycin can block the negative feedback loop starting from S6K1 to PI3K. Rapamycin inhibits mTORC2 in a cell selective manner while partially inhibiting mTORC1, long exposure of rapamycin leads to disruption of mTORC2 complex. Taking the effect of rapamycin on mTORC2 disassembly into account, it is intuitive to think that rapamycin inhibits cell growth

due to loss of Akt activation because of mTORC2 disruption. Rapamycin inhibitory activity towards mTORC2 in select cells is not clearly understood as mTORC2 disruption is not correlated with the efficacy of rapamycin. Irregular eIF4E/4E-BP1 axis in cancer also explains the poor efficacy of rapamycin in certain cases as it cannot inhibit 4E-BP1 phosphorylation. It was initially proposed that binding of rapamycin in FRB domain may hinder with Raptor-mTOR complex stability but recently discovered cryo-EM structure of mTORC1 has ruled out this possibility (Aylett et al., 2016).

The PI3K/Akt pathway lies upstream of mTOR and regulates various anabolic activities such as cellular proliferation and growth, survival and protein synthesis. Mutation or amplification of the PIK3CA gene is a frequent phenomenon that occurs in cancer cells. The frequency of aberrations in PI 3-K/AKT pathway in cancer has enhanced its importance for therapeutic uses. A wide range of PI3K/Akt cascade kinases has been validated as therapeutic targets. Since mTOR is a kinase, therefore the idea to target the catalytic site of mTOR led to the development of various ATP-competitive inhibitors.

Given the evidence that mTORC2 substrate Akt activation through PI3K pathway is involved in the regulation of mTORC1 activity through TSC1/2 axis, the researchers started to look for the ways to generate dual inhibition of PI3-Kinase and mTOR pathway. ATP-competitive inhibitors include both dual PI3Kinase/mTOR and selective mTOR inhibitors. The thought behind the development of dual PI3Kinase/mTOR ATP competitive inhibitors was to target both pathways at the same time to generate a more pronounced effect. In theory, an ATP competitive inhibitor can also target mTORC2 pathway. Torin, an ATP-competitive inhibitor of mTOR, inhibited mTORC1 phosphorylations in a greater range as compared to rapamycin (Thoreen et al., 2009). The development of PI3K α selective inhibitors such as PP242 and PP30 offers an opportunity to explore an expanded role of mTOR within the PI3K/Akt pathway. PP242 inhibited 4EBP1 phosphorylation at Thr36, Thr45 and Ser65 and hindered cell proliferation in a dose dependent manner (Feldman et al., 2009). These findings revealed the rapamycin insensitive components of the mTOR pathway and demonstrated that rapamycin is a partial inhibitor of mTOR pathway. Several studies have shown the effects of various selective and dual ATP competitive inhibitors however, an optimally good dual PI3K/mTOR catalytic inhibitor with equal selectivity and less toxicity towards normal cells is yet to be developed. Drug combination such as an Akt inhibitor along with mTOR inhibitor is another approach that can be used to fully inhibit proliferation with lower chances of activation of feedback loops that may recapitulate the growth process. One of the major challenges in the development of the combination drug is to deal with the toxic response of each drug.

Recently, the development of Rapalink, a third generation mTOR inhibitor has reached a new horizon in drug development process for the treatment of cancer (Rodrik-Outmezguine et al., 2016). It would be interesting to see how Rapalink or Rapalink alike drugs would behave in clinical setting. Intriguingly, screening of naturally occurring compounds might be anticipated to search for potential Rapalink-like molecules for future drug development. Lastly, mTOR inhibition remains an attractive option for therapeutic interventions for the treatment of cancer. Search for patterns in an evolving disease like cancer could pave a way for better target selection, development of novel drugs and overcome insurgence of resistance causing mutations.

1.6 INFLUX AND SIGNAL INTEGRATION UPSTREAM OF mTORC1

mTORC1 responds to a variety of signals including growth factors, hormones, cytokines, glucose, energy (AMP: ATP ratio), stress, oxygen levels and amino acids. All these inputs are channelled down through two distinct branches of the signaling cascade before they finally converge at mTORC1.

1.6.1 Signal convergence through the TSC/Rheb-GTPase axis

The transduction of signals such as growth factors, hormones and cytokines and several types of stress to mTORC1 is regulated at a midpoint where a heterodimer of Tuberous Sclerosis Complex 1 and 2 (TSC1/Hamartin and TSC2/Tuberin) acts as GTPase-activating protein (GAP) for the Ras homolog enriched in brain (Rheb) GTPase and promotes Rheb-GTP hydrolysis (Garami et al., 2003; Inoki et al., 2003; Tee et al., 2003; Zhang et al., 2003). In its activated state, GTP-bound Rheb is a major upstream activator of mTORC1 which acts by binding directly to mTORC1, this behavior of Rheb is observed concomitant of all stimuli including amino acids (Long et al., 2005). By acting as a GAP, TSC1/2 promotes the inactive state of Rheb, thereby preventing mTORC1 activation. TSC2 functions directly as a GAP for Rheb through a catalytic arginine located in a region homologous to the Rap1-GTPase-activating protein domain while TSC1 undertakes a scaffolding/regulatory function (Li et al., 2004). The basal GTP-bound levels of Rheb are high and there is no evidence for the existence of any Rheb GEF (Laplane and Sabatini, 2012). In the absence of TSC1/2 complex, mTORC1 is active even without upstream signals. This is observed as increased cell size both in TSC-null mouse embryonic fibroblasts (MEFs) and in Tuberous Sclerosis patients which spontaneously develop benign tumors known as hamartomas. However, it has been observed in

TSC2-null MEFs, that just Rheb activation is not sufficient for mTORC1 activation: in case of amino acids deficiency, some other components of the pathway which are not part of TSC-Rheb pathway can cause inactivation of mTORC1 (Long et al., 2005; Smith et al., 2005).

Physiologically, the mTORC1 activating signals act in different ways to neutralize the action of TSC1/2 complex thereby allowing Rheb to remain in its activated state. In the hormone/growth factor sensitive branch of mTOR signaling, known as PI3K-Akt-mTOR pathway, Akt phosphorylates TSC2 and disrupts the heterodimer assembly, which promotes the accumulation of GTP-bound Rheb GTPase (Inoki et al., 2002; Manning et al., 2002; Potter et al., 2002). Phosphatidylinositol-3-kinase (PI3K) mediates insulin-signaling effects through Akt. PI3K phosphorylates Phosphatidylinositol 4, 5-bisphosphate (PIP2) and converts it into Phosphatidylinositol (3, 4, 5)-trisphosphate (PIP3). Conversely, PIP3 can be dephosphorylated by a tumor suppressor phosphatase PTEN. Loss of function mutations in PTEN have been reported in different types of cancers. PDK1 (3-phosphoinositide dependent protein kinase-1) and Akt are recruited to the plasma membrane by PIP3, enabling PDK1 to phosphorylate Akt at Thr308 site. Active Akt phosphorylates tuberous sclerosis complex protein 2 (TSC2). Upon phosphorylation, TSC2 is dissociated from the complex and can no longer inhibit Rheb GTPase. GTP bound Rheb interacts and activates mTORC1 at the lysosomal surface.

Other pathways signaling to mTORC1 through TSC complex include proinflammatory cytokine signaling through I κ B kinase β (IKK β), MAP kinase signaling through Extracellular-signal-regulated kinase 1/2 (ERK1/2), canonical Wnt signaling through GSK3- β (in this case, GSK3- β -mediated phosphorylation of TSC2 promotes its GAP activity and Wnt pathway activation results in inhibition of GSK3- β). All these pathways result in inhibition of either TSC1 or 2 and consequently mTORC1 activation. On the other hand, sensing of stress conditions such as hypoxia and low energy levels (low ATP:AMP ratio) through Adenosine monophosphate-activated protein kinase (AMPK) results in phosphorylation and activation of TSC2 and consequently inactivation of mTORC1 (Laplante and Sabatini, 2012).

1.6.2 TSC-independent, Rag-mediated amino acid sensing

The TOR pathway evolved as a nitrogen sensor for environmental conditions in unicellular eukaryotes, which in mammals translates as amino acid sensing which acts in concert with other cues such as growth factors and hormones to coordinate cell growth in a multicellular context. It has been known for a long time that mTORC1 is activated by amino acids in a TSC-independent fashion (Smith et al., 2005), however, TSC antagonizes amino acid signaling to mTOR (Gao et al., 2002; Inoki et al., 2002; Tee et al., 2002). The presence of amino

acids is a necessary condition for the activation of mTORC1, even in the presence of other signals as discussed above (Hara et al., 1998). Despite its ancestral function, the mechanism for sensing intracellular amino acids remained unclear until 2008, when Kim et al., and Sancak et al., independently discovered the involvement of a family of small Ras-related GTP-binding protein (RRAGs) in amino acid dependent activation of mTORC1 (Kim et al., 2008; Sancak et al., 2008). In their activated state, promoted by amino acid sufficiency, these GTPases interact with mTORC1 and recruit it to the lysosomal surface where Rheb resides. This mechanism explains the need for both inputs (nutrients and growth factors) to fully activate mTORC1 signaling. The recent elucidation of the mechanisms of amino acid sensing is described in detail in the next section.

1.7 AMINO ACID SIGNALING TO mTORC1

In the past decade, a series of experiments led to the elucidation of an intricate network of proteins involved in amino acid sensing, starting with the discovery of Rag GTPases which are more proximal to mTORC1, followed by characterization of their positive and negative regulators and ultimately unravelling the structural basis for upstream leucine and arginine sensing.

Rags are small GTPases of the Ras superfamily, which exist as obligate heterodimers, contrasting with the majority of small GTPases, which are monomeric. In mammals, there are four Rag proteins which form obligate heterodimers: RagA or RagB dimerizes with RagC or RagD (Sekiguchi et al., 2001). They are orthologous to yeast proteins Gtr1 and Gtr2, respectively. These heterodimers seem to have a preference for opposite nucleotide loading states, such that when RagA/B is loaded with GTP, their partner RagC/D would be loaded with GDP. The nucleotide loading of RagA/B defines the activation state of the dimer (Bar-Peled et al., 2012). The active dimer, containing GTP bound RagA/B and GDP-bound RagC/D, interacts with Raptor component of mTORC1, consequently, mTORC1 translocates from cytoplasm to lysosomal surface, where it can now interact with Rheb GTPase to become active (Bar-Peled et al., 2012). Amino acids promote the GTP loading on RagA/B through an unknown mechanism (Jewell et al., 2013). Rag GTPase binds with a multisubunit complex of proteins called Ragulator (Sancak et al., 2010). The Rag-Ragulator complex pathway will be discussed in details later in the section about lysosomal regulation of mTORC1.

The activation and inactivation of GTPases rely on the bound state of GTP. GTP-bound small GTPases are active (meaning that they can recruit their effectors) while GDP-bound GTPases are inactive. Usually, the intrinsic hydrolysis of bound GTP to GDP is very slow in

small GTPases therefore they require a GTPase Activating Protein (GAP) to assist the hydrolysis of bound GTP to GDP. On the other hand, GEFs (Guanine nucleotide Exchange Factors) can remove the bound GDP and leave an empty site, promoting the binding of a GTP molecule, which is more abundant than GDP in the cytosolic environment and enters the GTPase active site by diffusion. In the case of Rags, the activated obligate heterodimer state is represented as RagA^{GTP}/RagC^{GDP} while the inactive state is RagA^{GDP}/RagC^{GTP} (where RagB might substitute for RagA, and RagD might substitute for RagC). The dimeric assembly suggests that each one of the monomers might have their own GAPs and GEFs, adding significant complexity to the system. After the discovery of Rag GTPases in amino acid sensing, an effort was initiated to find these regulatory factors, which might hold the answer to how amino acids affect the GTP loading of the Rags.

Amino acid signaling via mTORC1 pathway is regulated at both cytosolic and lysosomal level. Recent discovery of certain cytosolic proteins implicated in the regulation of mTORC1 pathway has revealed new alternative ways of manipulating the pathway for better understanding and treatment of pathologies associated to aberrations of the pathway.

1.7.1 Regulation of mTORC1 at the Lysosome by Regulator, V-ATPase and SLC38A9

Regulation of mTORC1 at lysosomal surface involves synchronization of several components. Regulator has emerged as an important attribute of the mTORC1 assembly primarily driven by amino acids signaling. Regulator is a pentameric complex of p18, MP1, p14, HBXIP and C7orf59. These proteins are also known as Lamtor 1,2,3,4 and 5 respectively. In contrast to many GTPases, Rags lack lipid-anchoring moiety, instead they rely on Regulator complex to interact with lysosomal surface. Recently, Regulator was identified as a Guanine Exchange Factor (GEF) for the Rag A/B (Bar-Peled et al., 2012). The pentameric complex received its name fittingly due to its substantial role as a scaffold protein and reported GEF activity towards Rag A and B GTPases. Activation of Rag-Regulator pathway involves two lysosomal integral membrane proteins: the v-ATPase complex and a solute carrier (SLC) named SLC38A9.

In 2011, Zoncu et al., showed that both V0 and V1 domains of v-ATPase (Forgac, 2007) interact with Regulator complex (Zoncu et al., 2011a). Along with the discovery of C7orf59-HBXIP complex as new components of Regulator complex with GEF activity, Bar Peled et al., proposed a model for v-ATPase interplay with Regulator (Bar-Peled et al., 2012). According to the proposed model, in the absence of amino acids, Rags, Regulator and v-ATPase remain tightly bound to each other and Regulator complex cannot perform its GEF activity on RagA/B.

The accumulation of luminal amino acids leads to v-ATPase dependent amino acid signaling that allows Ragulator to substitute GDP to GTP on RagA/B. The active RagA/B can now recruit mTORC1 to lysosomes from cytosol where it can interact with Rheb GTPase to become active (Bar-Peled et al., 2012) (**Figure 1.5**).

Throughout the discovery of Rag-Ragulator complex, Sabatini's group (Bar-Peled et al., 2012; Sancak et al., 2010) found peptides of SLC38A9 in the immunoprecipitation samples through mass spectrometry. Later on, SLC38A9 was studied and found to be an arginine sensor. Three independent studies demonstrated that SLC38A9 binds to arginine and interacts with Rag-Ragulator complex to activate mTORC1 (Jung et al., 2015; Rebsamen et al., 2015; Wang et al., 2015).

In 2015, Schweitzer et al., identified a novel Ragulator binding protein. c17orf59 does not bind with Rags. The overexpression of c17orf59 leads to the disruption of Rag-Ragulator complex at lysosome and loss in the mTORC1 activity. Although overexpression of c17orf59 seems to negatively regulate mTORC1 activity in a dose dependent manner, the loss of c17orf59 did not show any alteration in mTORC1 (Schweitzer et al., 2015).

1.7.2 Regulation of mTORC1 at cytosol–lysosome interface by GATOR, Sestrins and CASTOR

In 2013, Bar Peled et al. discovered a complex of three different proteins (DEPDC5, Npr12 and Npr13) which showed GAP activity towards RagA and B, and therefore the complex was named GATOR1 (GAP activity towards the Rags) (Bar-Peled et al., 2013). The hydrolysis of GTP to GDP on RagA or B would inactivate the GTPase. This inactivation of the Rag GTPase will directly reflect upon mTOR pathway as the active Rag GTPase is required to bind mTORC1 and promotes its localization at lysosomal surface. Here it is important to mention that GATOR1 acts specifically on RagA and B while the GAP for RagC and D is Folliculin-FNIP2 complex. Folliculin happens to be a tumor suppressor and surprisingly, behaves as a positive regulator of mTORC1 (Tsun et al., 2013). Previously, Leucyl t-RNA synthetase (LRS) had been reported to be involved in leucine sensing and functions as a GTPase activating protein (GAP) for RagD GTPase and not for RagA or B (Han et al., 2012). However, Tsun et al., did not reproduce the LRS GAP activity for RagD.

Another cytosolic complex called GATOR2 negatively regulates the GAP activity of GATOR1 complex. GATOR2 is composed of five proteins namely Mios, WDR24, WDR59, Sehi L, and Sec13. GATOR2 interacts with GATOR1 and inhibits its GAP activity towards RagA/B (Bar-Peled et al., 2013). The upstream leucine-sensitive regulators of GATOR2 are the Sestrins (Sesn), a family of evolutionary conserved genes involved in metabolic control. Sesn1,

2 and 3 are three members of sestrin gene family found in mammals. Numerous studies have reported the expression and activation of sestrin proteins by various stimuli such as stress, DNA damage and nutrient deprivation.

Two different groups have independently demonstrated the importance of sestrins in the regulation of GATOR2 complex. Budanov's group identified only sestrin 2 to interact with GATOR2 (Parmigiani et al., 2014) while Sabatini's group demonstrated sestrin 1 and 2 to bind GATOR2 and showed that sestrins do not affect GATOR1-GATOR2 interaction (Wolfson et al., 2016). Leucine bound sestrin cannot interact with GATOR2 thus indirectly inhibits GATOR1. Decrease in the level of cytosolic leucine would prevent sestrin bound GATOR2 to interact with GATOR1. Activated GATOR1 will be free to access and inhibit Rag GTPases. Hence, sestrin bound GATOR2 would indirectly prevent the translocation of mTORC1 from cytoplasm to lysosome (Chantranupong et al., 2014; Wolfson et al., 2016). The elucidation of this mechanism identified sestrins as the ultimate, long sought leucine sensors and opened the way for structural characterization of their interaction with leucine. Recently, the crystal structure of leucine bound sestrin has provided a solid rationale for its role as a leucine sensor in mTORC1 pathway (Saxton et al., 2016c), however, elucidation of the leucine-induced conformational changes would require the structure of apo Sestrin which is still lacking (Saxton et al., 2016b).

In a study somehow conflicting with reports from other groups, Peng et al., have demonstrated the direct interaction of sestrins with Rags. Since the sestrin protein shares homology with GDI1 (GDP dissociation inhibitor 1) protein, a regulator of Rab GTPases family members, it was hypothesized that sestrins might work as guanine dissociation inhibitors (GDIs) for Rags. The hypothesis was supported by an experiment where the mutations in the GDI motif hindered the ability of sestrins to inactivate mTORC1 activity and the sestrins regained inhibitory role by the delivery of GDI motif peptide (Peng et al., 2014).

Besides leucine, another amino acid gained a lot of importance during the discovery of various regulators of mTORC1. Various studies have shown the role of arginine in the stimulation of muscle growth, insulin secretion and immune response through activation of mTORC1. A recently identified protein named CASTOR1 (Cellular Arginine Sensor for mTORC1) has been reported to be an arginine sensor and GATOR2 interacting protein (Chantranupong et al., 2016); arginine binding to CASTOR1 is a part of cytosolic regulatory machinery for mTORC1 pathway. CASTOR1 is 63% homologous to another protein named CASTOR2 and CASTOR1/2 can form heterodimers, however, CASTOR2 does not show any affinity for arginine binding. Recently, two different groups have independently reported a

crystal structure of arginine bound CASTOR1 (Saxton et al., 2016a; Xia et al., 2016). The crystal structure of CASTOR1 has revealed that the homodimerization of the protein is essential for arginine binding. Arginine binding induces the dissociation of GATOR2 from CASTOR1 that further leads to activation of mTORC1 in a mechanism analogous to leucine sensing by sestrin (Saxton et al., 2016a; 2016c) These recent findings of GATOR1 and 2, sestrins and CASTOR1 have impressively established a structural insight into a better understanding of amino acid sensing by mTORC1 (**Figure 1.5**).

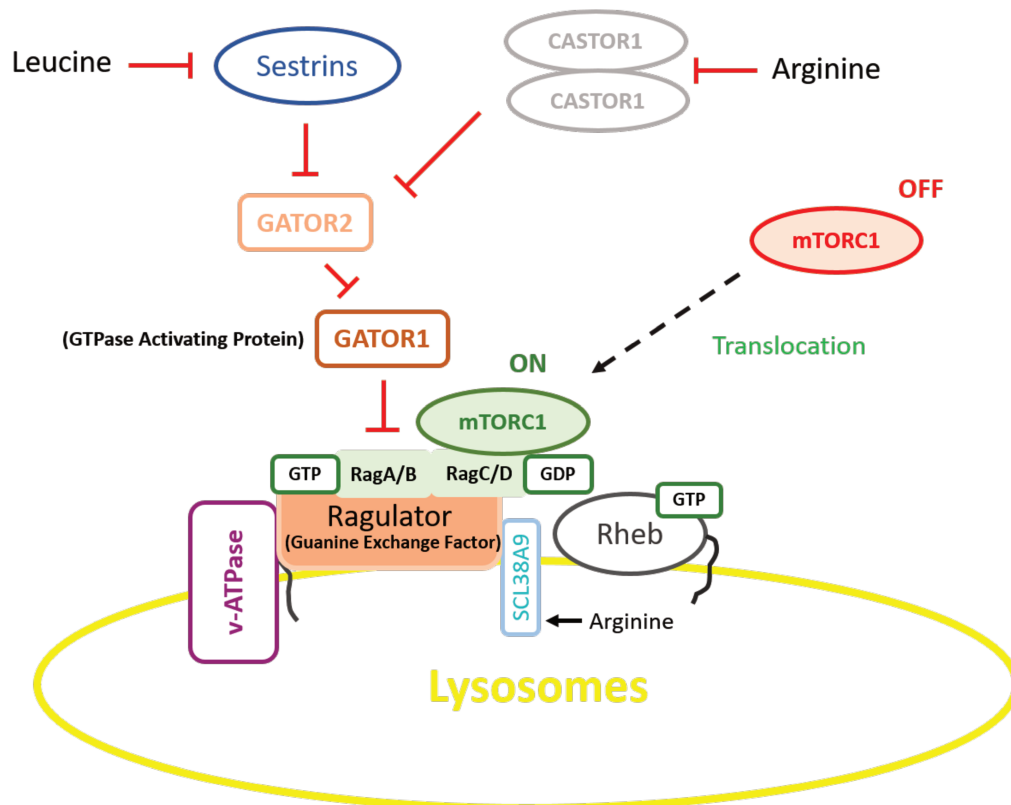


Figure 1.5. Amino acid sensitive mTOR signaling (inspired by Lim and Zoncu 2016)

1.7.3 Other proteins involved in nutrient sensing via mTORC1

David M. Sabatini (MIT-Howard University) is considered as one of the pioneers and leading names in the field of mTOR biology. Various studies led by different groups have not only been consistent but also validated the findings of his group. Here we report a few examples of published isolated data on the regulation of nutrient sensing through mTORC1 pathway. All the following mentioned studies are based on well-designed experiments published in peer-reviewed journals, however, at this point it is not clear how they connect with the mechanisms described in the previous sections.

SH3 domain-binding protein 4 (SH3BP4) was identified as a negative regulator of Rag GTPases. During amino acid starvation, SH3BP4 binds to GDP bound RagB GTPase through unknown mechanism while binding of SH3BP4 to RagC in complex with RagB GTPase depends upon the nucleotide loading state of RagB. Besides showing the direct interaction of SH3BP4 with RagB and RagC, the authors did not associate any GEF or GAP activity to SH3BP4 (Kim et al., 2012).

Duran et al., revealed an additional mechanism for the modulation of mTORC1 activation. p62 was identified as a Raptor binding protein, its binding stabilises the Raptor complex with downstream substrates. p62 plays significant role in the formation of active Rag heterodimer and is required for the Rag-mTORC1 interaction. No interactions between p62 and Ragulator complex subunits were observed, indicating that p62 forms an alternative docking site for mTORC1 activation (Duran et al., 2011).

Yan and colleagues proposed a regulatory model for mTORC1 activation via phosphorylated MAP4K3 (Ser170) in the presence of amino acids by discovering PP2A T61 epsilon as an inhibitor of MAP4K3. In amino acid starvation condition, PP2A in complex with its subunit PR61 epsilon dephosphorylates Ser170 MAP4K3 that leads to inhibition of mTORC1 activity (Yan et al., 2010).

1.7.4 Amino acid signaling through evolution

From evolutionary point of view, the Ego complex (EGOC), which resides at the vacuolar membrane, is involved in the regulation of TOR in yeast. EGOC is composed of Ego1, Ego3, Gtr1 and Gtr2. Like p18, Ego1 has a myristylation site that anchors it to the membrane and allows Ego1 to anchor Gtr1-Gtr2 (equivalent to Rag GTPase dimer) and TORC1 at the vacuolar membrane (Kogan et al., 2010). The exact function of Ego3 is still unknown but it shares structural similarity with MP1 and p14 and forms a homodimer that serves as yeast counterpart of MP1 and p14 heterodimer. There are no obvious orthologues of Ragulator in yeast, as EGOC and Ragulator complex do not share sequence similarity, but the overall homologous topology among the components is evident. Another variation in the pathways is of the GEF. Vam6 was identified as GEF for Gtr1 in yeast (Binda et al., 2009; Valbuena et al., 2012). Although mammals have a homologue for Vam6 called VPS39 (Vacuolar Protein Sorting 39), this protein does not show any GEF activity towards RagA/B; as previously mentioned Ragulator was identified as GEF for Rags which implies the divergence of the pathway in mammals in comparison to yeast (Bar-Peled et al., 2012). In contrast to GATOR1 complex in mammalian cells, SEACIT holds GAP activity towards Gtr1 and Gtr2 GTPases in

yeast. SEACIT and SEACAT are yeast orthologs of GATOR1 and GATOR2 respectively. Alike GATOR complex, SEA complex (SEAC) is also composed of eight proteins. Among these eight proteins, Iml1, Npr2, and Npr3 forms the SEACIT trimeric complex while Seh1, Sea2, Sea3, Sea4 and Sec13 forms a pentameric complex called SEACAT complex. SEACAT negatively regulates the GAP activity of SEACIT complex (Panchaud et al., 2013) (**Figure 1.6**).

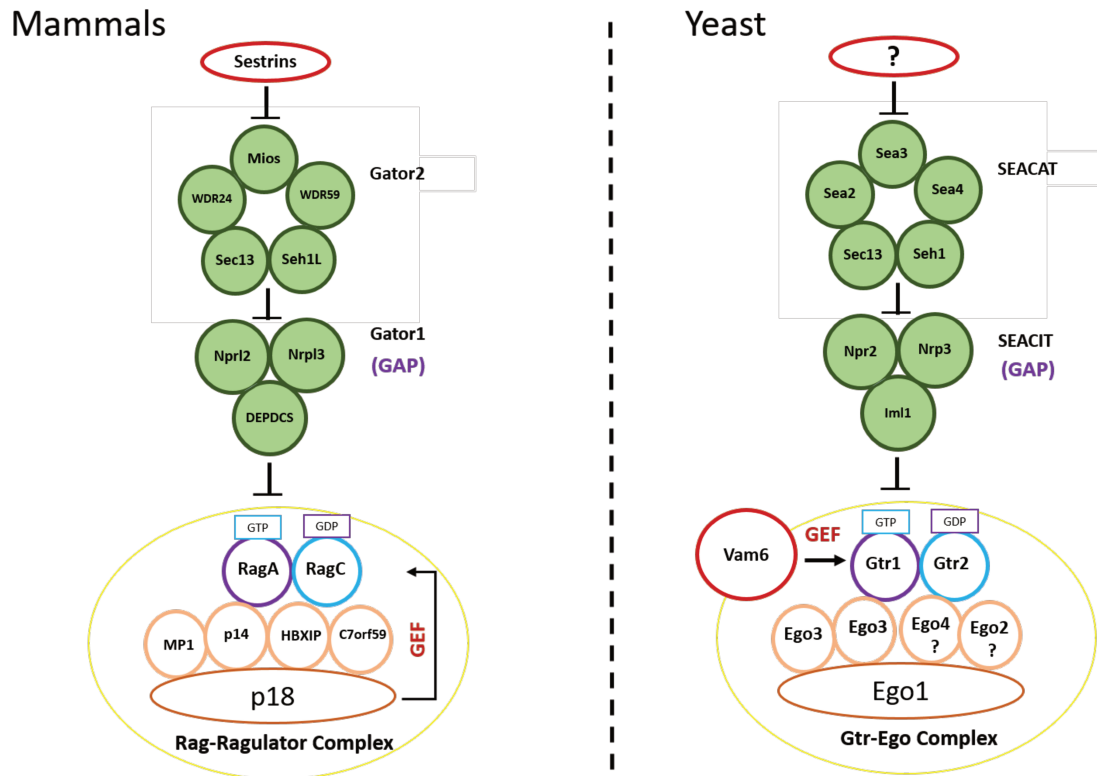


Figure 1.6. Evolutionary conservation of amino acid sensing in yeast and mammals (Inspired by Panchaud et al., 2013).

1.7.5 Structural features of Ragulator/Ego complex

Roadblock domain (RD) is closely related to longin domain (LD). LDs exhibit α - β - α topology with a 5-sheet β -meander with one helix on one side and two helices on the other side. A simple circular permutation of the last helix of an LD ($\beta\beta\alpha\beta\beta\alpha$) leads to the formation of a RD ($\alpha\beta\beta\alpha\beta\beta\alpha$) (**Figure 1.7**). From bacteria to eukaryotes, proteins with roadblock domains have been associated with small GTPases (Koonin and Aravind, 2000; Marat et al., 2011; Zhang et al., 2012). High-resolution crystal structures of MP1, p14, HBXIP and Gtr1-Gtr2 (in yeast) revealed the presence of roadblock domain in each of them (Garcia-Saez et al., 2011; Gong et al., 2011; Jeong et al., 2012; Kurzbauer et al., 2004; Lunin et al., 2004). The secondary structure prediction of C7orf59 also suggests a roadblock fold (Bar-Peled et al.,

2012). Contrary to the general observation, in addition to a GTPase domain, the four Rag GTPases also have an intrinsic RD at their C-terminal. In order to keep the GTPase domains away from the RD dimerization platform, the GTPase domains of Rags happen to conform a rotation. Perhaps, this rotational conformation of GTPase domain enables the Rags to interact with the RDs of the Ragulator complex (Gong et al., 2011; Jeong et al., 2012).

Despite the conservation of a prevalent α - β - α sandwich within the subunits of EgoC and Ragulator complex, there are few differences. The presence of a five-sheet β -meander within Ego3 homodimer makes it equivalent to the MP1-p14 heterodimer. However, the overall interface of the Ego3 homodimer differs from that of MP1-p14 heterodimer due to the presence of an unstructured loop between α 1 and β 1 on the lower side of the RDs of Ego3 homodimer (**Figure 1.8**). Two small yeast proteins namely Ycr075w-ap/Ego2 and Ynr034w-ap/Ego4 have been reported to be homologous to HBXIP and C7orf59. The structure of Ynr034w-ap exhibits an RD fold with a missing helix (α 3) just like the predicted model for C7orf59 ($\alpha\beta\beta\alpha\beta\beta$). On the other side, Ycr075w-ap lacks both the bottom surface helices ($\beta\beta\alpha\beta\beta$) (Levine et al., 2013).

Considering the reported crystal structures of MP1-p14 and HBXIP, and the predicted model of C7orf59, Ragulator complex consists of four roadblock domains, except p18, which does not contain a roadblock domain. p18 is predicted to be mostly alpha-helical with the presence of disordered regions. Biochemical characterization of p18 revealed molten globule characteristics (Magee and Cygler, 2011).

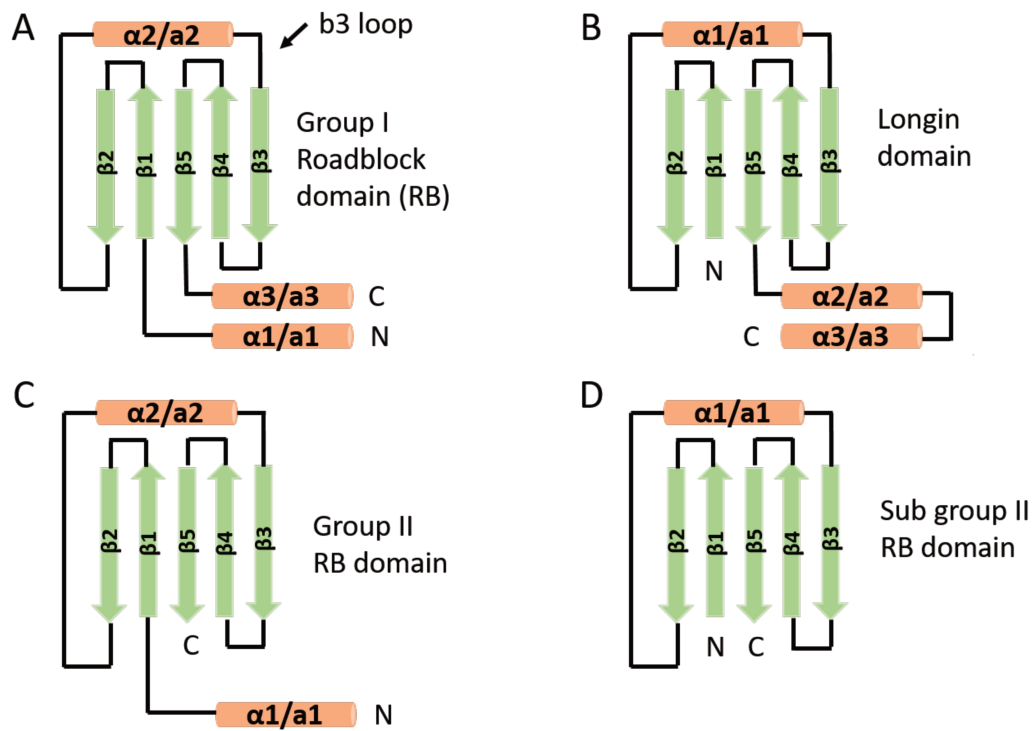


Figure 1.7. Schematic representation of different groups of roadblock fold and longin fold.

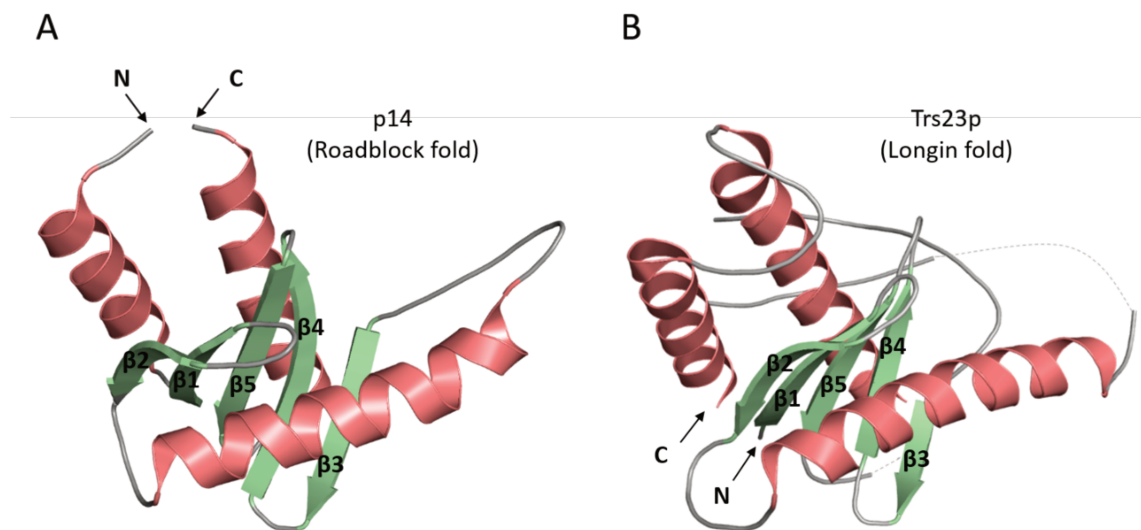


Figure 1.8 A: p14 adaptor protein, a Roadblock fold protein (PDB 1VET, chain B). **B:** yeast protein Trs23p, a Longin fold (PDB 3CUE).

1.7.6 Amino acid signaling: a target for therapeutic intervention

Besides cancer, over activation of mTOR pathway is also related to a number of other diseases. Drugs like rapamycin and mTORKis (mTOR Kinase inhibitors) are predominantly used in cancer treatment and display a wide range of cellular toxicities. In case of cancer, acute to modest toxicity spectrum can be taken into account due to the critical nature of the disease,

however in case of other pathologies such as diabetes, aging, obesity and benign tumors, mTOR pathway can be targeted through different means. Amino acid signaling holds great potential to control mTOR activity.

The term caloric restriction (CR) is a type of nutritional intervention comprised of reduced caloric intake without malnutrition. Initially, CR was thought to prevent the occurrence of chronic diseases and extend life span but studies carried on wild type mice and rhesus monkeys did not reduce cancer incidence or extend life span (Harper et al., 2006; Mattison et al., 2012), whereas mutations in the insulin-signaling pathway displayed positive effects on life span (Kenyon, 2010). Since amino acids and insulin signaling promote mTOR activity, therefore it was deduced that reduced mTOR signaling might extend life span (Evans et al., 2011; Laplante and Sabatini, 2012). Reduced mTOR activity and AMPK upregulation enhance the degradation of accumulated old cellular components through autophagy (Jiang et al., 2008). As self-explanatory, continuous replenishment with new cellular components slows down the aging process and promotes life span.

Over activation of the mTOR pathway via amino acids signaling stimulates p70-S6K dependent negative feedback activation that consequently leads to degradation of insulin receptor substrate 1 (IRS1) (Laplante and Sabatini, 2012). mTOR pathway also controls lipid synthesis by regulating the transcription factor sterol regulatory element binding protein 1c (SREBP-1c) (Peterson et al., 2011). mTORC2 positively regulates SREBP-1c by phosphorylating protein kinase C β (PKC β) which in turn activates SREBP-1c (Yamamoto et al., 2010). IRS1 degradation and SREBP-1c activation can lead to insulin resistance, which is one the major causes of Type 2 diabetes. It is a well-characterized observation that mTORC1 is also activated by insulin. In a review paper, Yoon and Choi explained the possible reason of constitutive hyperactivation of mTORC1 in insulin resistance (Yoon and Choi, 2016). Clinical studies have reported high circulating levels of branched chain amino acids (BCAAs) in type 2 diabetes and insulin-resistant obesity cases (Lackey et al., 2013; Olson et al., 2014). BCAAs include leucine, isoleucine and valine. These amino acids along with arginine and glutamine have been reported in the regulation of mTOR activity. Importance of leucine and arginine in the cytosolic regulation of mTOR has been discussed in details in section 1.7.2. A rat model with high blood levels of amino acids with sustained mTOR activity that led to insulin desensitization presents a strong case to target components of amino acid signaling for the treatment of type 2 diabetes (Newgard et al., 2009) (also reviewed by Choi and Yoon 2016).

Genetic diseases characterised by benign tumors including Tuberous sclerosis complex syndrome (TSCS), Cowden syndrome (CS) (Liaw et al., 1997) and Peutz-Jeghers syndrome

(PJS) are collectively termed as Hamartoma syndromes. Hamartoma syndromes are distinguished on the type of mutation originating the syndrome. Patients suffering from Hamartoma syndromes may grow benign tumors in vital organs of body such as brain, lungs, kidneys, skin and heart. Loss of function mutations in TSC1/TSC2 leads to hyperactivated mTOR pathway. In Cowden syndrome patients, continuous accumulation of active PIP3 due to the loss of PTEN phosphatase sustains active Akt feedback loop that keeps mTOR in hyperactive state. PJS is caused by the loss of LKB1 that prevents AMPK formation and keeps mTOR active even during oxidative stress (Inoki et al., 2005).

The importance of amino acid signaling axis in the regulation of mTOR pathway is evident in the above-described pathological conditions. For example, due to the mutations in TSC1/TSC2 (GAP for Rheb GTPase) in TSC syndrome, Rheb remains in active state that brings the other components of amino acid pathway machinery such as GATOR1/2, Rag GTPases, v-ATPase and Ragulator complex into spotlight as therapeutically important targets. It would be interesting to see how amino acid pathway can be selectively targeted for the treatment of various metabolic and physiological diseases. Recently, the discovery of regulatory mechanism for GATOR2 by leucine bound sestrins have made the amino acid signaling machinery more intriguing. It would be interesting to explore the assembly and stability of the Ragulator complex through potential positive and negative regulators. Hence, amino acid signaling offers numerous opportunities for therapeutic intervention.

2. Justification

Over the last few years, the gained structural insight into various components of mTORC1 signaling has paved the way to get better understanding of the regulation of the pathway. In this thesis, we present the structural and functional characterization of subunits of Ragulator complex. The present study was idealized in 2012 through a personal communication with David Sabatini, when the landmark paper by Bar-Peled et al was yet to be published. The unpublished discovery that Ragulator was actually a pentamer instead of trimer, and this pentameric assembly acted as a GEF for RagA/B, explained the failure of previous efforts of our group to produce a trimeric Ragulator for structural studies. Sabatini's group shared their expression construct for the newly discovered HBXIP-C7orf59 dimer and in 2013 this project was initiated as an effort to solve the structure of this dimer and gain insight into the assembly of pentameric Ragulator as a way to understand the structural basis of amino acid sensing, and maybe to allow future therapeutic interventions for cancer or other diseases.

We have employed various techniques such as protein crystallography, small angle X-ray scattering (SAXS), cross-linking coupled to mass spectrometry (XL-MS), hydrogen-deuterium exchange (HDX)/MS, mutagenesis and pulldown assays to elucidate the architectural complexity of Ragulator complex. In addition to structural characterization, functional studies using PKA modulators in cell culture have opened an exciting opportunity for future studies to unveil the possible cross talk between mTORC1 pathway and PKA.

Chapter 2

Crystal structure of C7orf59-HBXIP and insights into Ragulator assembly*

Nadia Rasheed¹, Tatiani B. Lima^{1,2}, Andrey F. Z. Nascimento³, Ana Luiza Savioli Silva¹, Marcel Nakahira², Germanna Lima Righetto¹, Liron Bar-Peled⁴⁻⁸, Kuang Shen⁴⁻⁸, David M. Sabatini⁴⁻⁸ Fabio C. Gozzo², Ricardo Aparicio², Juliana H. C. Smetana¹

1- Brazilian Biosciences National Laboratory (LNBio), Brazilian Center for Research in Energy and Materials (CNPEM), Zip Code 13083-970, Campinas, Sao Paulo, Brazil.

2- Institute of Chemistry, University of Campinas, Campinas, São Paulo 13083-970, Brazil.

3- Brazilian Synchrotron Light Laboratory (LNLS), Brazilian Center for Research in Energy and Materials (CNPEM), Zip Code 13083-970, Campinas, Sao Paulo, Brazil.

4- Department of Biology, Massachusetts Institute of Technology, Cambridge, Massachusetts 02139, USA.

5- Whitehead Institute for Biomedical Research, 9 Cambridge Center, Cambridge, Massachusetts 02142, USA.

6- Howard Hughes Medical Institute, Cambridge, Massachusetts 02139, USA.

7- Koch Institute for Integrative Cancer Research, 77 Massachusetts Avenue, Cambridge, Massachusetts 02139, USA.

8- Broad Institute of Harvard and Massachusetts Institute of Technology, 415 Main Street, Cambridge, Massachusetts 02142, USA.

Correspondence and requests for materials should be addressed to J.H.C.S (e-mail juliana.smetana@lnbio.cnpem.br)

* Submitted to Structure

SUMMARY

The Ragulator is a pentamer composed of MP1, p14, p18, C7orf59 and HBXIP, which acts as a lysosomal scaffold and GEF of the Rag GTPases in the amino acid sensitive branch of mTORC1 signaling. MP1, p14 and HBXIP are known to fold as Roadblock domains while C7orf59, the dimerization partner of HBXIP, is a poorly characterized protein predicted to display this same fold. Here we present the crystal structure of HBXIP-C7orf59 dimer at 2.9Å and explore its interaction with p18. The structure of the dimer revealed two Roadblock

domains associating to form an interface similar to MP1-p14, with the unexpected feature of an unfolded N-terminus in C7orf59 suggesting a closer connection to the yeast protein Ego2. We used a combination of cross-linking/mass spectrometry, site-directed mutagenesis/pulldown and spontaneous proteolysis to explore the HBXIP-C7orf59 interface with p18 in vitro and found a potential PKA phosphorylation site near this interface. PKA activation with Forskolin induced dissociation of the Ragulator complex, and the PKA inhibitor H-89 increased p18 binding to C7orf59. Our results confirm the essential role of HBXIP-C7orf59 dimer as an integral part of pentameric Ragulator and highlight potential evolutionary connections of the Roadblock fold, while shedding light on the elusive PKA-mTORC1 connection.

INTRODUCTION

In order to survive in nutrient insufficient/deprived conditions, eukaryotic organisms have a signaling pathway controlled by the protein kinase mTOR. The mammalian target of rapamycin (mTOR) is a serine/threonine protein kinase that belongs to phosphatidylinositol 3-kinase-related kinase protein family and is also known as mechanistic target of rapamycin or FK506 binding protein 12-rapamycin associated protein 1 (FRAP1) (Brown et al., 1994; Sabatini et al., 1994). mTOR signaling regulates growth, proliferation, motility, protein synthesis and transcription. Deregulation of mTOR can be observed in cancer, type 2 diabetes, obesity and various neurodegenerative diseases (Efeyan et al., 2012; Guertin and Sabatini, 2005; Laplante and Sabatini, 2012).

Kim et al and Sancak et al (Kim et al., 2008; Sancak et al., 2008) independently discovered the involvement of Rag GTPases in amino acid dependent activation of mTORC1. In mammals, four Rag proteins form obligate heterodimers; RagA or RagB dimerizes with RagC or RagD. Amino acids promote the GTP loading on RagA/B (Jewell et al., 2013). The GTP bound RagA/B dimer induces the translocation of mTORC1 from cytoplasm to lysosomal surface and Rag GTPase binds with a multisubunit complex called Ragulator (Sancak et al., 2010). Ragulator has emerged as an important regulator of the mTORC1 branch primarily driven by amino acids signaling. In contrast to many GTPases, Rags lack a lipid-anchoring moiety; instead, they rely on Ragulator complex to interact with lysosomal surface.

The Ragulator complex was originally identified as a trimer composed of the MP1-p14 dimer with p18, a lysosome-associated adaptor protein (Sancak et al., 2010). Shortly after, two additional subunits were identified as an integral part of the Ragulator which was found to act as a GEF for RagB only in the presence of all five subunits (Bar-Peled et al., 2012). These additional subunits are HBXIP, an antiapoptotic protein previously known to interact with the HBx protein of the Hepatitis B virus and inhibit viral replication (Marusawa et al., 2003; Melegari et al., 1998) and the uncharacterized C7orf59 protein.

The yeast counterpart of mammalian Ragulator is the Ego complex. Although the Ego complex shares functional and structural features with mammalian Ragulator such as vacuolar localization (functionally equivalent to lysosomal localization), interaction with the Rag orthologues Gtr1/Gtr2 and regulation of amino-acid sensing in the conserved TOR pathway, the evolutionary and structural relationships between Ragulator and Ego subunits are less than clear. The MP1-p14 heterodimer is related to a homodimeric Ego3 protein, while p18 shares structural features with Ego1. The putative yeast counterparts of HBXIP and C7orf59 are Ego2/Ycr075w-a and Ego4/Ynr034w-a (Levine et al., 2013). Ego2, but not Ego4, was shown

to be an essential part of the EgoTC complex by interacting directly with Ego1 and Ego3 forming a ternary complex (Ego-TC) which is required for the vacuolar localization of Gtr1/2 and TORC1 activation (Powis et al., 2015). Ego4 interacts genetically and physically with Gtr2 but the significance of this finding is yet to be determined (Powis et al., 2015).

A striking structural feature of both Ragulator/Rag and Ego/Gtr complexes is the presence of several Roadblock domains (RB), an ancient protein fold which functions as a protein interaction module. RB domains frequently interact to form either homo or heterodimers that function as platforms to anchor and regulate signaling proteins such as GTPases. Structurally, the RB domain consist of α - β - α sandwiches of approximately 100–120 amino acid residues in which a 5-sheet β -meander is flanked by one α -helix on one side (α_2) and two helices on the other side (α_1 and α_3). Several RB proteins lack the C-terminal α_3 helix, and this variation defines a subclass of Group II Roadblock domains (Powis et al., 2015). Less frequently, the N-terminal helix α_1 might be missing as well, for example in Ego2. The missing helices of these incomplete RBs can in some cases be replaced by α -helices from their interaction partners. The MP1-p14 heterodimer and the yeast Ego3 homodimers belong to Group I as they display all three helices characteristic of this fold, while HBXIP, C7orf59, Ego2 and Ego4 belong to Group II.

To gain further insight into the structure and function of the Ragulator complex, we have solved the crystal structure of the human complex of HBXIP and C7orf59 and explored its interaction with p18 by combining different biochemical techniques. We have also uncovered a potentially novel mechanism of PKA-mediated disassembly of the Ragulator complex, which might help to elucidate the unclear PKA-mTOR relationship.

RESULTS

Structure and dynamics of the XPOF dimer

We expressed and purified the HBXIP-C7orf59 dimer (called XPOF for simplicity – hbXiP/ c7OrF59) in *E. coli* from a bicistronic plasmid, recovering stoichiometric amounts of both proteins. Since only C7orf59 was expressed with an N-terminal hexahistidine tag, the copurification of untagged HBXIP indicated the formation of a stable dimer. HBXIP exists as a long isoform of 173 residues and a short isoform of 93 residues, both of which interacted with C7orf59 (**Figure 1A, B**). We chose the short isoform for structural characterization because the recombinant HBXIP-long was susceptible to proteolytic degradation.

The XPOF dimer crystallized in space group C2 with four dimers in the asymmetric unit (**Table 1**). The structure was deposited under PDB i.d. 5VOK. The crystals were small, plate-like and diffracted up to 2.95 Å. Residues 2 – 86 of C7orf59 and 2 – 90 of HBXIP are present in the electron density. The overall structure and dimer interface of XPOF are similar to the MP1-p14 dimer (Kurzbaue et al., 2004; Lunin et al., 2004a) and the C-terminal domains of Gtr1-Gtr2 (Gong et al., 2011; Jeong et al., 2012), except for the absence of a C-terminal helix which results in an exposed beta-sheet surface and a boat-like shape for C7orf59-HBXIP as compared to the prolate ellipsoid shape of MP1-p14, and the presence of an unfolded N-terminal region in C7orf59 corresponding to the N-terminal α -helix in HBXIP and other Roadblock proteins (**Figure 1C**). This unfolded segment (residues 1 - 15) displays an extended conformation, which is well defined in the electron density due to crystal packing. In the crystal, the N-terminal region of C7orf59 is stabilized by interactions with the exposed side of the beta-sheet in an adjacent XPOF dimer (**Supplementary Figure 1A**), which suggests a protein-binding potential for this surface. **Figure 1D** shows a superposition of the structures of C7orf59 and HBXIP. Despite their lack of sequence similarity, both proteins share a common fold except for the unfolded N-terminus of C7orf59. Another difference between the two proteins resides in the conformation of loop *b3*. The structure of HBXIP in the heterodimer was superimposed on the previously reported HBXIP structure (Garcia-Saez et al., 2011), with rmsd = 0.592, indicating that it does not undergo major conformational changes upon binding to C7orf59 (**Supplementary Figure 1B**).

The dimer interface buries an area of 910 Å² (13.4% of total surface area of C7orf59 and 16.1% of HBXIP) and is stabilized by hydrophobic contacts involving the α -helices *b – b**, hydrogen bonding involving main chain of strands $\beta3 – \beta3^*$ in each monomer, and contacts mediated by side chains in the loops connecting helix *b* and sheet 3 in each monomer (loop *b3*). The aliphatic side chains in the two-helix bundle formed by helix *b-b**, including Leu48,

Leu55, Ala40*, Ile43* and Val47*, engage in zipper-like hydrophobic interactions as reported previously for HBXIP homodimeric structure (Garcia-Saez et al., 2011) and MP1-p14 dimer (Kurzbaauer et al., 2004). The structural elements are named according to Kurzbaauer et al (Kurzbaauer et al., 2004) and asterisks indicate structural elements or residues from C7orf59 (**Figure 1E**).

A ConSurf analysis (**Supplementary Figure 2** and **Figure 2A**) indicated that the overall sequence conservation is low for both subunits, further confirming the notion that structural conservation goes well beyond sequence conservation in the Ragulator and Ego complexes. Both C7orf59 and HBXIP are highly hydrophobic, indicating that besides the heterodimer interface, most of their surfaces might be involved in protein-protein interactions with other Ragulator subunits (**Figure 2A**).

A closer inspection of the interface reveals that *b3** loop – *2b* pocket interaction appears to play a bigger role in stabilizing the dimer than the reciprocal *b3* loop – *2b** pocket. C7orf59 loop *b3** bends towards HBXIP accommodating its hydrophobic side chains (Cys51*, Phe53*, the aliphatic part of Arg54*, and Leu55*) in the *2b* pocket of HBXIP, in a way analogous to the interaction of MP1 loop *b3** with the *2b* pocket in p14 (Kurzbaauer et al., 2004) (**Figure 2B**). The edges of this pocket *2b* in HBXIP are lined by residues His41 and His87, which are well defined in the electron density, and Asn71 which is less defined. The *b3**–*2b* interface is mostly hydrophobic, however, it seems that it might be stabilized by a hydrogen bond between residues Arg54* in C7orf59 loop and Asn71 in HBXIP pocket due to the proximity of the side chains. The electron density of Phe53* side chain points to the dimer interface rather than the solvent.

Although the conformation of HBXIP *b3* loop indicates a less prevalent role of the *b3* loop – *2b** pocket interface in stabilizing the heterodimer, the striking sequence conservation of some residues close to C7orf59 *2b** pocket led us to probe this interface by site-directed mutagenesis. None of the side chains in HBXIP loop *b3* makes contacts with C7orf59, except for Leu55 which is actually part of helix *b*. Some of the most highly conserved residues of C7orf59 belong to loop *2b** (residues 31–36), which lines the *2b* pocket. However, mutation of either Glu34/Asn35 or Asp36/Glu37 to alanine did not affect the dimer integrity or p18 binding in an in vitro pulldown assay using recombinant proteins. Close to this loop lies the conserved Ser67*, located in the N-terminus of strand β 4*, which is a potential phosphorylation site according to KinasePhos 2.0 (Wong et al., 2007) and NetPhosK predictions. The close proximity of two negatively charged residues from HBXIP loop *b3* (Asp58 and Asp61) suggested that phosphorylation of Ser67* might result in electrostatic repulsion and dissociation

of the heterodimer. Ser67* was mutated to aspartate to test this hypothesis. Although this mutation did not affect stability of the heterodimer, it severely diminished the dimer's association with p18 (**Figure 2D**).

The structural relationships of HBXIP-C7orf59 and their putative yeast orthologues Ego2 and Ego4 are shown in **Figure 3**. The lack of both $\alpha 1$ and $\alpha 3$ in the structure of C7orf59 suggests that it is closely related to Ego2. While HBXIP appears to be more closely related to Ego4 due to the presence of $\alpha 1$ and lack of $\alpha 3$, the orientation of $\alpha 1$ is strikingly different in these two proteins. This feature, in combination with the fact that Ego4 does not behave as a bona fide Ego complex subunit (Powis et al., 2015), sheds doubt on whether HBXIP and Ego4 might be functionally related.

The purified XPOF dimer was analysed by hydrogen/deuterium exchange (HDX-MS) to evaluate its conformational dynamics and support crystallographic data (**Figure 4** and **Supplementary Figure 4**). In the C7orf59 structure, the regions showing highest relative deuterium incorporation were the unfolded N-terminus, sheets $\beta 2$ and $\beta 5$ and the N-terminal side of helix b^* . These regions displayed up to 50% deuterium incorporation after 2 hours. For HBXIP, the overall deuterium incorporation was lower, indicating a rigid fold. The only region where incorporation rates reached 50% in HBXIP was the C-terminal side of helix b , which is adjacent to the N-terminus of the corresponding helix in C7orf59 which also displayed high deuterium incorporation. The $b3^*$ loop displayed low deuterium incorporation, consistent with its tight interaction with the $2b$ pocket. These results confirm the unfolded nature of the C7orf59 N-terminus and highlight additional regions with high conformational flexibility in the dimer, which might be involved in interactions with other Regulator subunits.

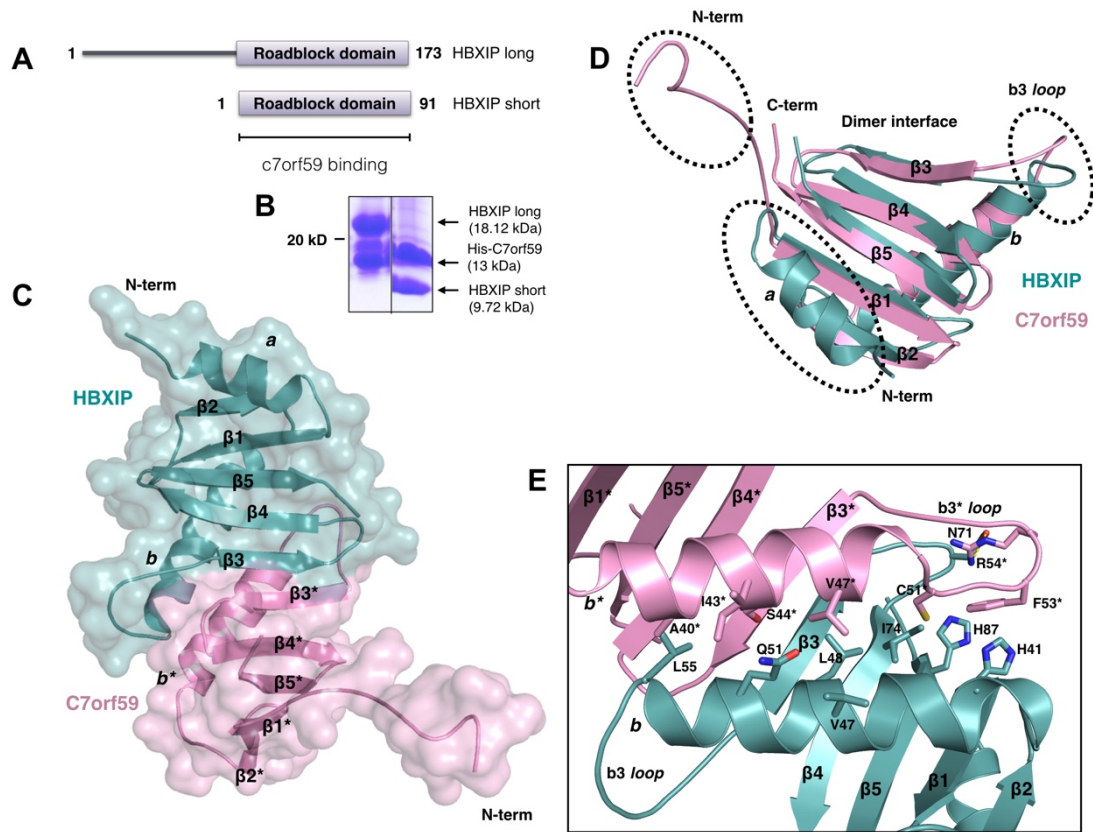


Figure 1. Structure of the HBXIP-C7orf59 dimer. **A:** The primary structure of HBXIP isoforms long and short, highlighting the Roadblock domain. **B:** Both isoforms of HBXIP copurify with C7orf59. Recombinant histidine-tagged C7orf59 was coexpressed with HBXIP long or HBXIP short and the dimers were isolated by affinity chromatography. **C:** Cartoon/space filling representation of the structure of HBXIP-C7orf59 dimer. **D:** Superposition of C7orf59 (pink) and HBXIP (cyan) highlighting the differences in conformation of loop *b3* and the N-terminus. **E:** Close up of the dimer interface.

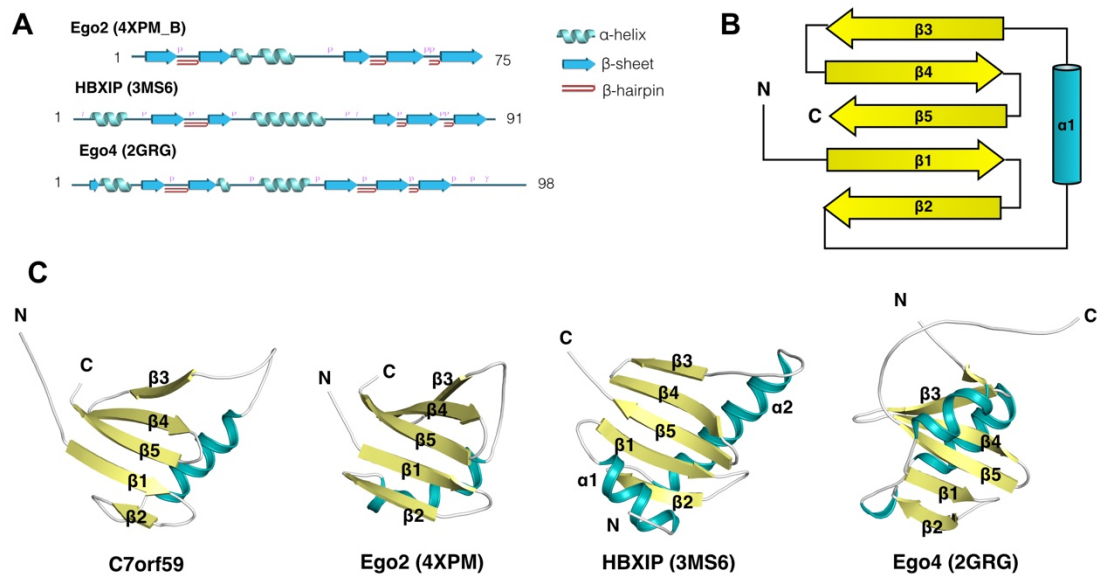


Figure 3. Structural relationships of group I Roadblock folds. **A:** PDBsum diagrams of secondary structure of human HBXIP (PDB 3MS6), yeast Ego2 (PDB 4XPM, chain B) and yeast Ego4 (PDB 2GRG). **B:** Topology of the C7orf59 roadblock fold. **C:** Structural comparison of human C7orf59/HBXIP and yeast Ego2/Ego4. Secondary structure elements are coloured as follows: beta-sheets in pale yellow, alpha helices in teal, loops in white. The structures are shown in the same orientation.

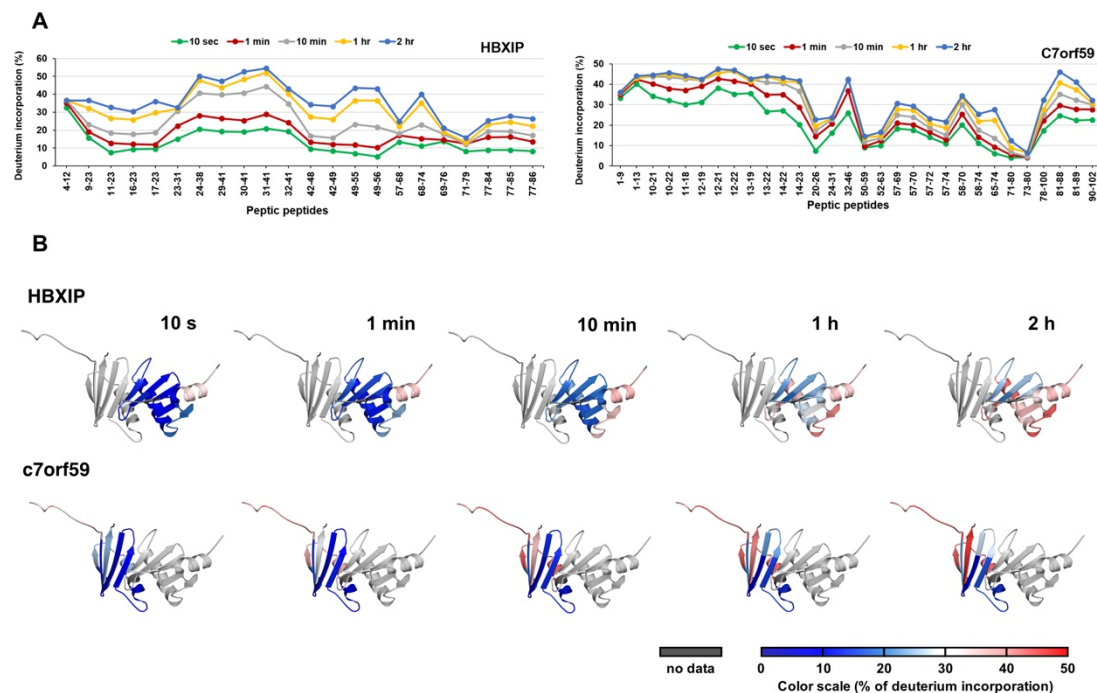


Figure 4. Dynamics of the HBXIP-C7orf59 dimer in solution. **(A)** HDX plot displaying the percentage of deuterium incorporation for each of the peptic peptides identified in HBXIP (left) and C7orf59 (right). **(B)** Structural representation of the relative deuterium incorporation of C7orf59 and HBXIP. Relative deuterium exchange (%) is represented from blue to red as indicated in the scale below.

Purification of a XPOF-p18 complex

To obtain a XPOF-p18 complex, the XPOF dimer was coexpressed in *E. coli* with an N-terminally truncated p18 construct (p18 Δ N, residues 8–161) in fusion with an N-terminal GST tag. When GST-p18 Δ N was expressed alone in *E. coli* and purified from the soluble fraction by GST-pulldown, a major band of 35 kD was detected indicating proteolytic degradation. Coexpression of the same GST-p18 Δ N construct with HBXIP-C7orf59 followed by Talon-pulldown yielded a 44 kD band, compatible with the predicted molecular weight of the GST-p18 Δ N fusion protein (**Figure 5A**), showing that recombinant XPOF dimer interacts with GST-p18 Δ N and prevents its degradation. Under the same conditions, MP1-p14 failed to form a stable complex with p18 (not shown), confirming that the XPOF dimer is a fundamental piece of the Ragulator complex which cannot be replaced by MP1-p14.

The affinity-purified trimeric complex was further purified by size exclusion chromatography in attempts to obtain a sample suitable for structural characterization. However, in spite of extensive efforts to stabilize the complex, the size exclusion elution profile invariably resulted in three peaks originating from spontaneous degradation of GST-p18 Δ N and

dissociation of XPOF dimer from the complex. SDS-PAGE analysis showed that the first peak corresponded mostly to intact XPOF/GST-p18 Δ N complex, although contaminated with a p18 degradation product, followed by a second peak characterized by further degradation of p18 and full dissociation of XPOF, and a third peak of XPOF dimer alone (**Figure 5B**). The apparent molecular weight of the p18 degradation intermediate indicates that it contains GST in fusion with the N-terminal half of p18, indicating that it dissociates from XPOF upon loss of its C-terminal half. LC/MS analysis on Synapt G1 HDMS after trypsinization of samples from similar preparation as shown in **Figure 5B** detected nontryptic peptides $_{105}$ LPPLPSLTSQPH $_{116}$ and $_{120}$ ASEPIPFSDLQQVSR $_{134}$, derived from the C-terminal half of p18 sequence as expected (**Figure 5C**). Both HBXIP and C7orf59 were identified in the same samples with high sequence coverage, thus validating the analysis (not shown).

To confirm the size exclusion and SDS-PAGE analysis, representative fractions from the first and third peaks of size exclusion were analysed by small-angle X-ray scattering (SAXS). The first peak showed signs of aggregation which prevented further analysis. For the third peak, the linear Guinier region of the scattering curve indicated that this sample was monodisperse, and allowed us to calculate radius of gyration (R_g), maximum distance (D_{max}) and molecular weight (MW). SAXS parameters calculated for the third peak (R_g : 2.29 nm, D_{max} : 7.83 nm, MW: 29.1 kDa) supported the idea that this peak corresponds mostly to XPOF dimer dissociated from GST-p18 Δ N (**Figure 5C**). A model was built from this curve and fitted to the crystallographic model, supporting the existence of the XPOF dimer in solution (**Supplementary Figure 4**).

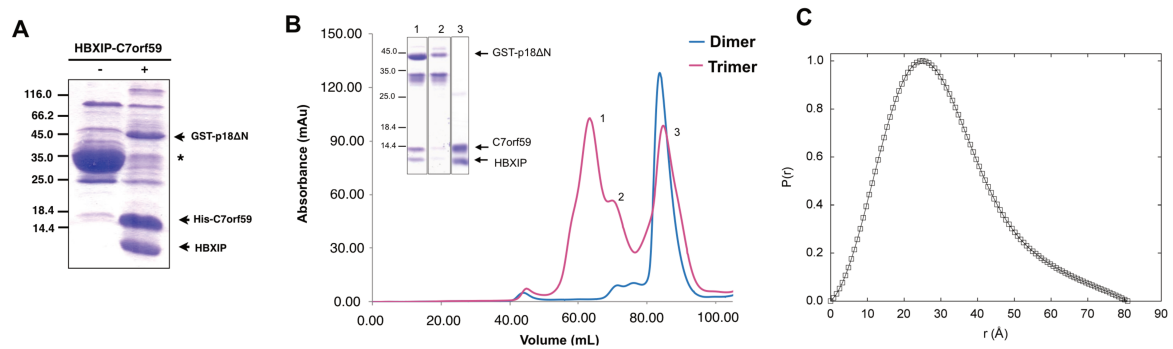


Figure 5. Spontaneous proteolysis and dissociation of the GSTp-18/XPOF complex **A:** Affinity-purified GST-p18ΔN migrates as a ~35 kD band on SDS-PAGE (indicated with an asterisk), while its complex with HBXIP-C7orf59 results in a band of ~44 kD indicating that GST-p18ΔN is protected from degradation in the presence of HBXIP-C7orf59. The sample shown in the first lane was purified using glutathione-sepharose beads and the second using Talon beads. **B:** Size exclusion elution profiles of the HBXIP-C7orf59 dimer (blue) and the dissociation products of the GST-p18ΔN + HBXIP-C7orf59 complex (magenta) on a Superdex 200 16/60 column. Inset: Coomassie stained SDS-PAGE analysis of representative fractions from the three peaks obtained from dissociation of the GST-p18ΔN + HBXIP-C7orf59 complex. **C:** Pair-distance distribution function of HBXIP-C7orf59 dimer bound to p18-derived fragments (peak 3 in panel b). The dimer used in SAXS analysis was His-tagged.

Different regions of p18 are required to bind XPOF and MP1-p14 dimers

The degradation and dissociation pattern of XPOF/GST-p18ΔN complex described above indicated that the C-terminal half of p18 was responsible for stable binding to XPOF. We then used a combined approach of cross-linking/mass spectrometry (XL/MS) and stop codon scanning to further explore this possibility.

Intact XPOF/GST-p18ΔN complex from the first peak of size exclusion shown in Figure 5B was analysed by cross-linking/mass spectrometry (XL/MS) using dysuccinyl suberate (DSS) as a probe. Lys60 of p18 was found cross-linked both to Lys64* and Lys88* of C7orf59 (**Figure 6A**). The same p18 residue was also detected in intramolecular cross-links with residues Lys20 and Lys103. The crosslinked peptides are shown in **Table 2**. The two C7orf59 residues found in p18-C7orf59 crosslink with Lys60 are structurally close to Ser67*, which we showed to be critical for p18 binding (**Figure 6B**). Lys60 is located in a highly conserved region of p18 which is predicted to adopt α -helical conformation.

To confirm our findings, stop codons were inserted by site-directed mutagenesis at positions 31, 35, 60, 74, 80, 103, 108, 130 and 149 of the GST-p18ΔN sequence (**Figure 6A**). These mutants were expressed in *E. coli* and Talon-pulldowns were performed with

coexpressed XPOF or MP1-p14 dimer. As a control, we performed GST-pulldowns of each construct expressed alone to verify the effects of these mutations on the expression levels and stability of GST- p18 Δ N (**Figure 6C**).

Both full length and 149_stop mutant of p18 interacted strongly with HBXIP-C7orf59 dimer, while all the other mutations substantially decreased this interaction. This indicates that the C-terminus of p18 (residues 130–149) is both required to interact with HBXIP-C7orf59 and is also stabilized by this interaction, since full length p18 is only detected in the presence of XPOF (**Figure 5A**). This region defined by stop codon scanning overlaps with the peptide 120 ASEPIPFSDLQQVSR $_{134}$, which coeluted with XPOF in size exclusion, indicating that residues 130–134 (QQVSR) might be particularly important for stable interaction with XPOF.

Surprisingly, deletion of residues 130–161 of p18 strongly favoured the interaction with MP1-p14, which was essentially undetectable both for full length p18 and 149_stop mutant (**Figure 6C**). This interaction was enhanced even further by deletion of residues 103–161 and 108–161 of p18, which correlates with the intrinsic stabilizing potential of these truncations, observed when GST-p18 and its deletion mutants were expressed alone (**Figure 6C**, lower panel).

All the p18 C-terminal deletion constructs smaller than 80 residues display very weak binding to MP1-p14 or XPOF, detectable only by Western blot (not shown), suggesting that the conserved p18 region surrounding Lys60 ($_{58}$ LAKTA $_{62}$) which was shown by XL-MS to interact with C7orf59 is not sufficient to stabilize the complex. We then used an alternative approach to confirm the importance of this region in the interaction with XPOF, by mutating all its polar residues to alanine (p18 mutant LAKTA–AAAAA). Although this mutation alone did not interfere in complex formation, an intriguing genetic interaction with the S67D mutant was observed, whereby the mutation was able to rescue p18 binding to Ser67* mutated XPOF (**Figure 6D**).

Taken together, these results indicate that multiple regions of p18 cooperate to assemble the pentameric Ragulator complex. The interaction with XPOF stabilizes recombinant p18 against proteolytic degradation, while the interaction with MP1-p14, instead, requires previous stabilization of p18, which can be achieved in vitro by deleting its C-terminus. In the cell, it is likely that the interaction with HBXIP-C7orf59 is a previous requirement to stabilize p18 in the right conformation to promote subsequent binding of MP1-p14.

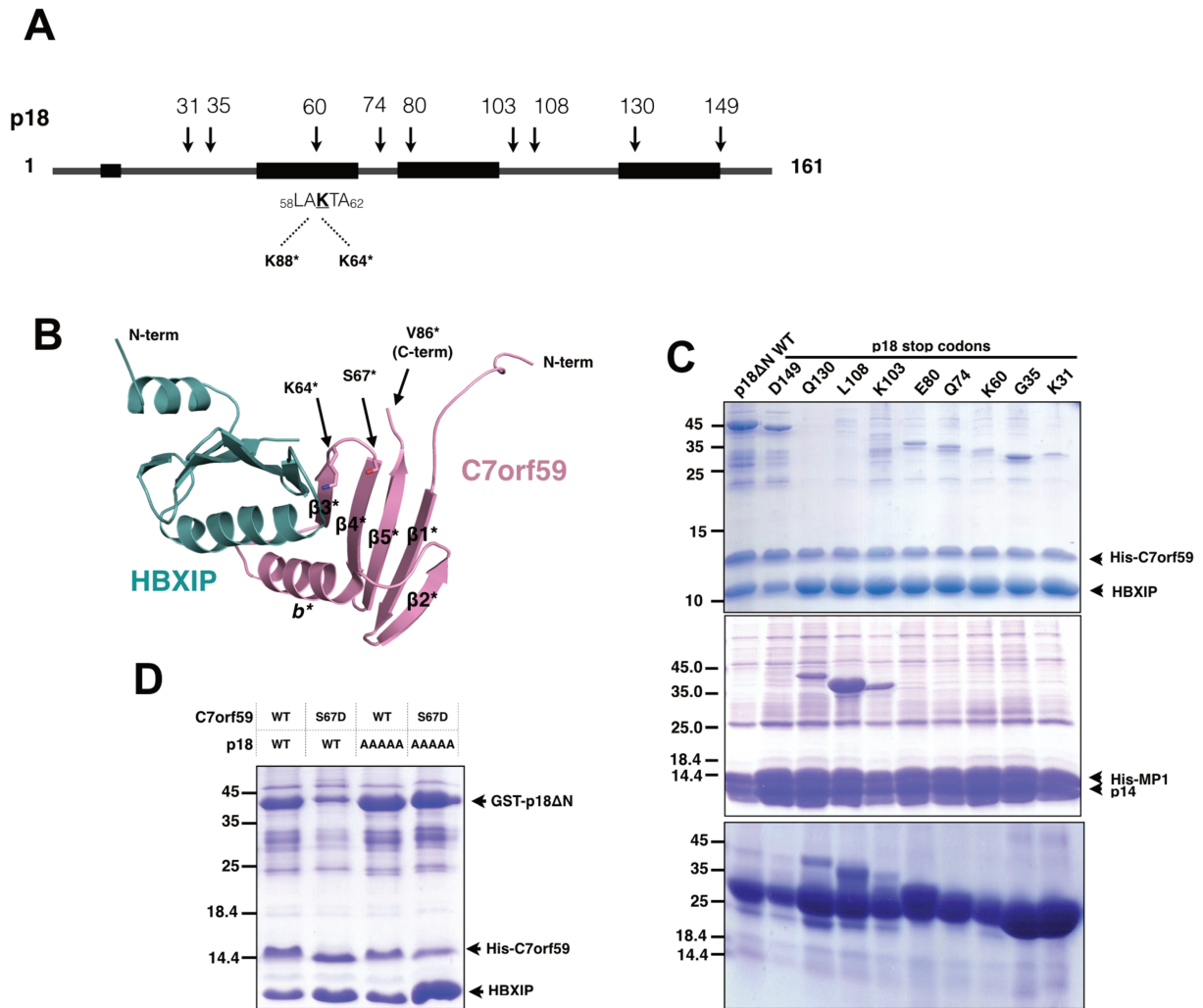


Figure 6. Distinct regions of p18 are responsible for interaction with HBXIP-C7orf59 and MP1-p14 dimers. **A:** Schematic representation of the p18 secondary structure, the identified crosslinks with C7orf59 and the constructs used in the stop codon scanning (arrows). The numbers indicate the positions of stop codon insertion by site-directed mutagenesis, and rectangles indicate the positions of predicted α -helices in p18 structure. **B:** Structure of the XPOF dimer highlighting the positions of residues Lys64*, Ser67* and Val86* (since Lys88 is not visible in the electron density, the closest residue is shown). **C:** Stop codon scanning of p18 sequence dissects its binding to the Ragulator subcomplexes HBXIP-C7orf59 and MP1-p14. Stop codons were inserted in GST-p18 Δ N sequence in the indicated positions by site-directed mutagenesis and the resulting constructs were coexpressed either with HBXIP-C7orf59 (upper panel) or MP1-p14 (middle panel) followed by Talon pull-down. The GST-p18 Δ N stop codon constructs were expressed and isolated by GST-pull-down to analyse the effects of C-terminal truncations on p18 degradation (lower panel). **D:** The p18 LAKTA-AAAAA mutation rescues its interaction with the S67D mutant of C7orf59.

PKA activation induces dissociation of the Ragulator complex

C7orf59 is an uncharacterized protein for which little information is available except for its role as a subunit of the Ragulator complex (Bar-Peled et al., 2012). To gain further insights into the regulation of *C7orf59*, we explored the role of the potential Ser67* phosphorylation site of *C7orf59* in regulating its interactions in cell culture. Sequence analysis with KinasePhos 2.0 (Wong et al., 2007) identified Ser67* as a potential PKA phosphorylation site with high score.

We expressed *C7orf59* in HEK293-T cells as an N-terminal FLAG fusion and the transiently transfected cells were stimulated with forskolin, an activator of adenylate cyclase which is widely used as a PKA agonist. The *C7orf59* interactions with p18, HBXIP and RagA were strongly reduced in the presence of forskolin, indicating that PKA activation results in breakdown of the Ragulator complex. However, besides PKA, forskolin has other cellular targets, for example PP2A. To further confirm that this effect could be attributed to PKA activation, we used the specific PKA inhibitor H-89. Incubation with this inhibitor markedly increased the amount of endogenous p18 coprecipitating with FLAG-*C7orf59*. The interactions with HBXIP and RagA were also slightly increased. Furthermore, pre-incubation with H-89 before addition of forskolin prevented the dissociation of p18, HBXIP and RagA from FLAG-*C7orf59* (**Fig. 7A**).

Immunolocalization in HeLa cells showed that endogenous *C7orf59* localizes in cytoplasmic vesicles. Colocalization with transfected DsRed-Rab7 indicates that these vesicles correspond to late endosomes/lysosomes, which is compatible with the role of *C7orf59* as a subunit of the Ragulator complex (**Fig. 7B**). It has been shown previously that the lysosomal localization of other Ragulator subunits and Rags depend on their interactions with p18, which is anchored on the lysosomal surface through N-terminal myristylation/palmytoilation (Gong et al., 2011; Kurzbauer et al., 2004; Nada et al., 2009; Sancak et al., 2010). Treatment of U2OS cell line with H-89 induced a concentration of endogenous *C7orf59* in vesicle-like spots, which is consistent with its increased binding to p18 (**Fig. 7C and Supplementary Fig 5**).

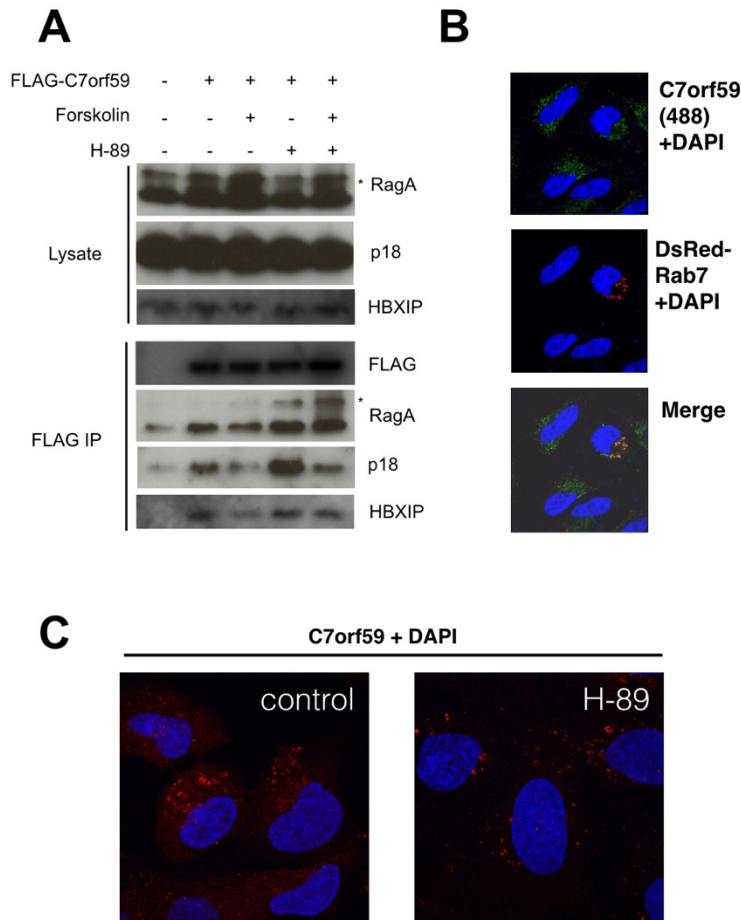


Figure 7. Stability of the Ragulator complex is affected by PKA activation **A:** Effect of PKA modulation on the Ragulator complex. HEK293-T cells were transiently transfected with FLAG-C7orf59 and treated with PKA modulators (Forskolin and H-89) as indicated. The interactions of FLAG-C7orf59 with endogenous proteins were detected by immunoprecipitation using FLAG-specific antibody and Western blot using antibodies specific to p18, HBXIP and RagA. **B:** Colocalization of endogenous C7orf59 (stained with Alexa 488, green) and transfected DsRed-Rab7, a marker of late endosomes and lysosomes, in HeLa cells. **C:** Effect of PKA inhibition with H-89 on the subcellular distribution of endogenous C7orf59 (stained with Alexa 647, red) in U2OS cells. Nuclei are stained with DAPI (Blue).

DISCUSSION

The roadblock fold is present in the MP1-p14 dimer (Kurzbaauer et al., 2004; Lunin et al., 2004b) and HBXIP (Garcia-Saez et al., 2011). Our study showed that C7orf59 also folds as a roadblock domain, confirming previous predictions and thus highlighting this structural motif as a major theme in the pentameric Ragulator. As expected based on sequence analysis, the C7orf59 fold lacks the C-terminal helix present in Group II roadblock proteins such as MP1 and p14. Unexpectedly, it also lacks the N-terminal α -helix, resulting in an overall topology, which is more closely related to yeast protein Ego2 than Ego4. Therefore, the crystal structure reported here suggests that C7orf59 is more likely to be the human orthologue of Ycr075w-a/Ego2. This would be difficult to infer based on sequence information only and this new information allows a better comparison of the mammalian and yeast systems.

By close inspection of the crystal structure of XPOF heterodimer, we came across known elements of Roadblock domain interfaces such as the continuous β -sheet and the hydrophobic helix-helix contacts, as well as an unexpected key-lock interface that structurally relates with MP1-p14. Surface hydrophobicity analysis of the XPOF crystal structure revealed the presence of a hydrophobic pocket in HBXIP, comparable to the 2*b* pocket identified in p14 by Kurzbaauer et al (Kurzbaauer et al., 2004). The *b3** loop of C7orf59 is inclining towards the 2*b* hydrophobic pocket of HBXIP and the side chains of residues Phe53* and Arg54* within this loop assume conformations that indicate the presence of an intersubunit hydrophobic key-lock motif within the XPOF structure. This observation is supported by the presence of well-defined electron density around critical residues such as Phe53* of C7orf59 and His41 and His87 of HBXIP (which form the outer less hydrophobic edges of the 2*b* pocket). Arg54* is possibly involved in a hydrogen bond with Asn71 of HBXIP. These contacts might explain the existence of the C7orf59–HBXIP heterodimer, considering that HBXIP is also known to form homodimers which do not display this lock-and-key feature (Garcia-Saez et al., 2011).

In addition to solving the structure of XPOF dimer, we also explored its interaction with p18. We have shown by cross-linking/MS and mutagenesis that an evolutionarily conserved region of p18 where residue Lys60 is located is closely associated with a conserved region of C7orf59 comprising loop 2*b** and adjacent Ser67* residue. Mutation of Ser67* of C7orf59 to aspartate reduced its binding to p18 without affecting the C7orf59-HBXIP interaction, and mutation of the p18 residues surrounding Lys60 (LAKTA–AAAAA mutation) rescued the loss of binding to S67D mutant, indicating a genetic interaction of Ser67* mutation and LAKTA–AAAAA mutation. However, this interaction is likely to be secondary in determining the stability of the p18 association with HBXIP-C7orf59, as this region of p18 failed to associate stably with

the dimer either upon mutagenesis-mediated deletion of other C-terminal p18 regions or by spontaneous proteolysis, while other regions located closer to the C-terminus of p18 were able to do so. Intriguingly, a single region of p18 was both strongly associated with HBXIP-C7orf59 upon spontaneous degradation of p18 (residues 92 – 103) and essential for the binding of p18 to MP1-p14 dimer as determined by stop codon scanning (residues 81 – 103). This region is likely to be important in the assembly of pentameric Ragulator due to its unique ability to associate with the two dimers.

Many protein interactions are known to be regulated by reversible phosphorylation. The presence of a conserved serine residue (Ser67*) in a loop close to the dimer interface led us to investigate a potential phosphorylation site in C7orf59 and the consequences of its phosphorylation on the stability of the Ragulator complex. Because Ser67* is predicted to be a PKA site, we investigated the effect of PKA modulation on the Ragulator complex. The C7orf59-HBXIP and C7orf59-p18 interactions were negatively affected by specific activation of cAMP-dependent protein kinase A (PKA), while PKA inhibition resulted in a marked increase in the amount of p18 bound to C7orf59 and in the subcellular redistribution of C7orf59 resulting in a less diffuse and more vesicle-like pattern. These results suggest that PKA phosphorylation of Ser67 in C7orf59 or other residues induces the regulated breakdown of the Ragulator complex and subsequent mTOR inactivation, although further experiments are required to demonstrate this observation. PKA is involved in metabolic regulation downstream of GPCR/cAMP signaling and one of its important upstream activators is the hormone glucagon (Pearce et al., 2010). Therefore, PKA is activated in response to nutritional scarcity to stimulate catabolism, in contrast with mTOR, which is activated by nutrient availability to stimulate anabolism. It would not be surprising if these two pathways could negatively regulate each other. However, while it is widely accepted that there exists a PKA-mTORC1 crosstalk, the exact mechanisms are not completely understood and cAMP may either activate or inactivate mTOR depending on cell type (Brown et al., 1994; Sabatini et al., 1994; Xie et al., 2011). Our results suggest a mechanism for mTORC1 regulation by PKA involving direct modulation of Ragulator stability by PKA activation. Further investigation of this novel mechanism might shed light on the crosstalk of these important pathways.

METHODS

Plasmids

All plasmids used in this study were constructed using standard molecular biology techniques. Details about cloning procedures are given in Supplemental Methods. The MP1-p14 expression plasmid was a kind gift from Dr. Lukas Huber (Kurzbaue et al., 2004). DsRed-Rab7 expression plasmid was obtained from Addgene (Plasmid #12661).

Purification and crystallization of XPOF

The 6xHis-tagged XPOF dimer was expressed in *E. coli* BL21(DE3) from the plasmid pACYC-Duet-C7orf59-HBXIP for 16 hours at 30°C after induction with 0.5 mM IPTG. Protein purification was done by affinity chromatography using Talon resin, followed by proteolytic removal of the tag and size exclusion chromatography on Superdex 200 16/60 column (GE Healthcare). The initial crystallization attempts were performed in the high throughput crystallization facility of the Brazilian National Biosciences Laboratory, RoboLab. Crystals were grown by vapor diffusion (hanging drop) at 18°C. Diffraction quality crystals were fully grown after 25-30 days in conditions: 4M sodium Formate with 5% glycerol (as a main refinement condition) and 0.01M barium Chloride as an additive. Further information can be found in Supplemental Methods.

In silico model building of C7orf59-HBXIP heterodimer

A computational model of the C7orf59 protein was built on the Phyre2 server (<http://www.sbg.bio.ic.ac.uk/phyre2>) (Kelley et al., 2015; Kim et al., 2008). The model displaying a Roadblock fold was one of the highest scoring models and was used for docking. Docking of predicted model over monomeric structure of HBXIP (PDB:3MS6) was performed using ClusPro server (Comeau et al., 2004; Kozakov et al., 2017) (<https://cluspro.bu.edu>). Among the options returned by ClusPro, a dimer displaying the expected roadblock interface was selected.

Data collection and structure solution

Native data for HBXIP-C7orf56 crystals was collected at 100K on the I24 beamline at the Diamond Light Source (Didcot, United Kingdom). Data sets were processed by the automatic pipeline at beamline with *xia2* using *DIALS* (Waterman et al., 2016; Winter, 2009), and then scaled and merged with *AIMLESS* using $CC_{1/2}$ cutoffs (Evans and Murshudov, 2013;

Karplus and Diederichs, 2012; Winn et al., 2011). Initially, the data sets have been automatically assigned to one of the space groups I222, C2 or P1. The phase problem was firstly solved using the best crystal, indexed in space group I222. An automated molecular replacement procedure as implemented in *MrBUMP* (Keegan and Winn, 2007; Winn et al., 2011) was employed, using as search models PDB files for HBXIP (3MSH, 3MS6) and an *in silico* modelling for C7orf59, both in their original forms and as additional modified models obtained with *PDBClip* (Winn et al., 2011), *MOLREP* (Vagin and Teplyakov, 1997) *CHAINSAW* (Stein, 2008), *SCULPTOR* (Bunkóczi and Read, 2011) and *PDBset* (Winn et al., 2011). Multiple alignment and structural analysis were done with *ClustalW2* (Larkin et al., 2007) and *SCOP* (Murzin et al., 1995), respectively. After automated model preparation, molecular replacement solutions were obtained independently with *MOLREP* (Vagin and Teplyakov, 1997) and *PHASER* (McCoy et al., 2007), and subjected to a preliminary refinement with *REFMAC5* (Murshudov et al., 2011).

A total of 23 solutions have been output by *MrBUMP*, the top solution with a R_{free} value of 0.493. Curiously, overall inspection with *PyMOL* (Schrödinger, 2016) showed that, with a few exceptions, most of the solutions corresponded to a same orientation within the asymmetric unit (with crystallographic symmetry taken into account if necessary). Surprisingly, a representative of the main solution cluster, the top solution, which was found by *PHASER*, was complementary to a different orientation found by *MOLREP*, as judged by the expected HBXIP-C7orf59 dimer interface obtained by *in silico* modelling. These two partial solutions were then manually combined to give an initial model. After a few rounds of refinement and model rebuilding, R_{free} decreased to 0.425. Despite the indication of a successful solution, it was difficult to obtain a reliable and stable refinement, which led us to consider a lower symmetry space group. Further refinement then proceeded to completion with data from the same crystal now processed in space group C2, using the available pre-refined model in a simple molecular replacement procedure done with *PHASER*. All through the process, Free R flag was the same, ensuring the accuracy of the crystal structure. The model was improved by iteratively model rebuilding in *COOT* (Emsley et al., 2010) and refined using *REFMAC5*, *PDB_REDO* and *phenix.refine* (Adams et al., 2010; Afonine et al., 2012; Joosten et al., 2014; Murshudov et al., 2011; Winn et al., 2011). Data collection and refinement statistics are given in **Table 1**. *PyMOL 1.7* was used to prepare the crystallographic models figures.

ConSurf analysis of evolutionary conservation

Evolutionary conservation profiles of HBXIP and C7orf59 were estimated using ConSurf version 3.0 (Ashkenazy et al., 2010; Glaser et al., 2003; Landau et al., 2005) (consurf.tau.ac.il). A CSI-BLAST search for homologs of the sequences was performed against the UNIREF-90 database with 3 iterations, an E-value cutoff 0.0001, minimal % ID of 35% for homologs and maximal % ID of 90% between sequences. A total of 50 sequences that sample the list of homologues were retrieved and aligned using MAFFT (with the accurate option L-INS-i). Calculation of position-specific conservation scores was performed using the Bayesian method. Evolutionary substitution model was set to default. The sequence conservation pattern was color coded by ConSurf from the most variable (turquoise) through intermediately conserved positions (white) to the most conserved (burgundy), and mapped onto the three-dimensional structure of the dimer.

Pulldown assays

The expression plasmids for GST-p18ΔN, HBXIP-C7orf59 or MP1-p14, or the respective mutated constructs were cotransformed into *E. coli* BL21(DE3) and expression was induced by adding 0.5 mM IPTG and incubating for 16 hours at 30°C at 200 rpm. The pellets were lysed using 0.2 mg ml⁻¹ lysozyme combined with sonication in pH 7.4 PBS buffer supplemented with 5% glycerol, 2 mM β-mercaptoethanol and 5 mM of imidazol (the latter used only for Talon pulldowns). Glutathione sepharose beads (Glutathione-Sepharose 4B, GE Healthcare) or Talon beads (Clontech) were added to the cleared lysates, which were incubated for 3 hours at 4°C on an agitator at a very slow speed. The samples were washed five times with lysis buffer and the beads were eluted with Laemmli buffer and analyzed by coomassie stained SDS-PAGE 15%.

Cell culture, transfection, coimmunoprecipitation and localization

HEK293-T, HeLa or U2OS cells were grown in DMEM containing 10% fetal bovine serum (FBS) at 37° C with 5% CO₂. Transient transfections were performed with PEI (Boussif et al., 1995). Cells were transfected with FLAG-tagged C7orf59 wild type. After 48h of transfection, cells were treated with Forskolin 40 μM or the PKA inhibitor H-89 (20μM), both from Sigma-Aldrich. Cells were lysed in lysis buffer (150 mM NaCl, 30 mM Tris, 3 mM EDTA and 0.3%(v/v) IGEPAL pH 8.0) supplemented with phosphatase inhibitor (10 mM beta glycerophosphate and 20 mM NaF) and incubated with FLAG-agarose affinity beads (Sigma-

Aldrich) for 3-4 hours at 4°C. The beads were washed four times with lysis buffer and bound proteins were eluted in Laemmli buffer. The samples were analysed by Western blot with antibodies anti-FLAG (Sigma), anti-p18/LAMTOR1, anti-HBXIP and anti-RagA (Cell Signaling Technology). For immunolocalization of endogenous C7orf59, cells were fixed with paraformaldehyde after the indicated treatments, and stained with primary C7orf59 antibody (Cell Signaling Technology) and secondary anti-rabbit antibody conjugated to Alexa647 or Alexa488 (Life Technologies) as indicated. Nuclei were stained with DAPI. Lysosomes/ late endosomes were stained with transfected DsRed-Rab7 where indicated. Images were captured in a TCS SP8 Leica confocal microscope at 63x magnification.

Hydrogen-deuterium exchange

Hydrogen-deuterium exchange was started by diluting the sample of purified HBXIP-C7orf59 1:15 in deuterated buffer (50 mM Tris.DCl, 100 mM NaCl, 2 mM β -mercaptoethanol, 5% glycerol, pD 7.4) at 25°C and stopped at different time points (10s, 1 min, 10 min, 1h and 2h) by adding equal volumes of quench buffer (800 mM Guanidine-HCl, 0.8% formic acid (vol/vol), 20 mM DTT, pH 2.5) at 4°C. A control sample was collected at time = 0. Samples were injected into a nano Acquity UPLC system with HDX technology coupled to Synapt G1 HDMS (Waters Corporation, USA). Online digestion was performed on an immobilized pepsin column (2x30 mm, Applied Biosystem, USA) for 4 minutes at 15°C with 35 μ L.min⁻¹ flow. The resulting peptides were desalted on an ACQUITY UPLC BEH C18 pre-column (1.7 μ m, VanGuard, Waters) at 0°C and separated on an analytical column (ACQUITY UPLC BEH C18 1.7 μ m, 1 mm x 100 mm, Waters) at 0°C with 50 μ L.min⁻¹ flow. The runs were processed by Protein Lynx Global Server v.2.4. (Waters Corporation, USA) and DynamX v.3.0 (Waters Corporation, USA). For C7orf59, a total 33 of peptides were detected, with 96.1% sequence coverage, and 3.76 redundancy, while for HBXIP, a total 34 of peptides were detected, with 91.3% coverage and 4.00 redundancy.

Chemical crosslinking/ Mass spectrometry analysis

The HBXIP-C7orf59-GST-p18 Δ N complex resultant from the first peak of purification by size-exclusion chromatography was submitted to chemical cross-linking combined with mass spectrometry. Cross-linking reactions were performed as previously described (Iglesias et al., 2009; 2010). The raw data from spectrometer were processed using Mascot Distiller 2.4.3

(Matrix Science) and the spectra were used for crosslinked peptide identification using SIM-XL (Lima et al., 2015). Further information in Supplemental material.

Small angle X-ray scattering

Small-angle X-ray scattering (SAXS) curves were recorded at the SAXS-1 beamline at Laboratório Nacional de Luz Síncrotron (Brazilian Synchrotron Light Laboratory, LNLS), equipped with a Dectris Pilatus 300K detector (84 mm × 107 mm) and a capillary sample holder. Sample-to-detector distance was 1606.50 mm and radiation wavelength was 1.55 Å, with q ranging from 0.0063 to 0.2787 Å⁻¹ ($q=4\pi\sin\theta/\lambda$, where 2θ is the scattering angle). Further information in Supplementary material.

Table 1. Data collection and refinement statistics.

	HBXIP-C7orf59
Wavelength (Å)	0.9686
Resolution range (Å)	81.85 - 2.89 (3.07 - 2.89)
Space group	C 1 2 1
Cell dimensions	
a,b,c (Å)	180.88, 64.76, 79.23
α,β,γ (°)	90.00, 115.18, 90.00
Total reflections	125792 (20673)
Unique reflections	18719 (3004)
Multiplicity	6.7 (6.9)
Completeness (%)	99.5 (99.1)
Mean I/sigma(I)	6.5 (0.7)
Wilson B-factor (Å ²)	86.24
R-merge	0.171 (3.50)
R-meas	0.186 (3.79)
CC1/2	0.993 (0.337)
Reflections used in refinement	18629 (3020)
Reflections used for R-free	949 (158)
R-work	0.3077 (0.4642)
R-free	0.3548 (0.4572)
Number of non-hydrogen atoms	5079
macromolecules	5077
solvent	2
Protein residues	688
RMS deviation (bonds) (Å)	0.007
RMS deviation (angles) (°)	1.24
Ramachandran favored (%)	88.02
Ramachandran allowed (%)	8.83
Ramachandran outliers (%)	3.14
Rotamer outliers (%)	19.76
Clashscore	11.37
Average B-factor (Å ²)	95.78
macromolecules	95.79
solvent	77.61
Number of TLS groups	1

Statistics for the highest-resolution shell are shown in parentheses.

Table 2. Crosslinking/MS analysis of XPOF and XPOF-GST-p18ΔN complexes.

Protein 1			Protein 2		
Peptide sequence	Subunit	Cross-linked Residue	Peptide sequence	Subunit	Cross-linked Residue
TDEQALLSSILAKTASNIIDVSAADSQGM EQHEYMDR	p18	Lys 60	LAVLSSSLTHWKK	p18	Lys 103
TDEQALLSSILAKTASNIIDVSAADSQGM EQHEYMDR	p18	Lys 60	KLLDPSSPPTK	p18	Lys 20
TDEQALLSSILAKTASNIIDVSAADSQGM EQHEYMDR	p18	Lys 60	VFVVKR	C7orf59	Lys 88
TDEQALLSSILAKTASNIIDVSAADSQGM EQHEYMDR	p18	Lys 60	GMNVPFKR	C7orf59	Lys 64
EOHEYMDR TDEQALLSSILAKTASNIIDVSAADSQGM	p18	Lys 60	LLDPSSPPTKALNG	p18	Lys 31
EOHEYMDR LLDPSSPPTKALNGAEPNYHSLPSAR	p18	Lys 31	AEPNYHSLPSAR GMNVPFKR	C7orf59	Lys 64

ACKNOWLEDGEMENTS

This work was funded by Fundação de Amparo à Pesquisa do Estado de São Paulo (FAPESP). N. R. was recipient of CNPq-TWAS fellowship (190174/2012-9). J.H.C.S was recipient of FAPESP Grant 2014/12445-0. T. B. L. and A. F. Z. N. were recipients of CAPES fellowships. R. A. and F. C. G. were recipients of CNPq productivity fellowships. We thank Mario T. Murakami, Priscila O. Giuseppe, José Brandão-Neto and Pierre Aller for help with data collection. We thank LNBio/CNPEM for financial support and access to the facilities, LNLS for access to beamline SAXS-1 and Diamond Light Source for access to beamline I24.

Supplemental Data

SUPPLEMENTAL METHODS

Plasmid construction and mutagenesis

The pET-Duet-C7orf59-HBXIP bicistronic expression plasmid was obtained by subcloning both cDNAs sequentially into a modified version of pET-Duet-1 plasmid (Clontech) harbouring a PreScission site. C7orf59 was cloned between the *Bam*HI and *Not*I sites in frame with an N-terminal hexahistidine tag followed by the PreScission protease cleavage site, and HBXIP was cloned between *Nde*I and *Xho*I restriction sites. The pACYC-Duet-C7orf59-HBXIP plasmid was constructed by subcloning the bicistronic cassette 6xHis-PreScission-HBXIP-C7orf59 from pET-Duet-C7orf59-HBXIP into pACYC-Duet (Clontech) using the *Nco*I and *Xho*I restriction sites. p18ΔN was subcloned into pGEX-4T-1 from pET302. C7orf59 was subcloned from pACYC-Duet into pCDNA-FLAG (*Bam*HI and *Not*I). Site-directed mutagenesis (except for LAKTA_AAAAA mutation) was performed by thermal cycling with *Pfu* (Thermo Scientific) and digestion of parental DNA with *Dpn*I (Thermo Scientific), followed by transformation into DH5α and clone confirmation by sequencing. A total of nine stop codon mutants of GST-p18ΔN were constructed (D149, Q130, L108, K103, E80, Q74, K60, G35, K31). Three mutants of C7orf59 i.e., E34A/N35A, D36A/E37A and S67D were also designed to target the conserved residues of the protein. GST-p18ΔN LAKTA_AAAAA mutant was obtained by PCR with the primers shown in Supplemental Table 1 using *Pfu* polymerase followed by ligation with T4 DNA ligase. All the five residues were mutated in the same PCR reaction. All the mutant clones were confirmed through sequencing before proceeding to the pull down experiments. The sequences of mutagenic primers are given in **Supplementary Table 1**.

Expression of His-C7orf59-HBXIP

The expression of His-C7orf59-HBXIP dimer was done in *E. coli* strain BL21(DE3) using IPTG as an inducer. Initially, protein expression of dimers with either long or short HBXIP was tested at 25° C and 30° C, for 4 to 16 hours at 200 rpm in LB medium in the presence of 0.5 mM IPTG. Small-scale affinity purification was performed with Talon resin to test the quality of the expression from the soluble fraction. The short HBXIP isoform was chosen for further experiments due to the lack of degradation bands. Large-scale expression of His-C7orf59-HBXIP was induced with 0.5 mM IPTG at 30° C for 16 hours at 200 rpm in 20 liters of LB medium.

Affinity purification

Large-scale affinity purification of His-C7orf59-HBXIP was performed using PBS pH 7.4 (1X) with 5% glycerol, 2 mM β -mercaptoethanol and 5 mM of imidazole as resuspension/lysis buffer. The resuspended lysate was supplemented with 1 mM PMSF and protease inhibitor cocktail (1X), incubated with lysozyme ($0.1 \text{ mg}\cdot\text{ml}^{-1}$) for 1 hour at 4°C on ice and then lysed by sonication (5 to 6 cycles of 15 seconds at 1 min interval apart). The cleared lysate obtained after centrifugation at 16000 g for 1-2 hour at 4°C was subjected to batch affinity purification using Talon resin (Clontech). After incubation with resin, lysate was centrifuged at 650 rpm at 4°C to remove the flow through. The Talon beads were washed five times with the resuspension buffer and proteins were eluted with PBS pH 7.4 (1X) supplemented with 300 mM imidazole, 5% glycerol and 2 mM β -mercaptoethanol. The cleared lysates were divided into two batches before proceeding to the washing and elution steps. To remove the excess imidazole, the sample was dialysed in PBS buffer (1X) pH 7.4 with 5% glycerol, 2 mM β -mercaptoethanol and later cleaved with 80 units of PreScission protease (GE Healthcare) for 16 hours at 4°C to remove the His tag from C7orf59.

Size exclusion chromatography

The cleaved sample was concentrated to 2 ml using a centrifugal filter device (GE Healthcare, MWCO 3.000/ 3kDa) and size exclusion chromatography was performed on a Superdex 200 column 16/60 (GE healthcare) connected to an ÄKTA FPLC system using 50 mM Tris-HCl (pH 7.4) supplemented with 2 mM of β -mercaptoethanol, 5% glycerol and 100 mM of NaCl. UV absorbance was monitored at 280 nm to indicate the presence of proteins. The peak fractions were collected and concentrated using a centrifugal filter device (GE Healthcare, MWCO 3.000) until the desired concentration was achieved for the follow up crystallization experiments. The final concentration of the pure protein was determined from the UV absorption at 280 nm using a NanoDrop spectrophotometer. ProtParam was used for the calculation of molar extinction coefficient of proteins (<http://www.expasy.ch/tools/protparam.html>).

Chemical crosslinking/ Mass spectrometry analysis

The protein complex was incubated with DSS (suberic acid bis (N-hydroxysuccinimide ester) in dry dimethylformamide (Merck, 27 mM stock) to a final 1:50 complex/DSS ratio for 2 hours at 25°C . Thereafter, reduction and alkylation reactions of cysteine (thiol groups) was

performed by reduction with 0.24 mM DTT (dithiothreitol in 0.1M ammonium bicarbonate, 30 min at 60°C) followed by a alkylation with 1.4 mM IAA (iodoacetamide in 0.1M ammonium bicarbonate, 30 min at room temperature in dark), and digested with trypsin (20 $\mu\text{g}\cdot\text{mL}^{-1}$) to a final 1:20 trypsin/protein ratio for 16 hours at 37°C (all these reagents from Sigma-Aldrich). The digested samples were desalted and enriched by fractionation using cartridge Oasis HLB (Waters), eluted with different concentrations of acetonitrile (10, 20, 30 and 70% acetonitrile aqueous solution), and dried in vacuum concentration for a final volume of 20 μL (in water). In mass spectrometer, the fractions containing peptides were separated on nano-LC system (Easy-nLC 1000, Thermo Fisher Scientific) at reverse-phase separation at a flow rate 300 nL/min using the following mobile phase gradient from 5 to 35% B (50 min); 35-70% B (2 min); 70% B (8 min) (solvents A: 5% ACN, 0.1% formic acid in water, and B: 95% ACN, 0.1% formic acid in water). The system was connected to a nano-ESI source coupled to Q-Exactive mass spectrometer (Thermo Fisher Scientific). Each full MS scan, acquired in the orbitrap over a mass rang of m/z 400-1800 at resolution of 70000 (m/z 400), was followed by ten data-dependent acquisition (DDA) mode controlled by XCalibur 2.0 software. The ten most intense signals in the mass spectrum were selected for collision-induced dissociation (CID) and fragments were detected by Orbitrap at resolution of 35000 (m/z 400).

Small angle X-ray scattering

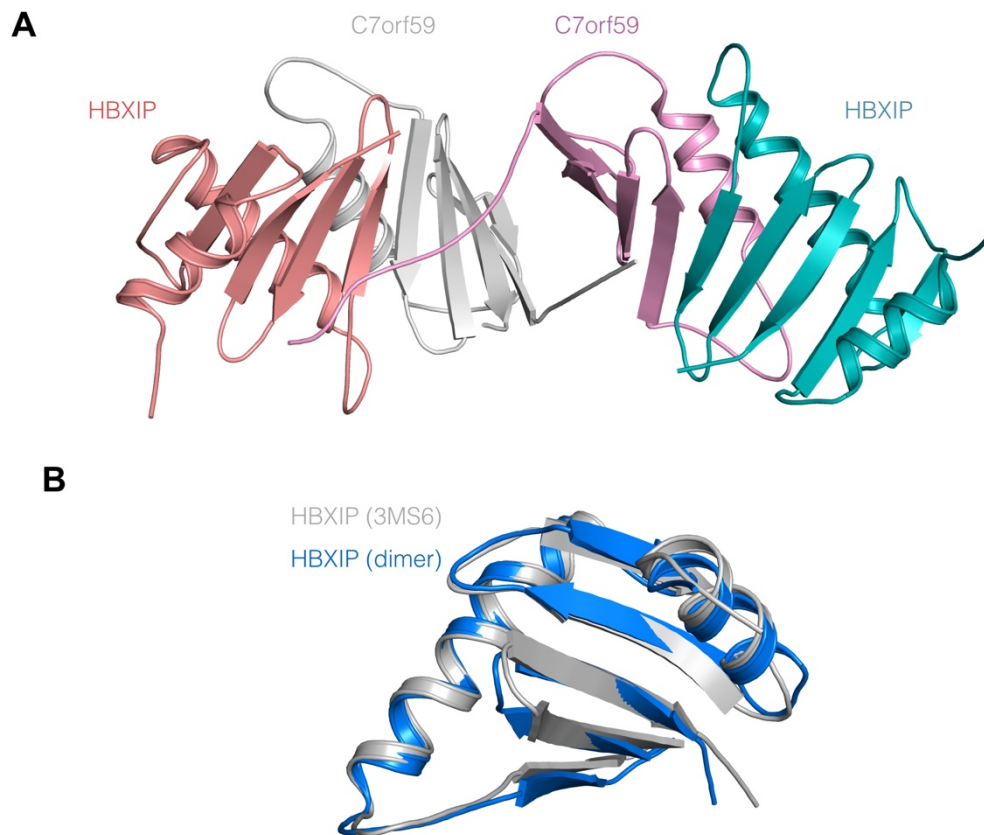
Small-angle X-ray scattering (SAXS) curves were recorded at the SAXS-1 beamline at Laboratório Nacional de Luz Síncrotron (Brazilian Synchrotron Light Laboratory, LNLS), equipped with a Dectris Pilatus 300K detector (84 mm \times 107 mm) and a capillary sample holder. Sample-to-detector distance was 1606.50 mm and radiation wavelength was 1.55 Å, with q ranging from 0.0063 to 0.2787 \AA^{-1} ($q=4\pi\sin\theta/\lambda$, where 2θ is the scattering angle). Fractions from size exclusion chromatography were collected and analysed immediately after centrifugation at 13000 g for 10 min at 4°C, and the size exclusion buffer was used as reference for buffer subtraction. A series of increasing exposure times (5, 30, 90 sec.) was employed to assess potential radiation damage. Fit2D (Hammersley et al., 1996) was used for data integration, normalization to the intensity of the transmitted beam and sample attenuation, and buffer scattering subtraction. Absolute calibration of scattering data was performed using water as a secondary standard (Mylonas and Svergun, 2007; Orthaber et al., 2000). ATSAS (Petoukhov et al., 2012) and GNUPLOT (<http://www.gnuplot.info>) were used for data analysis and plotting. The radius of gyration (R_g) and the zero-angle scattering intensity ($I(0)$) were

obtained from the Guinier approximation $I(q) = I(0)\exp(-q^2R_g^2/3)$, valid for $qR_g \lesssim 1.3$, and by the indirect Fourier transform method implemented in the program GNOM (Svergun, 1992). The pair-distance distribution function, $P(r)$, was calculated from the scattering curve using GNOM. Molecular mass was estimated by a concentration-independent method based on the Porod invariant ($\int q^2 I(q) dq$). For model construction, forty dummy atom models of the HBXIP-C7orf59 dimer were generated from the scattering curve using DAMMIF (Franke and Svergun, 2009) in mode 'slow', without enforcing any symmetry (P1) or anisotropy restrictions. This model set was clustered using DAMCLUST (Konarev et al., 2006). The biggest cluster consisting of 18 models for the HBXIP-C7orf59 dimer was averaged and superposition of the final model on the crystal structure of HBXIP-C7orf59 was done with SUPCOMB (Kozin and Svergun, 2001) after removing the flexible N-terminus of C7orf59 (residues 1–15). Images were generated using *PyMOL 1.7* (Schrödinger, 2016). Computational jobs were automated with C shell scripts.

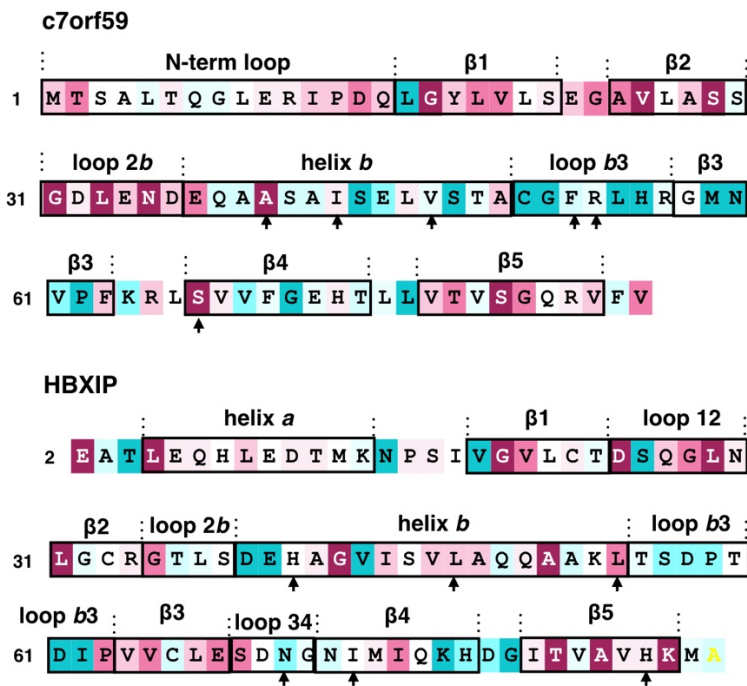
Supplementary Table 1. Mutagenic primers.

<i>Mutation</i>	<i>Protein</i>	<i>Primer Sequence (5' – 3')</i>	<i>Type</i>
<i>K31</i>	p18	CTCCATTGAGAGCTTAGGTAGGGGGGCTGC	Forward
<i>K31</i>	p18	GCAGCCCCCTACCTAAGCTCTCAATGGAG	Reverse
<i>G35</i>	p18	GGGCTCGGCTCAATTGAGAGCTTTGGTAGGG	Forward
<i>G35</i>	p18	CCCTACCAAAGCTCTCAATTGAGCCGAGCCC	Reverse
<i>K60</i>	p18	ATGTTGCTGGCTGTCTAGGCAAGGATGGAAGAG	Forward
<i>K60</i>	p18	CTCTTCCATCCTTGCTAGACAGCCAGCAACAT	Reverse
<i>Q74</i>	p18	CTCCATGCCCTATGAGTCTGCAGCAGACACATC	Forward
<i>Q74</i>	p18	GATGTGTCTGCTGCAGACTCATAGGGCATGGAG	Reverse
<i>E80</i>	p18	CGGTCCATGTACTAATGTGCTCCATGCCC	Forward
<i>E80</i>	p18	GGGCATGGAGCAGCATTAGTACATGGACCG	Reverse
<i>K103</i>	p18	CGGTGGCAGCTTCTACCAATGGGTCAGGC	Forward
<i>K103</i>	p18	GCCTGACCCATTGGTAGAAGCTGCCACCG	Reverse
<i>L108</i>	p18	GCTGGTAAGAGACGGCTACGGTGGCAGCTTCTTC	Forward
<i>L108</i>	p18	GAAGAAGTGCCACCGTAGCCGTCTTACCAGC	Reverse
<i>Q130</i>	p18	TCCTGGAGACCTGCTACAATCAGAGAACGGG	Forward
<i>Q130</i>	p18	CCCGTTCTCTGATTTGTAGCAGGTCTCCAGGA	Reverse
<i>D149</i>	p18	AACCAGCTCCTCTTTTGCCTACACACGGATCTGAGAAAG	Forward
<i>D149</i>	p18	CTTTCTCAGATCCGTGTGTAGGCAAAGAGGAGCTGGTT	Reverse
<i>LAKTA_AAAAA</i>	p18	CGCCGCCAGCAACATCATTGATGTGTCTG	Forward
<i>LAKTA_AAAAA</i>	p18	GCGGCGGCGATGGAAGAGAGCAGGGC	Reverse
<i>E34A/N35A</i>	C7orf59	GGCTGCCTGCTCATCAGCCGCCAGGTCCCCAGATGA	Forward
<i>E34A/N35A</i>	C7orf59	TCATCTGGGGACCTGGCGGCTGATGAGCAGGCAGCC	Reverse
<i>D36A/E37A</i>	C7orf59	CACTGGCTGCCTGCGCAGCATTCTCCAGGTCC	Forward
<i>D36A/E37A</i>	C7orf59	GGACCTGGAGAATGCTGCGCAGGCAGCCAGTG	Reverse
<i>S67D</i>	C7orf59	GTTCTCAAAGACCACATCCAGGCGCTTGAAGGGCA	Forward
<i>S67D</i>	C7orf59	TGCCCTTCAAGCGCCTGGATGTGGTCTTTGGAGAAC	Reverse
<i>S67A</i>	C7orf59	CTCCAAAGACCACAGCCAGGCGCTTGAAGGG	Forward
<i>S67A</i>	C7orf59	CCCTTCAAGCGCCTGGCTGTGGTCTTTGGAG	Reverse

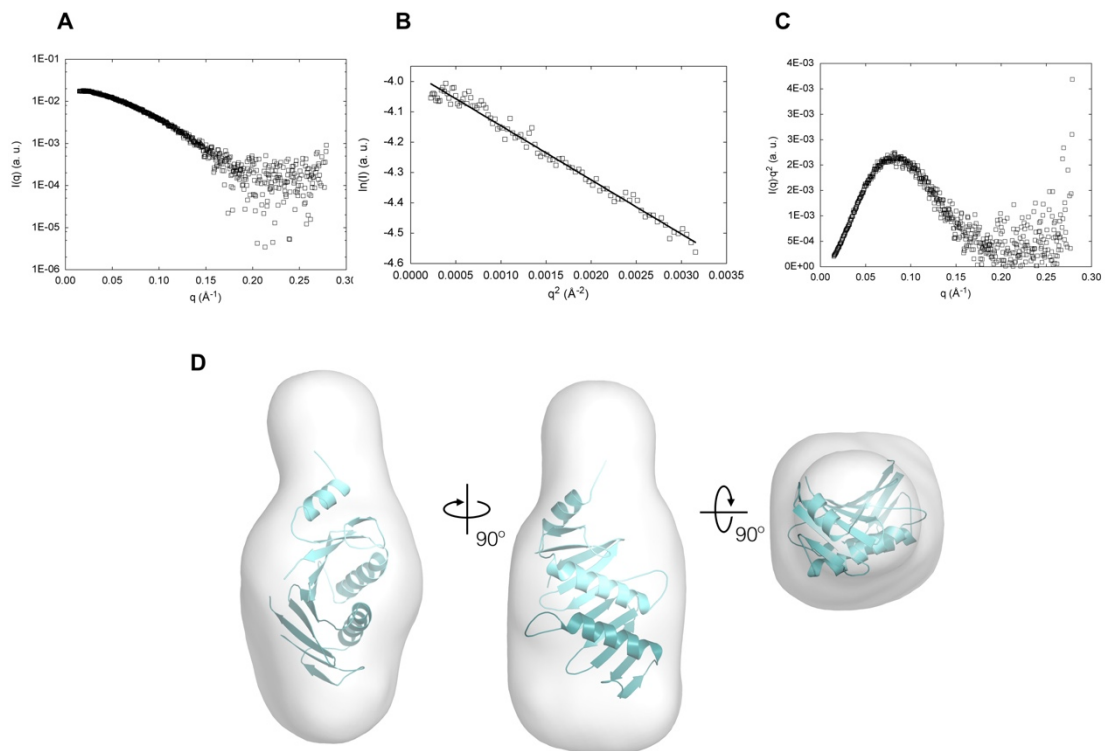
SUPPLEMENTAL FIGURES



Supplementary Figure 1. A: Packing of the dimers in the crystal lattice stabilizes the flexible N-terminal region of C7orf59. Two of the four dimers present in the asymmetric unit are shown. **B:** Superposition of the HBXIP structure reported previously (PDB:3MS6, in grey) and the HBXIP structure from this study in the complex with C7orf59 (blue).

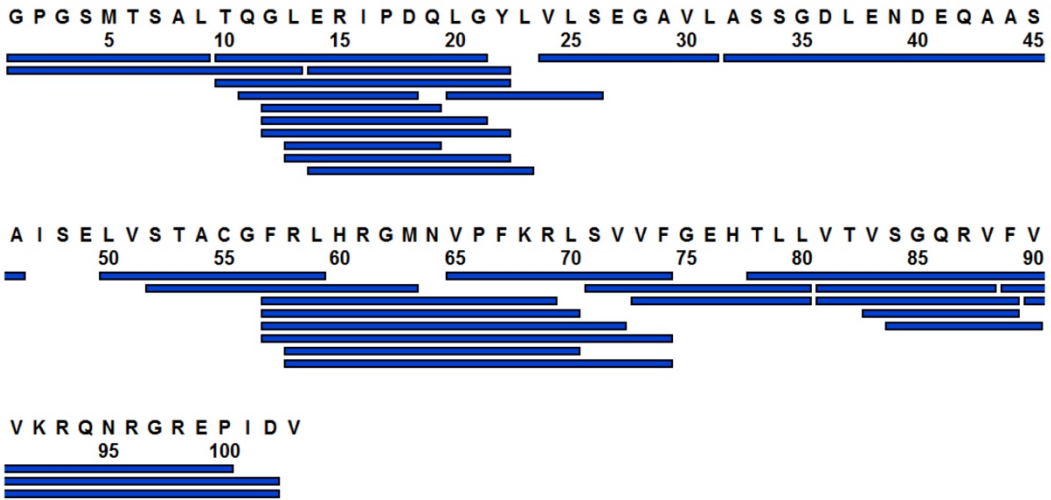


Supplementary Figure 2. Sequences and secondary structure elements of C7orf59 and HBXIP coloured according to the ConSurf conservation analysis. The arrows indicate potentially important residues identified in the crystal structure.



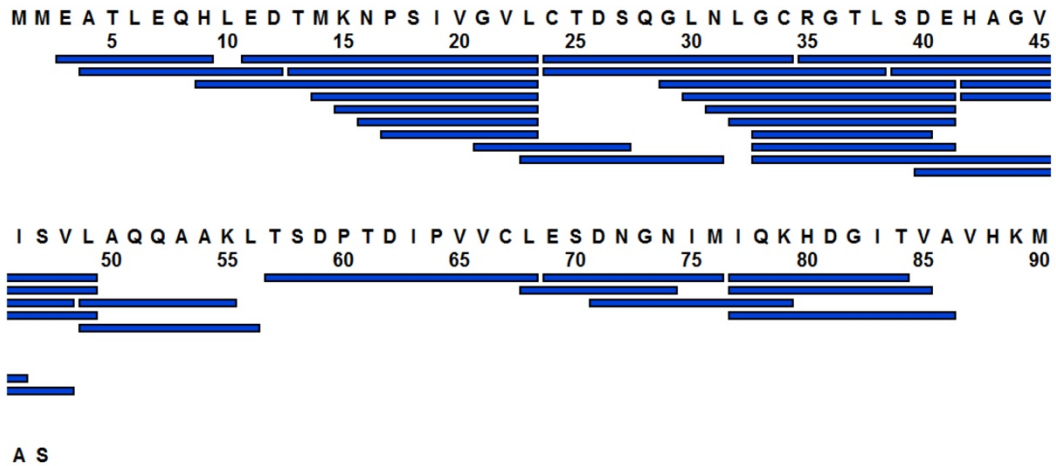
Supplementary Figure 3. Small angle X-ray scattering analysis of the XPOF dimer bound to p18-derived peptide, obtained from spontaneous dissociation of the XPOF-GST-p18 Δ N trimer. **A:** Scattering curve **B:** Guinier region. **C:** Krakty plot. **D:** SAXS envelope fitted to the XPOF dimer. The flexible N-terminal residues of C7orf59 were removed for this analysis. HBXIP is in light cyan and C7orf59 is in dark cyan.

c7orf59



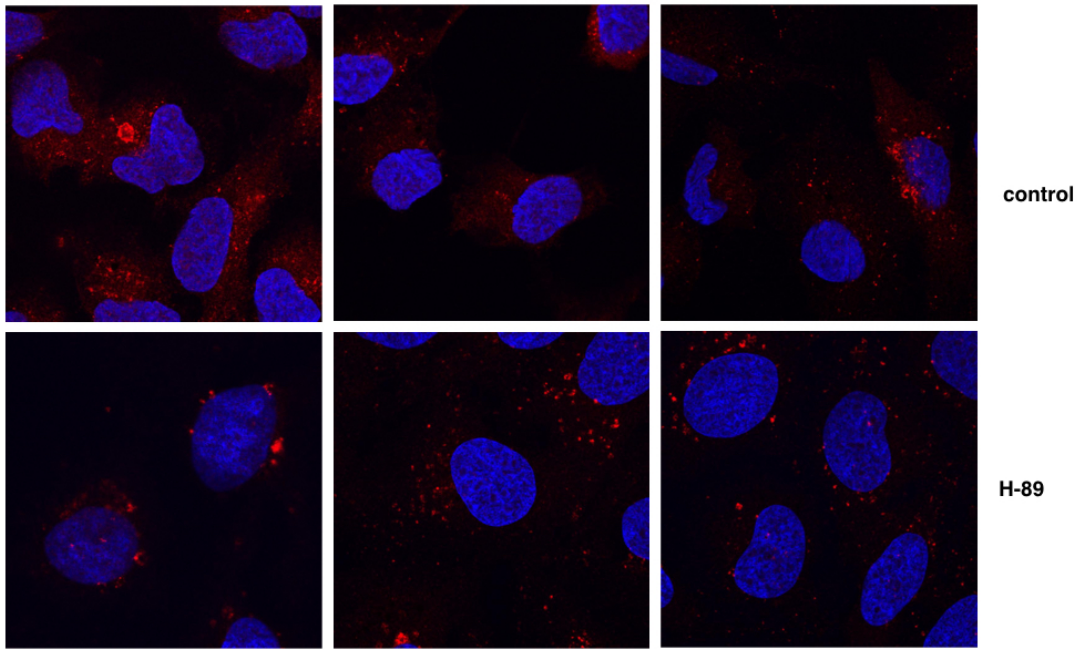
Total: 33 Peptides, 96.1% Coverage, 3.76 Redundancy

HBXIP



Total: 34 Peptides, 91.3% Coverage, 4.00 Redundancy

Supplementary Figure 4. Sequence coverage of HBXIP and C7orf59 in the HDX-MS experiment.



Supplementary Figure 5. Additional images from the experiment shown in Figure 7C.

References

- Adams, P.D., Afonine, P.V., Bunkóczi, G., Chen, V.B., Davis, I.W., Echols, N., Headd, J.J., Hung, L.-W., Kapral, G.J., Grosse-Kunstleve, R.W., et al. (2010). PHENIX: a comprehensive Python-based system for macromolecular structure solution. *Acta Crystallogr. D Biol. Crystallogr.* *66*, 213–221.
- Afonine, P.V., Grosse-Kunstleve, R.W., Echols, N., Headd, J.J., Moriarty, N.W., Mustyakimov, M., Terwilliger, T.C., Urzhumtsev, A., Zwart, P.H., and Adams, P.D. (2012). Towards automated crystallographic structure refinement with phenix.refine. *Acta Crystallogr. D Biol. Crystallogr.* *68*, 352–367.
- Ashkenazy, H., Erez, E., Martz, E., Pupko, T., and Ben-Tal, N. (2010). ConSurf 2010: calculating evolutionary conservation in sequence and structure of proteins and nucleic acids. *Nucleic Acids Res.* *38*, W529–W533.
- Bar-Peled, L., Schweitzer, L.D., Zoncu, R., and Sabatini, D.M. (2012). Ragulator Is a GEF for the Rag GTPases that Signal Amino Acid Levels to mTORC1. *Cell* *150*, 1196–1208.
- Boussif, O., Lezoualc'h, F., Zanta, M.A., Mergny, M.D., Scherman, D., Demeneix, B., and Behr, J.P. (1995). A versatile vector for gene and oligonucleotide transfer into cells in culture and in vivo: polyethylenimine. *Proc. Natl. Acad. Sci. U.S.A.* *92*, 7297–7301.
- Brown, E.J., Albers, M.W., Shin, T.B., Ichikawa, K., Keith, C.T., Lane, W.S., and Schreiber, S.L. (1994). A mammalian protein targeted by G1-arresting rapamycin-receptor complex. *Nature* *369*, 756–758.
- Bunkóczi, G., and Read, R.J. (2011). Improvement of molecular-replacement models with Sculptor. *Acta Crystallogr. D Biol. Crystallogr.* *67*, 303–312.
- Comeau, S.R., Gatchell, D.W., Vajda, S., and Camacho, C.J. (2004). ClusPro: a fully automated algorithm for protein-protein docking. *Nucleic Acids Res.* *32*, W96–W99.
- Efeyan, A., Zoncu, R., and Sabatini, D.M. (2012). Amino acids and mTORC1: from lysosomes to disease. *Trends Mol Med.*
- Emsley, P., Lohkamp, B., Scott, W.G., and Cowtan, K. (2010). Features and development of Coot. *Acta Crystallogr. D Biol. Crystallogr.* *66*, 486–501.
- Evans, P.R., and Murshudov, G.N. (2013). How good are my data and what is the resolution? *Acta Crystallogr. D Biol. Crystallogr.* *69*, 1204–1214.
- Franke, D., and Svergun, D.I. (2009). DAMMIF, a program for rapid ab-initio shape determination in small-angle scattering. *J Appl Crystallogr* *42*, 342–346.

- Garcia-Saez, I., Lacroix, F.B., Blot, D., Gabel, F., and Skoufias, D.A. (2011). Structural characterization of HBXIP: the protein that interacts with the anti-apoptotic protein survivin and the oncogenic viral protein HBx. *J. Mol. Biol.* *405*, 331–340.
- Glaser, F., Pupko, T., Paz, I., Bell, R.E., Bechor-Shental, D., Martz, E., and Ben-Tal, N. (2003). ConSurf: identification of functional regions in proteins by surface-mapping of phylogenetic information. *Bioinformatics* *19*, 163–164.
- Gong, R., Li, L., Liu, Y., Wang, P., Yang, H., Wang, L., Cheng, J., Guan, K.-L., and Xu, Y. (2011). Crystal structure of the Gtr1p-Gtr2p complex reveals new insights into the amino acid-induced TORC1 activation. *Genes Dev.*
- Guertin, D.A., and Sabatini, D.M. (2005). An expanding role for mTOR in cancer. *Trends Mol Med* *11*, 353–361.
- Hammersley, A.P., Svensson, S.O., Hanfland, M., Fitch, A.N., and Hausermann, D. (1996). Two-dimensional detector software: From real detector to idealised image or two-theta scan. *High Pressure Research* *14*, 235–248.
- Iglesias, A.H., Santos, L.F.A., and Gozzo, F.C. (2009). Collision-induced dissociation of Lys-Lys intramolecular crosslinked peptides. *J. Am. Soc. Mass Spectrom.* *20*, 557–566.
- Iglesias, A.H., Santos, L.F.A., and Gozzo, F.C. (2010). Identification of cross-linked peptides by high-resolution precursor ion scan. *Anal. Chem.* *82*, 909–916.
- Jeong, J.-H., Lee, K.-H., Kim, Y.-M., Kim, D.-H., Oh, B.-H., and Kim, Y.-G. (2012). Crystal structure of the Gtr1p(GTP)-Gtr2p(GDP) protein complex reveals large structural rearrangements triggered by GTP-to-GDP conversion. *Journal of Biological Chemistry* *287*, 29648–29653.
- Jewell, J.L., Russell, R.C., and Guan, K.-L. (2013). Amino acid signalling upstream of mTOR. *Nat. Rev. Mol. Cell Biol.* *14*, 133–139.
- Joosten, R.P., Long, F., Murshudov, G.N., and Perrakis, A. (2014). The PDB_REDO server for macromolecular structure model optimization. *IUCrJ* *1*, 213–220.
- Karplus, P.A., and Diederichs, K. (2012). Linking crystallographic model and data quality. *Science* *336*, 1030–1033.
- Keegan, R.M., and Winn, M.D. (2007). Automated search-model discovery and preparation for structure solution by molecular replacement. *Acta Crystallogr. D Biol. Crystallogr.* *63*, 447–457.
- Kelley, L.A., Mezulis, S., Yates, C.M., Wass, M.N., and Sternberg, M.J.E. (2015). The Phyre2 web portal for protein modeling, prediction and analysis. *Nat Protoc* *10*, 845–858.
- Kim, E., Goraksha-Hicks, P., Li, L., Neufeld, T.P., and Guan, K.-L. (2008). Regulation of

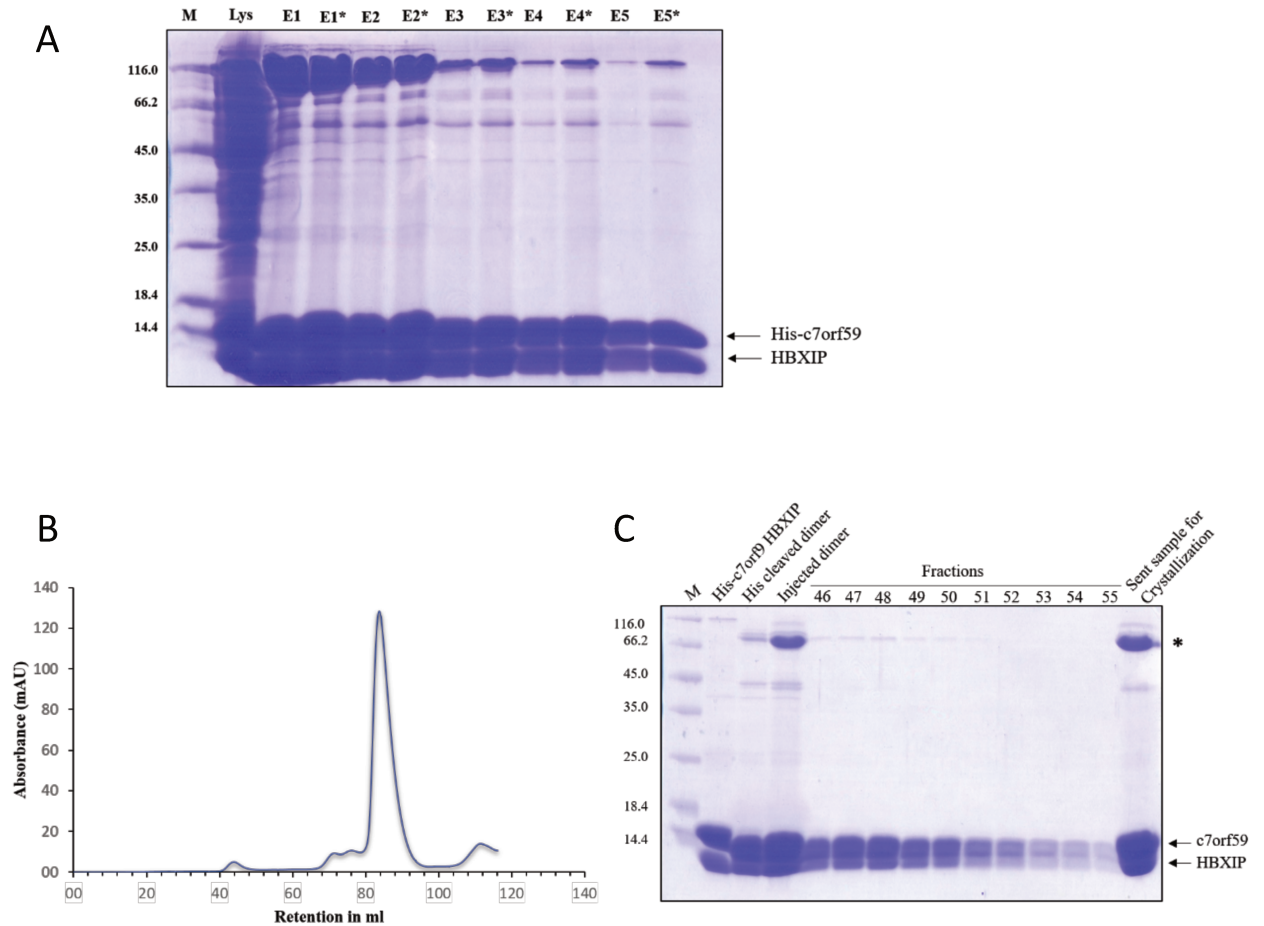
- TORC1 by Rag GTPases in nutrient response. *Nat. Cell Biol.* *10*, 935–945.
- Konarev, P.V., Petoukhov, M.V., Volkov, V.V., and Svergun, D.I. (2006). ATSAS2.1, a program package for small-angle scattering data analysis. *J Appl Crystallogr* *39*, 277–286.
- Kozakov, D., Hall, D.R., Xia, B., Porter, K.A., Padhorny, D., Yueh, C., Beglov, D., and Vajda, S. (2017). The ClusPro web server for protein-protein docking. *Nat Protoc* *12*, 255–278.
- Kozin, M.B., and Svergun, D.I. (2001). Automated matching of high-and low-resolution structural models. *J Appl Crystallogr*.
- Kurzbaueer, R., Teis, D., de Araujo, M.E.G., Maurer-Stroh, S., Eisenhaber, F., Bourenkov, G.P., Bartunik, H.D., Hekman, M., Rapp, U.R., Huber, L.A., et al. (2004). Crystal structure of the p14/MP1 scaffolding complex: how a twin couple attaches mitogen-activated protein kinase signaling to late endosomes. *Proc. Natl. Acad. Sci. U.S.a.* *101*, 10984–10989.
- Landau, M., Mayrose, I., Rosenberg, Y., Glaser, F., Martz, E., Pupko, T., and Ben-Tal, N. (2005). ConSurf 2005: the projection of evolutionary conservation scores of residues on protein structures. *Nucleic Acids Res.* *33*, W299–W302.
- Laplante, M., and Sabatini, D.M. (2012). mTOR signaling in growth control and disease. *Cell* *149*, 274–293.
- Larkin, M.A., Blackshields, G., Brown, N.P., Chenna, R., McGettigan, P.A., McWilliam, H., Valentin, F., Wallace, I.M., Wilm, A., Lopez, R., et al. (2007). Clustal W and Clustal X version 2.0. *Bioinformatics* *23*, 2947–2948.
- Levine, T.P., Daniels, R.D., Wong, L.H., Gatta, A.T., Gerondopoulos, A., and Barr, F.A. (2013). Discovery of new Longin and Roadblock domains that form platforms for small GTPases in Ragulator and TRAPP-II. *Small GTPases* *4*, 62–69.
- Lima, D.B., de Lima, T.B., Balbuena, T.S., Neves-Ferreira, A.G.C., Barbosa, V.C., Gozzo, F.C., and Carvalho, P.C. (2015). SIM-XL: A powerful and user-friendly tool for peptide cross-linking analysis. *J Proteomics* *129*, 51–55.
- Lunin, V.V., Munger, C., Wagner, J., Ye, Z., Cygler, M., and Sacher, M. (2004a). The structure of the MAPK scaffold, MP1, bound to its partner, p14. A complex with a critical role in endosomal map kinase signaling. *J. Biol. Chem.* *279*, 23422–23430.
- Lunin, V.V., Munger, C., Wagner, J., Ye, Z., Cygler, M., and Sacher, M. (2004b). The structure of the MAPK scaffold, MP1, bound to its partner, p14. A complex with a critical role in endosomal map kinase signaling. *J. Biol. Chem.* *279*, 23422–23430.
- Marusawa, H., Matsuzawa, S.-I., Welsh, K., Zou, H., Armstrong, R., Tamm, I., and Reed, J.C. (2003). HBXIP functions as a cofactor of survivin in apoptosis suppression. *Embo J.* *22*, 2729–2740.

- McCoy, A.J., Grosse-Kunstleve, R.W., Adams, P.D., Winn, M.D., Storoni, L.C., and Read, R.J. (2007). Phaser crystallographic software. *J Appl Crystallogr* 40, 658–674.
- Melegari, M., Scaglioni, P.P., and Wands, J.R. (1998). Cloning and characterization of a novel hepatitis B virus x binding protein that inhibits viral replication. *J. Virol.* 72, 1737–1743.
- Murshudov, G.N., Skubák, P., Lebedev, A.A., Pannu, N.S., Steiner, R.A., Nicholls, R.A., Winn, M.D., Long, F., and Vagin, A.A. (2011). REFMAC5 for the refinement of macromolecular crystal structures. *Acta Crystallogr. D Biol. Crystallogr.* 67, 355–367.
- Murzin, A.G., Brenner, S.E., Hubbard, T., and Chothia, C. (1995). SCOP: a structural classification of proteins database for the investigation of sequences and structures. *J. Mol. Biol.* 247, 536–540.
- Mylonas, E., and Svergun, D.I. (2007). Accuracy of molecular mass determination of proteins in solution by small-angle X-ray scattering. *J Appl Crystallogr.*
- Nada, S., Hondo, A., Kasai, A., Koike, M., Saito, K., Uchiyama, Y., and Okada, M. (2009). The novel lipid raft adaptor p18 controls endosome dynamics by anchoring the MEK-ERK pathway to late endosomes. *Embo J.* 28, 477–489.
- Orthaber, D., Bergmann, A., and Glatter, O. (2000). SAXS experiments on absolute scale with Kratky systems using water as a secondary standard. *Journal of Applied Crystallography.*
- Pearce, L.R., Komander, D., and Alessi, D.R. (2010). The nuts and bolts of AGC protein kinases. *Nat. Rev. Mol. Cell Biol.* 11, 9–22.
- Petoukhov, M.V., Franke, D., Shkumatov, A.V., Tria, G., Kikhney, A.G., Gajda, M., Gorba, C., Mertens, H.D.T., Konarev, P.V., and Svergun, D.I. (2012). New developments in the ATSAS program package for small-angle scattering data analysis. *J Appl Crystallogr* 45, 342–350.
- Powis, K., Zhang, T., Panchaud, N., Wang, R., Virgilio, C.D., and Ding, J. (2015). Crystal structure of the Ego1-Ego2-Ego3 complex and its role in promoting Rag GTPase-dependent TORC1 signaling. *Cell Res.* 25, 1043–1059.
- Sabatini, D.M., Erdjument-Bromage, H., Lui, M., Tempst, P., and Snyder, S.H. (1994). RAFT1: a mammalian protein that binds to FKBP12 in a rapamycin-dependent fashion and is homologous to yeast TORs. *Cell* 78, 35–43.
- Sancak, Y., Bar-Peled, L., Zoncu, R., Markhard, A.L., Nada, S., and Sabatini, D.M. (2010). Regulator-Rag complex targets mTORC1 to the lysosomal surface and is necessary for its activation by amino acids. *Cell* 141, 290–303.
- Sancak, Y., Peterson, T.R., Shaul, Y.D., Lindquist, R.A., Thoreen, C.C., Bar-Peled, L., and Sabatini, D.M. (2008). The Rag GTPases bind raptor and mediate amino acid signaling to

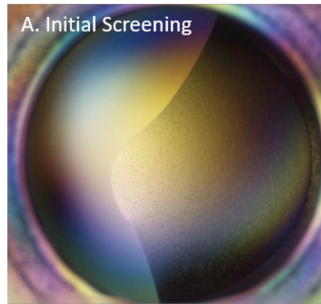
- mTORC1. *Science* 320, 1496–1501.
- Schrödinger, L. (2016). The PyMOL Molecular Graphics System, Version 1.8 Schrödinger, LLC.
- Stein, N. (2008). CHAINSAW: a program for mutating pdb files used as templates in molecular replacement. *J Appl Crystallogr.*
- Svergun, D.I. (1992). Determination of the regularization parameter in indirect-transform methods using perceptual criteria. *J Appl Crystallogr.*
- Vagin, A., and Teplyakov, A. (1997). MOLREP: an automated program for molecular replacement. *J Appl Crystallogr.*
- Waterman, D.G., Winter, G., Gildea, R.J., Parkhurst, J.M., Brewster, A.S., Sauter, N.K., and Evans, G. (2016). Diffraction-geometry refinement in the DIALS framework. *Acta Crystallogr D Struct Biol* 72, 558–575.
- Winn, M.D., Ballard, C.C., Cowtan, K.D., Dodson, E.J., Emsley, P., Evans, P.R., Keegan, R.M., Krissinel, E.B., Leslie, A.G.W., McCoy, A., et al. (2011). Overview of the CCP4 suite and current developments. *Acta Crystallogr. D Biol. Crystallogr.* 67, 235–242.
- Winter, G. (2009). xia2: an expert system for macromolecular crystallography data reduction. *J Appl Crystallogr.*
- Wong, Y.-H., Lee, T.-Y., Liang, H.-K., Huang, C.-M., Wang, T.-Y., Yang, Y.-H., Chu, C.-H., Huang, H.-D., Ko, M.-T., and Hwang, J.-K. (2007). KinasePhos 2.0: a web server for identifying protein kinase-specific phosphorylation sites based on sequences and coupling patterns. *Nucleic Acids Res.* 35, W588–W594.
- Xie, J., Ponuwei, G.A., Moore, C.E., Willars, G.B., Tee, A.R., and Herbert, T.P. (2011). cAMP inhibits mammalian target of rapamycin complex-1 and -2 (mTORC1 and 2) by promoting complex dissociation and inhibiting mTOR kinase activity. *Cell. Signal.* 23, 1927–1935.

ADDITIONAL SUPPLEMENTAL FIGURES

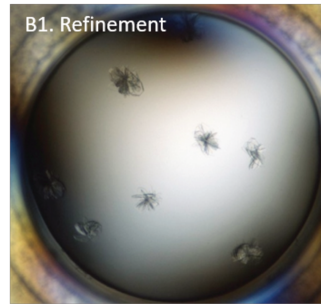
(These additional supplemental figures are not part of the submitted manuscript)



Supplemental Figure 1: Purification of the XPOF dimer. **A:** 15% SDS PAGE gel of elutions of His-C7orf59-HBXIP dimer through affinity purification. Total lysate was divided into two batches and protein was eluted using PBS 1X (pH 7.4) supplemented with 2 mM of β -mercaptoethanol, 5% glycerol and 300 mM imidazole. **B:** Gel filtration peak profile of C7orf59-HBXIP dimer, performed on a Superdex 200 column 16/60 (GE healthcare) connected to an AKTA FPLC system using 50 mM of Tris-HCl (pH 7.4) supplemented with 2 mM of β -mercaptoethanol, 5% glycerol and 100mM of NaCl. **C:** 15% SDS PAGE gel of gel filtration representing the eluted fractions. Fraction 46 to 55 were concentrated to 17 mg/ml and sent for crystallization. The Asterisk (*) represents an anomalous migration band of C7orf59, only observed when the sample is concentrated.



A. Initial Screening
4 M Sod. Formate
18 °C



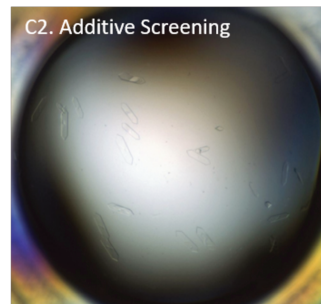
B1. Refinement
4 M Sod. Formate
3% Glycerol, 4°C



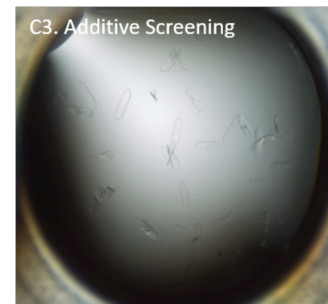
B2. Refinement
4 M Sod. Formate
5% Glycerol, 4°C



C1. Additive Screening
4 M Sod. Formate
5% Glycerol
0.01 M Barium Chloride, 18°C



C2. Additive Screening
4 M Sod. Formate
5% Glycerol
0.05 M Sod. Fluoride, 18°C



C3. Additive Screening
4 M Sod. Formate
5% Glycerol
4% 1-Propanol, 18°C

Supplemental Figure 2: Selected images of microcrystals from initial screening to mono 2D crystals of C7orf59 HBXIP heterodimer obtained from additive screening (Hampton Kit).

Chapter 3

Additional data on Ragulator complex and its subunits

INTRODUCTION

After optimizing the expression protocol of C7orf59-HBXIP heterodimer, the expression of full Ragulator complex was set up. The expression of p18 alone enhanced its degradation even in the presence of GST-tag but the co-expression of GST-p18 Δ N WT and C7orf59-HBXIP dimer led to the formation of trimer complex (**Chapter 2**). We tried to construct the pentameric complex by mixing the XPOF-p18 trimer and MP1-p14 dimer. We were able to obtain Ragulator complex after a gel filtration step, but due to the intrinsically unstable nature of p18, the complex went through subsequent degradation. Later, pull down experiments using the stop codon mutants of p18 explained the importance of full-length p18 for the formation of XPOF-p18 trimer complex (**consult Chapter 2**). This chapter depicts the efforts made to establish an understanding of the pentameric complex in parallel to the results described in Chapter 2. Here, we describe the protocol for the large-scale purification of XPOF-p18 trimer complex along with an overview of the structural analysis of Ragulator complex through crosslink and SAXS data. Although several experiments provide insight at how p18 peptides interact with other subunits of the complex, yet we refrain from predicting any structural model for the recombinant Ragulator complex in this dissertation.

MATERIALS AND METHODS

Expression vectors

Table 1 shows all the vectors used for the expression of subunits of Ragulator complex. His-C7orf59-HBXIP and GST-p18 Δ N-His-C7orf59-HBXIP trimer complex were cotransformed and coexpressed in *E. coli* BL21(DE3) while MP1-p14 dimer was expressed separately. Both the trimer and dimer subunits were expressed using 0.5 mM of IPTG as inducer in LB medium at 30° C for 16 hours at 200 rpm. GST-p18 Δ N-His-C7orf59-HBXIP trimer and His-C7orf59-HBXIP were always expressed in large volumes up to twenty litres (20L) due to low yield. Five litres (5L) expression of of MP1-p14 provided good yield.

Protein purification

Talon beads were used to purify both trimer and dimer subunits through affinity batch purification. PBS pH 7.4 (1X) with 5% glycerol, 2mM β -mercaptoethanol and 5mM of imidazole was used for resuspension of bacterial pellets. The resuspended lysate was supplemented with 1 mM PMSF and protease inhibitor cocktail (1X), incubated with lysozyme (0.1 mg.ml^{-1}) for 1 hour at 4°C on ice and later lysed by sonication (5 to 6 cycles of 15 seconds at 1 min interval apart). After sonication step, the lysates were centrifuged at 16000 g for 1 hour at 4°C . The cleared lysates were incubated with resin for 2 to 3 hours. Later, lysates were centrifuged at 650 rpm at 4°C to remove the flow through. The talon beads were washed five times with the resuspension buffer and proteins were eluted with PBS pH 7.4 (1X) supplemented with 300 mM imidazole, 5% glycerol and 2mM β -mercaptoethanol. For the assembly of pentameric Ragulator complex, both dimer and trimer complexes were mixed and concentrated together. The concentrated sample was passed through Superdex 200 column 16/60 (GE) connected to an AKTA FPLC system using 50 mM Tris-HCl (pH 7.4) supplemented with 2 mM β -mercaptoethanol, 5% glycerol and 100mM NaCl.

Crosslinking, SAXS, mutagenesis and pull down analysis of the pentamer

Consult **Chapter 2** for methods.

RESULTS AND DISCUSSION

Strategy for complex assembly

We developed a strategy to assemble pentameric Ragulator *in vitro* from the combination of MP1-p14 dimer and XPOF-GST-p18 Δ N trimer. As reported in Chapter 2, we had found that only the XPOF dimer, and not MP1-p14, can stabilize p18 against degradation. The formation of the pentamer was confirmed by size exclusion using the samples **A** and **B** of **Figure 3.1**. The pentamer peak is actually a dimer of pentamers due to the presence of GST, which forms a dimer. Surprisingly, it also showed the formation of a tetramer His-C7orf59-HBXIP + MP1-p14 (**Figure 3.2A**) which is a completely new information. We assumed that the tetramer complex does not exist based on the previously published data (Bar-Peled et al., 2012). However, the bands observed in the analysis of the fractions by SDS-PAGE indicate the presence of the MP1, p14, C7orf59 and HBXIP proteins, but not of GST-p18 Δ N WT. Mass spectrometric analysis of the sample revealed two peptides from p18 in the assumed tetramer. Peptide sequence VDAKEELVVQFGIP, which corresponds to the C-terminal of p18 (148-161

a.a) and RLAVLSSSLTHW (91-102 a.a) were found in the tetramer complex. The identification of peptides in the tetramer sample indicated that the tetramer is a proteolytically modified pentamer, and not a complex of the two dimers only. To verify that the “tetramer” formation requires p18, a sample of only the two dimers XPOF and MP1-p14 combined was analysed by size exclusion under the same conditions (data not shown), which did not lead to the formation of tetramer. The data suggest that the tetramer is actually a version of the pentamer with attached p18 peptides; however, due to the small size of these p18 fragments, the sample was still treated as a tetramer in the SAXS analyses.

Large-scale purification of GST-p18 Δ N–C7orf59-HBXIP trimer

As reported in **Chapter 2**, the GST-p18 Δ N–C7orf59-HBXIP trimer undergoes spontaneous proteolysis and dissociation, resulting in a sample which appears to be a dimer but still has a p18-derived peptide associated with it. This appears to be analogous to the tetramer originating from the pentamer, as described above. Considering that spontaneous proteolysis can remove flexible regions and sometimes promote crystallization, we developed a large-scale purification protocol for this trimer-derived “dimer” to obtain samples for crystallization assays. We chose Talon beads over Glutathione resin (GST beads) to carry out the large-scale affinity purification of trimer complex to promote enrichment of full-length p18, which is associated with the XPOF dimer, by capturing his-tagged C7orf59 instead of GST-tagged p18. Use of Talon beads to pool only dimer bound GST-p18 Δ N WT, later on proved to be a better strategy. The dimer purification protocol was used for the affinity purification and size exclusion/gel filtration of trimer complex. Due to intrinsic proteolysis of p18, the gel filtration protocol needs further optimization. **Figure 3.3** shows the affinity purification and gel filtration chromatogram of the injected trimer. Fractions from both trimer and dimer peak are shown in **Figure 3.4**. The dimer complex that was the product of the subsequent degradation of trimer was sent for mass spectrometry analysis. As suspected peptides of p18 were found in the sample. The p18 peptide bound dimer complex has been subjected to initial crystallization screening (data not shown). Microcrystals were obtained from initial screening, the crystallization condition may require several refinement cycles.

GST-p18 Δ N LAKTA_AAAAA mutant does not interact with MP1-p14

To further explore the results shown in chapter 2 for the LAKTA-AAAAA mutant, we decided to evaluate the effect of mutation in the LAKTA region of p18 in its binding to MP1-p14 by combining this p18 mutation with stop codons at K103 and L108, which were previously

shown to increase the detection of p18 interaction with MP1-p14. We performed a pull down experiment using GST-p18 Δ N LAKTA_AAAAA (K103 stop codon) and GSTp18 Δ N LAKTA_AAAAA (L108 stop codon) with His-MP-p14 WT. **Figure 3.5 A** shows that these mutants continue to interact with MP1-p14 dimer, while GSTp18 Δ N LAKTA_AAAAA (WT) mutant did not show any binding to MP1-p14 just like GSTp18 Δ N WT (**Figure 3.5 B**).

SAXS data analysis

The fractions obtained from size exclusion (**Figure 3.2**) were subjected to small angle X-rays scattering technique (SAXS) at the SAXS1 beamline of LNLS to determine the overall low-resolution molecular envelopes of the complexes. Considering the sensitivity of SAXS data collection process and to ensure the quality of the collected data, fresh samples were purified and used on the same day. The fractions considered as “tetramer” were monodisperse (especially fraction 22 which was used in the analysis) and with good signal to noise ratio, contrasting with the peak of intact pentamer containing GST which showed signs of aggregation. **Figure 3.6** shows the scattering curves, Guinier Region, Krakty plot and distance distribution function of the tetramer (fraction 22 shown in **Figure 3.2 A**). The Krakty plot indicates a compact and well-folded shape. The calculated parameters for the tetramer were Rg 2.93 nm and Dmax 10.04 nm. The molecular weight calculated as the Porod volume divided by 1.6 was 51.4, which agreed well with the molecular weight calculated from the sequences of the four subunits MP1, p14, HBXIP and C7orf59 (50.9 kDa). We superimposed all SAXS data of tetramer over data from XPOF and MP1-p14 samples to highlight the increased size of the tetramer complex through distance distribution function (**Figure 3.7**). The distance distribution function indicates a prolate ellipsoid shape. Due to the lack of a reliable model of the pentamer, it was not possible to fit a model in the SAXS envelope.

Crosslinking evidence

In addition to XPOF dimer and its complex with p18, the protein samples used for the assembly of pentamer were also sent for crosslink coupled-mass spectrometric analysis using DSS to our collaborator Prof. Dr. Fabio Gozzo (IQ-Unicamp). Two MP1-p18 lysine crosslinks were detected in the pentamer, in addition to a p18 intramolecular crosslink. A search for serine crosslinks identified MP1-HBXIP, p14-HBXIP, and p18-C7orf59 crosslinks. The limited number of crosslinks involving MP1 and p14 prevented any conclusion about the three dimensional arrangement of the Regulator subunits. **Table 2 (Chapter 3)** shows the detected

crosslinks within the subunits of Ragulator complex. For detailed protocol of crosslink and mass spectrometry experiment, consult **Chapter 2**.

Table 1: List of all the vectors used for expression of subunits of Ragulator complex and for the preparation of mutant clones.

VECTOR	RESISTANCE	FUSION TAG	PROTEASE RECOGNITION	SOURCE
PET-302-p18ΔN	Ampicillin	His, N-term	--	D.M. Sabatini
PGEX-4T3-p18ΔN	Ampicillin	GST, N-term	thrombin	This Project
PET28A-MP1-p14	Kanamycin	His, C-term (MP1)	--	T. Clausen
PET-DUET- C7orf59-HBXIP (LONG)	Ampicillin	His, N-term (C7orf59)	PreScission	D. Sabatini
PET-DUET-C7orf59-HBXIP (SHORT)	Ampicillin	His, N-term (C7orf59)	PreScission	D. Sabatini
PACYC-DUET- C7orf59-HBXIP (SHORT)	chloramphenicol	His, N-term (C7orf59)	PreScission	This Project

Table 2: List of detected crosslink in the pentameric Ragulator.

Protein 1			Protein 2		
Peptide sequence	Subunit	Cross-linked Residue	Peptide sequence	Subunit	Cross-linked Residue
TDEQALLSSILAKTASNIIDVSAADSQGMEQHEYMDR	p18	Lys 60	KLLLDPPSPPTK	p18	Lys 20
TDEQALLSSILAKTASNIIDVSAADSQGMEQHEYMDR	p18	Lys 60	FLYKK	MP1	Lys 12
KLPLPLSLTSQPHQVLASEPIPFSDLQQVSR	p18	Lys 104	FLYKK	MP1	Lys 12
GTLSDEHAGVISVLAQQAAKLTSDPDIPVVCLESDNGNIMIQ KHDGITVAVHK	HBXIP	Lys 78	AQALVQYLEEPLTQVAAS	p14	Ser 125
LPPLPLSLTSQPHQVLASEPIPFSDLQQVSR	p18	Ser 110	GMNVPFKR	C7orf59	Lys 64
LPSVEGLHIVVSDR	MP1	Ser 15	HDGITVAVHKMAS	HBXIP	Lys 88

FIGURES

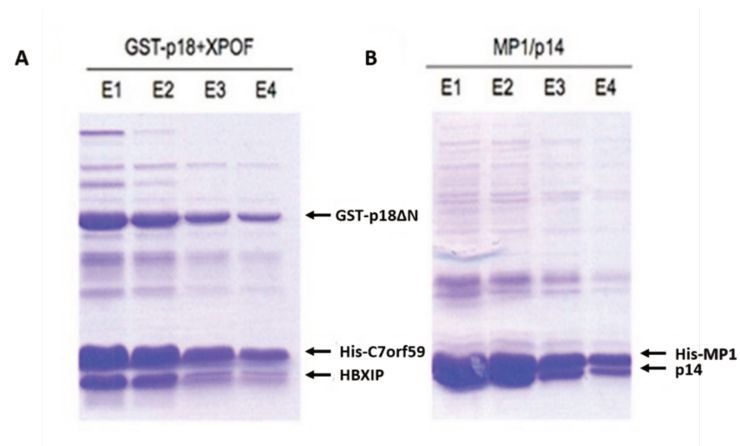


Figure 3.1: 16% SDS acrylamide gel showing elutions from affinity purification of GST-p18ΔN WT + His-C7orf59-HBXIP trimer and His-MP1-p14 dimer. Talon beads were used for the affinity purification. The elutions from both trimer and dimer were later mixed and concentrated together and subjected to size exclusion chromatography.

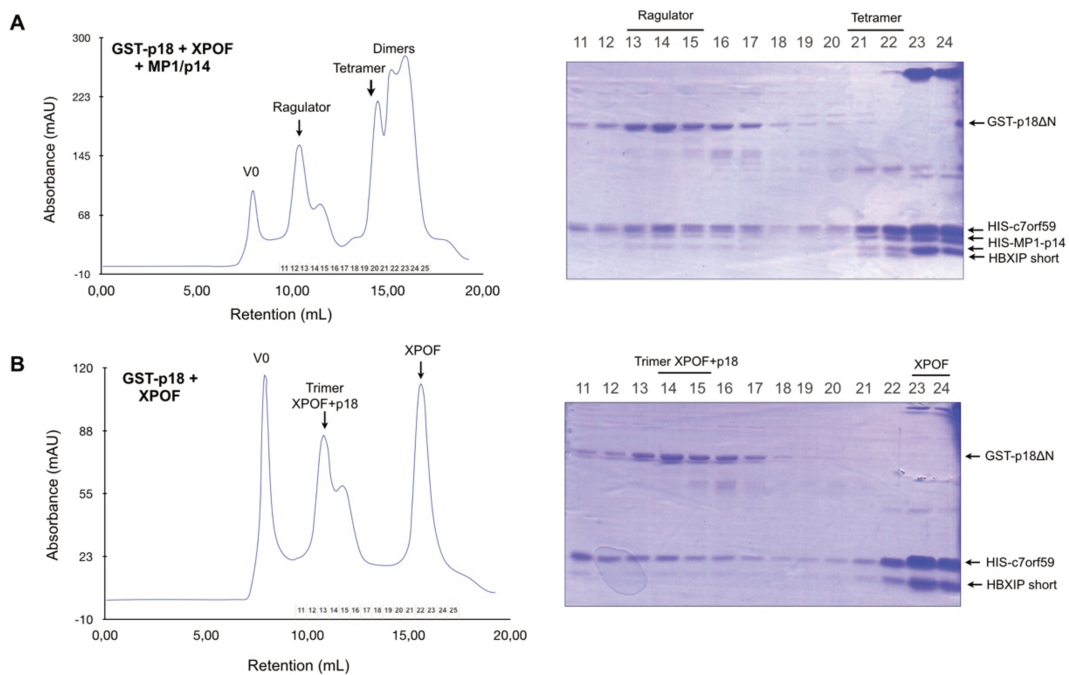


Figure 3.2: A- Size exclusion chromatography of pentameric Ragulator starting from the affinity purification of the dimer-MP1-p14 and XPOF-GST-p18ΔN (left) and 16% SDS PAGE analysis of the fractions eluted from gel filtration column. Peptides of p18 within the tetramer complex were only detected by mass spectrometry. B- Control run of size exclusion chromatography showing XPOF-GST-p18ΔN trimer and its subsequent degradation leading to XPOF dimer, using the same trimer sample

that was used for the assembly of pentamer showed above (left panel). Right panel: 16% SDS-PAGE analysis of the trimer and dimer fractions.

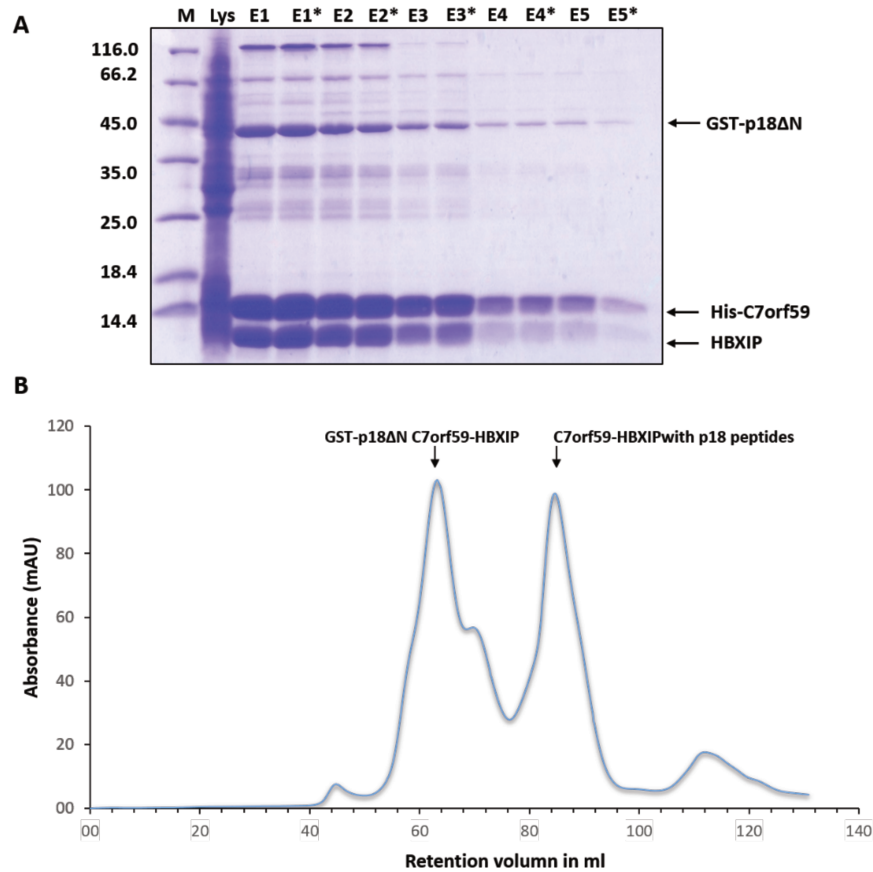


Figure 3.3: **A**-Affinity purification of GST-p18 Δ N WT-C7orf59-HBXIP trimer. Due to large amount of lysate, sample was divided into two batches before carrying out washing and elution steps. Samples were run on 15% SDS acrylamide gel. **B**-Gel filtration of GST-p18 Δ N WT-C7orf59-HBXIP trimer (His-cleaved) and its subsequent degradation leading to XPOF dimer formation. p18 peptides were only found in the dimer sample through mass spectrometry analysis.

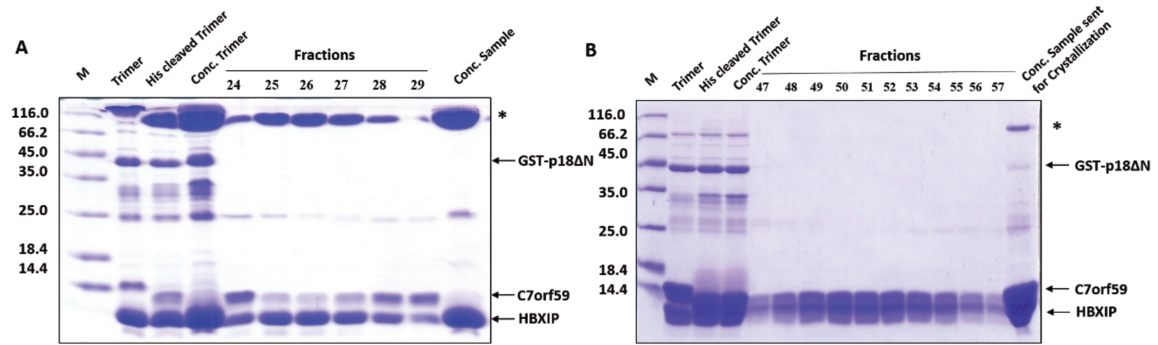


Figure 3.4: **A-**15% SDS acrylamide gel demonstrating GST-p18 Δ N WT-C7orf59-HBXIP trimer fractions. Shift in the migration pattern of C7orf59 can be seen due to His-tag cleavage. Asterisk represents an anomalous band that only appears when dimer complex is concentrated. **B-** His-cleaved fractions of dimer peak. The fractions were concentrated and sent for initial crystallization screening.

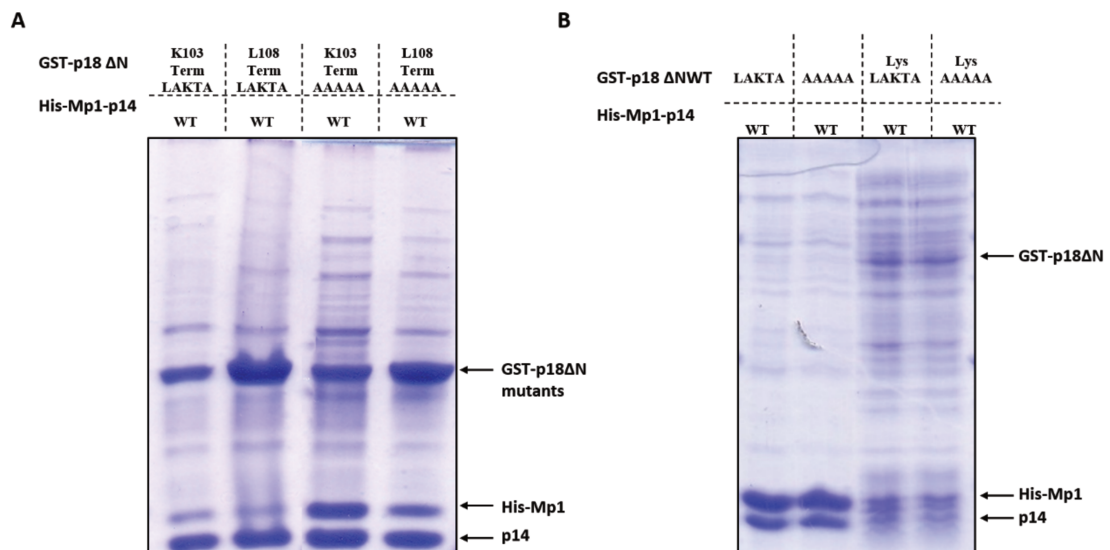


Figure 3.5: **A-** His-MP1-p14 dimer continues to interact with GSTp18 Δ N K103 and L103 stop codon mutants independent of LAKTA site mutation. **B-** While MP1-p14 dimer does not show any significant binding to GST-p18 Δ N WT irrespective of AAAAA mutation inserted in the LAKTA region of GST-p18 Δ N WT. Both pull down experiments were performed using Talon resin.

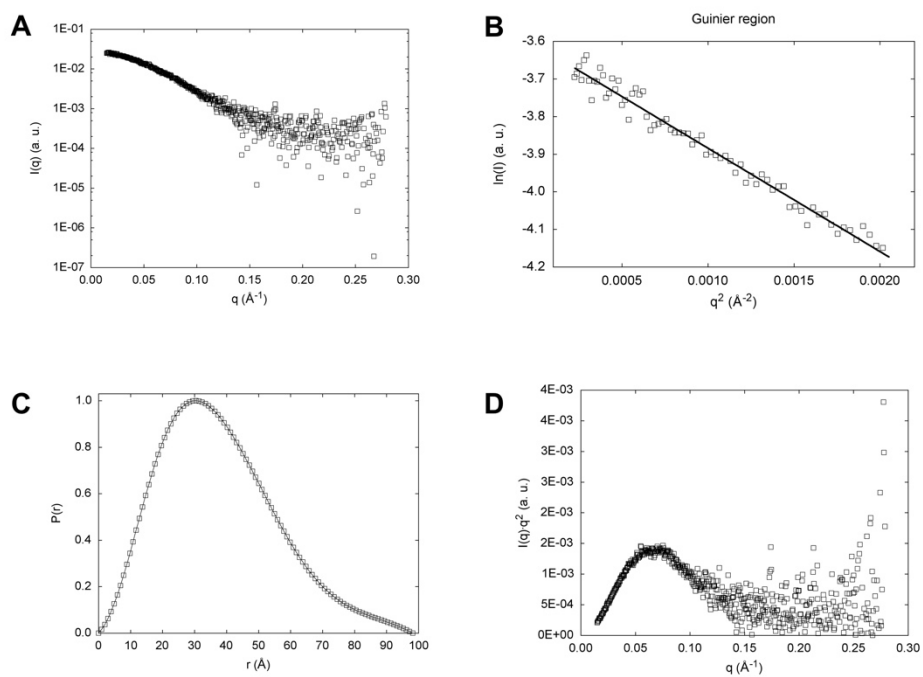


Figure 3.6: Small angle X-ray scattering analysis of the XPOF-MP1-p14 tetramer bound to p18-derived peptide, obtained from spontaneous dissociation of the XPOF-MP1-p14-GST-p18 Δ N pentamer. **A:** Scattering curve. **B:** Guinier region. **C:** Distance distribution function $p(r)$. **D:** Kratky plot.

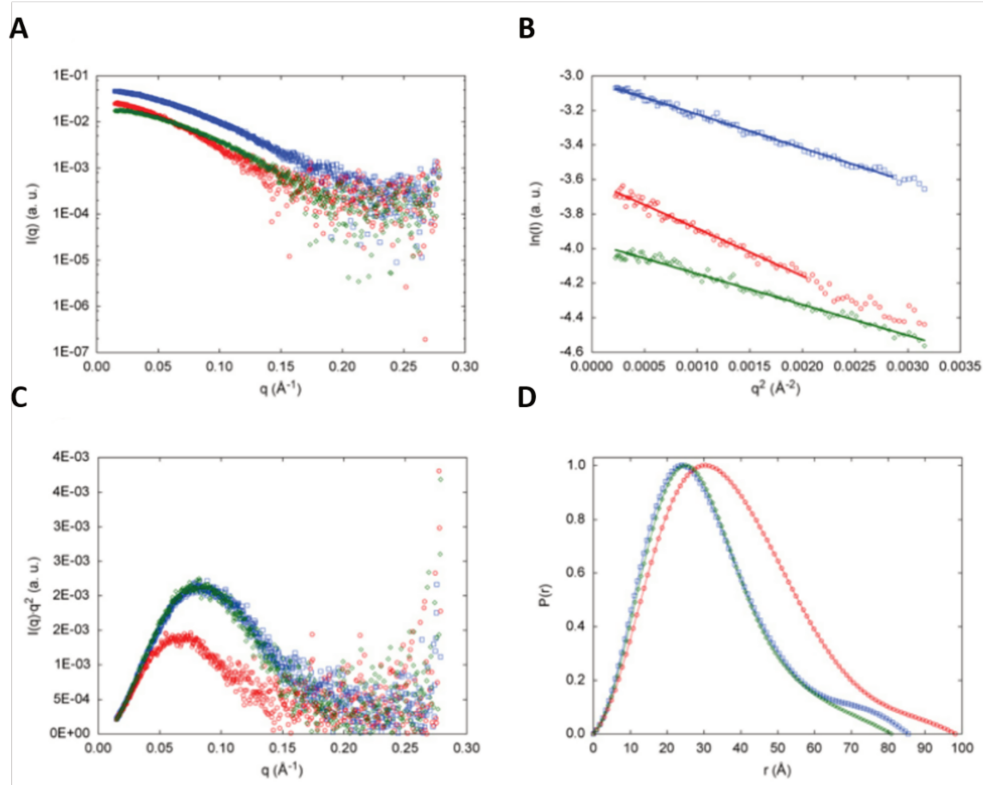


Figure 3.7: SAXS data analysis panel for MP1/p14 (green), C7orf59-HBXIP (blue) and tetramer C7orf59-HBXIP + MP1/p14 (red); **A-** Scattering Curve; **B-** Guinier region; **C-** Kratky Plot; **D-** distance distribution function $p(r)$.

Chapter 4

CONCLUSION AND FUTURE DIRECTIONS

Over the last few years, the understanding of the mTORC1 pathway through amino acid signaling has expanded in an exponential manner. The identification of several components of the pathway through cell culture, biochemical techniques and mass spectrometry has provided valuable information about the regulatory mechanisms of the pathway. The crystal structures of some of components of the pathway has facilitated the process of discovering their molecular activity through which amino acids are sensed and later how this signal leads to the translocation of mTORC1 to lysosomes. The signal propagation mechanism involves Rag GTPases. The activation of Rag GTPases heavily depends upon the integrity of the Ragulator complex, which consists of MP1, p14, p18, HBXIP and C7orf59. The Ragulator complex displays an important regulatory role in the activation of mTORC1 at lysosomal surface. The crystal structures of MP1, p14 and HBXIP are already available. In this thesis, we present the crystal structure of C7orf59-HBXIP heterodimer (named XPOF for simplicity) at 2.95 Å resolution. The unstructured N-terminal of C7orf59 links back to the evolutionary conservation of some of the structural features within the regulatory constituents of the TOR pathway in yeast.

Before solving the crystal structure of the dimer, we had relied on a computational model to interpret and guide our findings (**Figure 4.1**), including results from crosslinking/mass spectrometry and site-directed mutagenesis. Although this model had correctly predicted most of the features about the fold of C7orf59 and interface of the dimer, analysis of crystal structure of XPOF dimer revealed a new set of information that could not be observed in the computational model, including important differences in the conformation of the N-terminus and *b3* loop of C7orf59 as well as in the positions of specific residues (**Figure 4.2** and **4.3**).

The crystal structure of XPOF not only displays the same fold as MP1-p14, but it also demonstrates a putative intersubunit key-lock motif. In the crystal structure of MP1-p14, two hydrophobic residues Leu63 and Leu65 of MP1 interact with the p14 residues Ile48, Ile52, Met74, Val81, Ile83, and Tyr94, which form a hydrophobic pocket. Kurzbauer et al referred to this hydrophobic pocket as *2b* pocket (Kurzbauer et al., 2004). In the crystal structure of XPOF, the key-lock motif constitutes of *b3** loop of C7orf59 inclining towards *2b* pocket of HBXIP just like the structurally equivalent *b3* loop of MP1 pointing towards *2b* pocket of p14. Although many of the side chains are barely visible in the electron density due to low data quality, some residues such as Phe53 in *b3** loop of C7orf59 and His41 and His87 of HBXIP that form the

edges of the hydrophobic *2b* pocket, display good electron density in the crystallography data, probably as a consequence of their tight packing in the interface. Although Asn71 of HBXIP lies in the region with less defined electron density, yet we tend to assume that this residue is likely to make hydrogen bond with Arg54 of C7orf59 in regards to their close proximity with each other. Interestingly, side chain of Arg54 of C7orf59 presents an odd angle within the *b3** loop, which in case of the absence of *2b* pocket of HBXIP would be facing the solvent suggesting that the *2b* pocket of HBXIP is protecting the Arg54 of C7orf59 from solvent access. The computational model did predict the right fold and helical and β -sheet interfaces for the heterodimer but the presence of this hydrophobic key-lock motif was only observed in the crystal structure. The *in silico* model of the heterodimer showed both loops on either side of helical interface to be away from each other. This conformational behaviour of the flanking loops can also be observed in the homodimer of HBXIP (**Figure 4.4**).

The C7orf59-HBXIP heterodimer is remarkably different from the crystal structure of HBXIP homodimer due to the presence of unstructured N-terminal of C7orf59 and the intersubunit hydrophobic key-lock motif. In the HBXIP homodimer, the equivalent *b3* loop of a monomer is seemingly less hydrophobic which would not fit within the *2b* hydrophobic pocket of dimerization partner (**Figure 4.5**). These differences suggest the likelihood of the prevalent existence of heterodimer over homodimer under physiological conditions, which could further be proved through future studies.

The orientation of the key-lock motif and the presence of a well-defined pocket in HBXIP to accommodate C7orf59 loop *b3* also strongly points at the possibility of this interface being druggable. We aim to perform site directed mutagenesis to demonstrate the importance of this interface for the stability of the heterodimer, by mutating Arg54 and Phe53 to alanine and performing pulldowns with recombinant proteins.

Generally, only conserved residues are considered important for the stability and functional activity of the protein. Our observation regarding XPOF structure presents an unconventional case. The subunits of Ragulator complex do share similar fold with their yeast orthologs but they lack sequence homology. Additionally, the putative yeast orthologs for C7orf59 and HBXIP are yet to be fully characterized as members of EGO complex. This study revealed that C7orf59 appears as Ego2 with a distinct unstructured N-terminal region. Contrary to the heterodimer of C7orf59-HBXIP, Ego2 forms a homodimer that led us to assume that hypothetically during evolution MP1-p14 might be the first to evolve as a heterodimer with a much-conserved dimer interface, on the other hand, C7orf59 evolved later as dimerization partner of HBXIP. It is considerable to understand that the subunits of Ragulator complex might

have gone through structural modifications to support the cellular organizational complexity during evolutionary changes.

In the beginning of the project, based on the computational model, we assumed that sequence conservation was critical to find important residues in the dimer interface as well as the dimer-p18 interface. We designed E34A_N35A and D36A_E37A C7orf59 double mutants based on the high sequence conservation of these residues. These mutants neither affected the stability of the heterodimer nor its interaction with p18. Another conserved residue, Ser67 in C7orf59, was mutated to Aspartate to mimic phosphorylation. This mutation showed significant difference in terms of interaction with p18, but not HBXIP. Later, by solving the crystal structure it became clear that these residues lie close to the HBXIP *b3* loop - C7orf59 *2b* pocket interface, which has a pseudo-symmetric relationship with the C7orf59 *b3* loop - HBXIP *2b* pocket, which is a less conserved interface, yet appears to be more important for the stability of the heterodimer.

The expression of recombinant XPOF in *E. coli* BL21(DE3) did not lead to high yield and the purification protocol needed a lot of optimization. Later, we also faced difficulties in crystallizing the complex. Several attempts led to 2D monocrystals, which were sent to Diamond Synchrotron Light Source for X-ray diffraction. The presence of 4M sodium formate in the crystallization condition could work as cryoprotectant, therefore further treatment with better cryoprotectants were avoided due to the fragile nature of crystals. After long sought analysis of diffraction data with low defined electron density in certain regions of the heterodimer, we still managed to gain some structural insight into the critical regions of the heterodimer. Further investigation in finding the scope of the unstructured N-terminal along with the putative druggable hydrophobic *b3** loop-*2b* pocket of XPOF heterodimer in the assembly of Ragulator complex is beyond the timeframe associated with this dissertation.

In this project, we also studied the p18 interaction pattern with XPOF and MP1-p14 dimers. Intriguingly, deletion of a C-terminal region of p18 abrogated its interaction with XPOF, while the same type of deletion promoted the interaction with MP1-p14, likely due to the increased stability of C-terminally deleted p18. We have tried to develop a protocol for the purification of GST-p18-C7orf59-HBXIP trimer complex. Due to low yield of trimer, the protocol requires adjustments to accommodate the intrinsic proteolysis of p18.

Recently, we have also found an important piece of information regarding the possible involvement of PKA in the regulation of mTORC1 activity through Ragulator complex. The hypothesis of PKA regulation came from the observation that the conserved Ser67 of C7orf59, which we found to be important for p18 binding, is a potential PKA phosphorylation site.

Mutation of this residue to Aspartate inserts a negative charge, which mimics the presence of phosphate group and results in partial dissociation of p18 in a pulldown assay with recombinant proteins. The results documented in **Chapter 2** of this dissertation demonstrate the changes in the interaction pattern of the subunits of Ragulator complex and RagA GTPase when treated with PKA modulators such as Forskolin (PKA activator) and H-89 (PKA inhibitor), as well as subcellular redistribution of endogenous C7orf59 in U2OS cells upon H-89 treatment. These results clearly showed that PKA activation results in dissociation of the Ragulator complex. However, it is not clear at this point if this effect is mediated by phosphorylation of C7orf59 on Ser67, as mutations on this site seemed to behave in the same way as the wild type protein (data not shown). Future experiments, including in vitro phosphorylation of Ragulator subunits with PKA, detection of phosphorylation events by mass spectrometry and design of additional mutations should clarify this issue. Considering the fact that mTORC1 controls multiple anabolic activities of the cell, the crosstalk with a major catabolic pathway such as PKA signaling may likely be involved in the regulation of mTOR. Hopefully, future experiments would increase our understanding of the prospects of PKA involvement in mTORC1 activity through Ragulator complex.

FIGURES

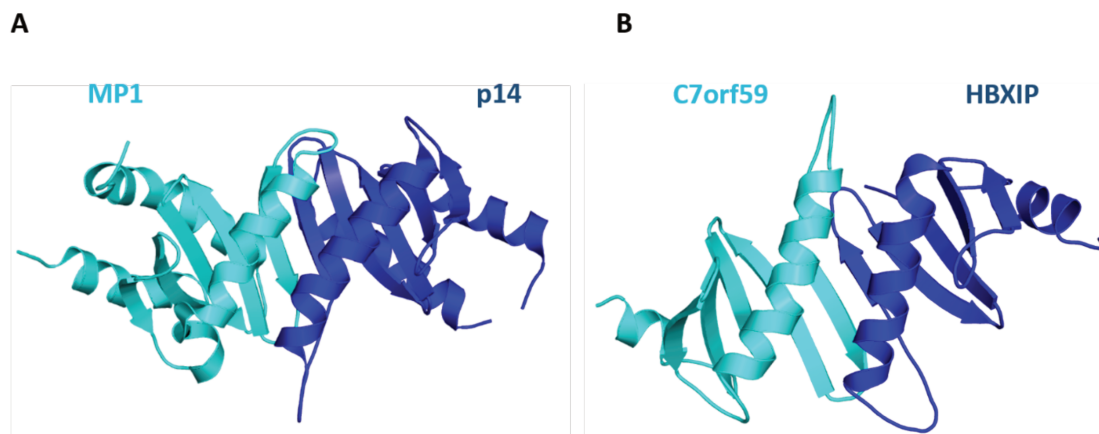


Figure 4.1: **A-**The Structure of MP1 and p14. MP1 forms a stable heterodimer with p14 (Kurzbaue et al., 2004). **B -** Predicted structural model of the dimer C7orf59-HBXIP. The structural model of C7orf59 was obtained through the QuickPhyre server and docking was done using ClusPro server. The model suggests the presence of roadblock domain.

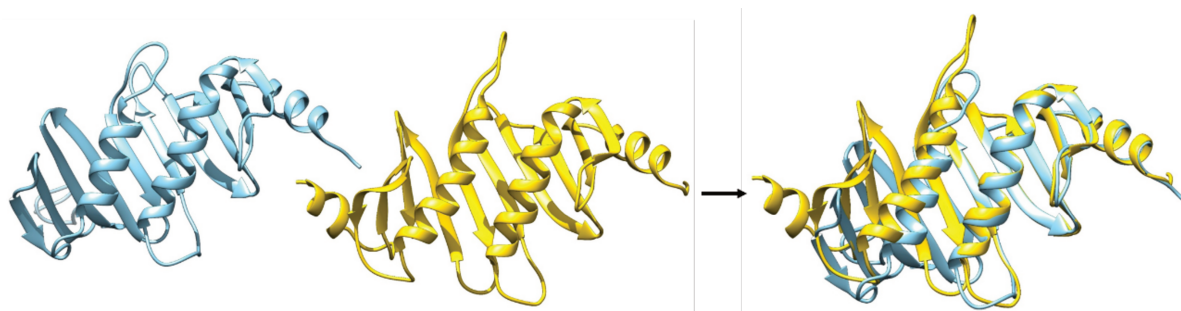


Figure 4.2: Superposition of crystal structure of XPOF (in light blue) over predicted structural model of the dimer (in golden yellow).

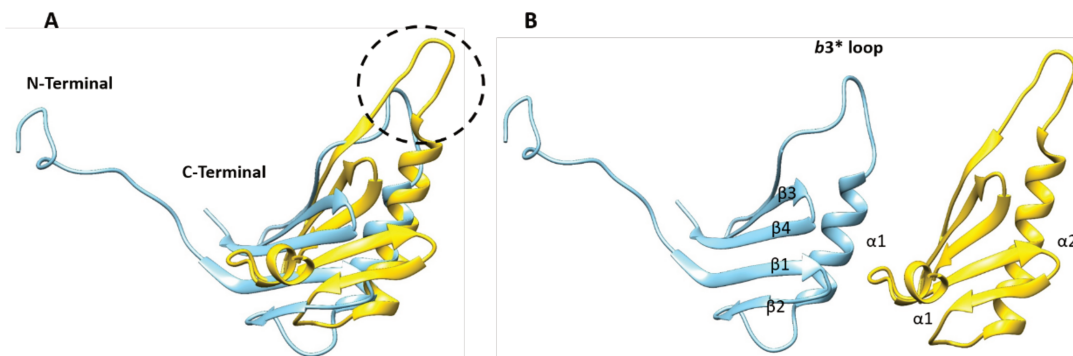


Figure 4.3: A-Superposition of crystal structure of C7orf59 (in light blue) over *in silico* model of C7orf59 (in golden yellow). B-Unstructured N-Terminal, change in the helix size and variations in the orientation of $b3^*$ loop are evident.

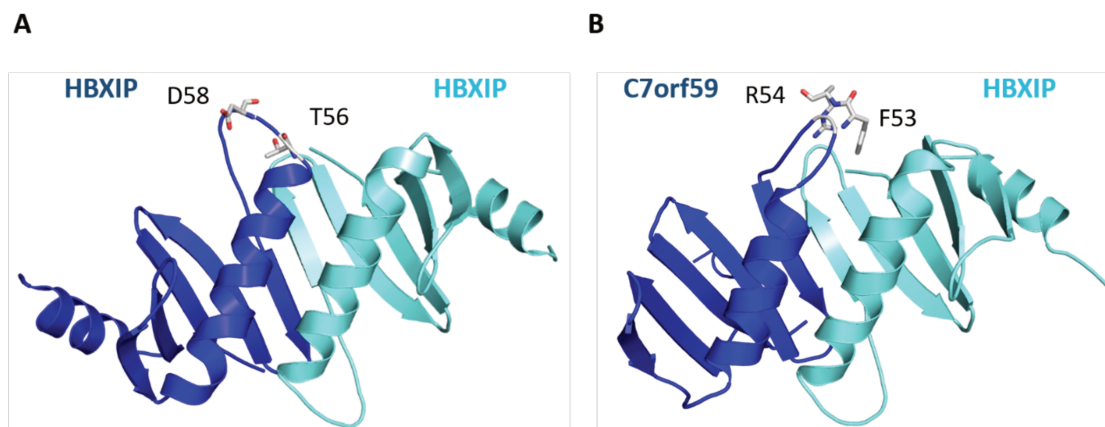


Figure 4.4: A- Crystal structure of HBXIP homodimer. B- Crystal structure of C7orf59-HBXIP heterodimer. Variation in the orientation of $b3$ loop residues can be observed in both structures.

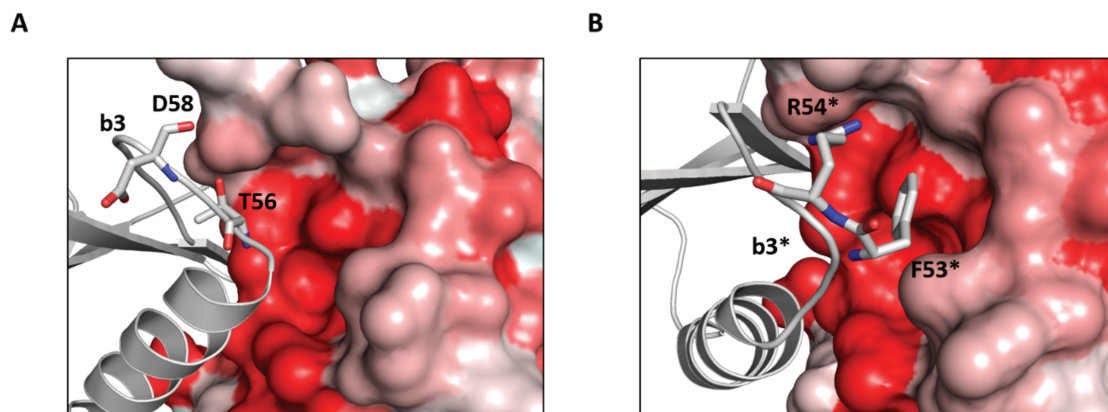


Figure 4.5: **A-**Surface view representation of hydrophobic *2b* pocket of HBXIP and important residues of *b3* loop can be observed deviating away from the pocket formed by the dimerization partner in the crystal structure of HBXIP homodimer. **B-** F53 and R54 of *b3** loop residues of C7orf59 inclining towards the hydrophobic *2b* pocket of HBXIP in the crystal structure of XPOF.

REFERENCES

- Adams, P.D., Afonine, P.V., Bunkóczi, G., Chen, V.B., Davis, I.W., Echols, N., Headd, J.J., Hung, L.-W., Kapral, G.J., Grosse-Kunstleve, R.W., et al. (2010). PHENIX: a comprehensive Python-based system for macromolecular structure solution. *Acta Crystallogr. D Biol. Crystallogr.* *66*, 213–221.
- Afonine, P.V., Grosse-Kunstleve, R.W., Echols, N., Headd, J.J., Moriarty, N.W., Mustyakimov, M., Terwilliger, T.C., Urzhumtsev, A., Zwart, P.H., and Adams, P.D. (2012). Towards automated crystallographic structure refinement with phenix.refine. *Acta Crystallogr. D Biol. Crystallogr.* *68*, 352–367.
- Alain, T., Morita, M., Fonseca, B.D., Yanagiya, A., Siddiqui, N., Bhat, M., Zammit, D., Marcus, V., Metrakos, P., Voyer, L.A., et al. (2012). eIF4E/4E-BP Ratio Predicts the Efficacy of mTOR Targeted Therapies. *Cancer Res.* *72*, 6468–6476.
- Arsham, A.M., Howell, J.J., and Simon, M.C. (2003). A novel hypoxia-inducible factor-independent hypoxic response regulating mammalian target of rapamycin and its targets. *J. Biol. Chem.* *278*, 29655–29660.
- Ashkenazy, H., Erez, E., Martz, E., Pupko, T., and Ben-Tal, N. (2010). ConSurf 2010: calculating evolutionary conservation in sequence and structure of proteins and nucleic acids. *Nucleic Acids Res.* *38*, W529–W533.
- Aylett, C.H.S., Sauer, E., Imseng, S., Boehringer, D., Hall, M.N., Ban, N., and Maier, T. (2016). Architecture of human mTOR complex 1. *Science* *351*, 48–52.
- Bar-Peled, L., Chantranupong, L., Cherniack, A.D., Chen, W.W., Ottina, K.A., Grabiner, B.C., Spear, E.D., Carter, S.L., Meyerson, M., and Sabatini, D.M. (2013). A Tumor suppressor complex with GAP activity for the Rag GTPases that signal amino acid sufficiency to mTORC1. *Science* *340*, 1100–1106.
- Bar-Peled, L., Schweitzer, L.D., Zoncu, R., and Sabatini, D.M. (2012). Ragulator Is a GEF for the Rag GTPases that Signal Amino Acid Levels to mTORC1. *Cell* *150*, 1196–1208.
- Baretić, D., Berndt, A., Ohashi, Y., Johnson, C.M., and Williams, R.L. (2016). Tor forms a dimer through an N-terminal helical solenoid with a complex topology. *Nat Commun* *7*, 11016.
- Ben-Sahra, I., Howell, J.J., Asara, J.M., and Manning, B.D. (2013). Stimulation of de novo pyrimidine synthesis by growth signaling through mTOR and S6K1. *Science* *339*, 1323–1328.
- Benjamin, D., Colombi, M., Moroni, C., and Hall, M.N. (2011). Rapamycin passes the torch: a new generation of mTOR inhibitors. *Nature Publishing Group* *10*, 868–880.

- Bentzinger, C.F., Romanino, K., Cloëtta, D., Lin, S., Mascarenhas, J.B., Oliveri, F., Xia, J., Casanova, E., Costa, C.F., Brink, M., et al. (2008). Skeletal muscle-specific ablation of raptor, but not of rictor, causes metabolic changes and results in muscle dystrophy. *Cell Metabolism* 8, 411–424.
- Bernardi, R., Guernah, I., Jin, D., Grisendi, S., Alimonti, A., Teruya-Feldstein, J., Cordon-Cardo, C., Simon, M.C., Rafii, S., and Pandolfi, P.P. (2006). PML inhibits HIF-1 α translation and neoangiogenesis through repression of mTOR. *Nature* 442, 779–785.
- Binda, M., PEli-Gulli, M.-P., Bonfils, G., Panchaud, N., Urban, J., Sturgill, T.W., Loewith, R., and De Virgilio, C. (2009). The Vam6 GEF controls TORC1 by activating the EGO complex. *Mol. Cell* 35, 563–573.
- Boussif, O., Lezoualc'h, F., Zanta, M.A., Mergny, M.D., Scherman, D., Demeneix, B., and Behr, J.P. (1995). A versatile vector for gene and oligonucleotide transfer into cells in culture and in vivo: polyethylenimine. *Proc. Natl. Acad. Sci. U.S.a.* 92, 7297–7301.
- Brown, E.J., Albers, M.W., Shin, T.B., Ichikawa, K., Keith, C.T., Lane, W.S., and Schreiber, S.L. (1994). A mammalian protein targeted by G1-arresting rapamycin-receptor complex. *Nature* 369, 756–758.
- Bunkóczi, G., and Read, R.J. (2011). Improvement of molecular-replacement models with Sculptor. *Acta Crystallogr. D Biol. Crystallogr.* 67, 303–312.
- Cafferkey, R., Young, P.R., McLaughlin, M.M., Bergsma, D.J., Koltin, Y., Sathe, G.M., Faucette, L., Eng, W.K., Johnson, R.K., and Livi, G.P. (1993). Dominant missense mutations in a novel yeast protein related to mammalian phosphatidylinositol 3-kinase and VPS34 abrogate rapamycin cytotoxicity. *Mol. Cell. Biol.* 13, 6012–6023.
- Chantranupong, L., Scaria, S.M., Saxton, R.A., Gygi, M.P., Shen, K., Wyant, G.A., Wang, T., Harper, J.W., Gygi, S.P., and Sabatini, D.M. (2016). The CASTOR Proteins Are Arginine Sensors for the mTORC1 Pathway. *Cell*.
- Chantranupong, L., Wolfson, R.L., Orozco, J.M., Saxton, R.A., Scaria, S.M., Bar-Peled, L., Spooner, E., Isasa, M., Gygi, S.P., and Sabatini, D.M. (2014). The Sestrins Interact with GATOR2 to Negatively Regulate the Amino-Acid-Sensing Pathway Upstream of mTORC1. *Cell Reports*.
- Chiu, M.I., Katz, H., and Berlin, V. (1994). RAPT1, a mammalian homolog of yeast Tor, interacts with the FKBP12/rapamycin complex. *Proc. Natl. Acad. Sci. U.S.a.* 91, 12574–12578.
- Choo, A.Y., Yoon, S.-O., Kim, S.G., Roux, P.P., and Blenis, J. (2008). Rapamycin differentially inhibits S6Ks and 4E-BP1 to mediate cell-type-specific repression of mRNA translation. *Proceedings of the National Academy of Sciences* 105, 17414–17419.

- Comeau, S.R., Gatchell, D.W., Vajda, S., and Camacho, C.J. (2004). ClusPro: a fully automated algorithm for protein-protein docking. *Nucleic Acids Res.* 32, W96–W99.
- Copp, J., Manning, G., and Hunter, T. (2009). TORC-specific phosphorylation of mammalian target of rapamycin (mTOR): phospho-Ser2481 is a marker for intact mTOR signaling complex 2. *Cancer Res.* 69, 1821–1827.
- Cunningham, J.T., Rodgers, J.T., Arlow, D.H., Vazquez, F., Mootha, V.K., and Puigserver, P. (2007). mTOR controls mitochondrial oxidative function through a YY1-PGC-1 α transcriptional complex. *Nature* 450, 736–740.
- Davies, M.P.A., Barraclough, D.L., Stewart, C., Joyce, K.A., Eccles, R.M., Barraclough, R., Rudland, P.S., and Sibson, D.R. (2008). Expression and splicing of the unfolded protein response gene XBP-1 are significantly associated with clinical outcome of endocrine-treated breast cancer. *Int. J. Cancer* 123, 85–88.
- DeYoung, M.P., Horak, P., Sofer, A., Sgroi, D., and Ellisen, L.W. (2008). Hypoxia regulates TSC1/2-mTOR signaling and tumor suppression through REDD1-mediated 14-3-3 shuttling. *Genes Dev* 22, 239–251.
- Dowling, R.J.O., Topisirovic, I., Alain, T., Bidinosti, M., Fonseca, B.D., Petroulakis, E., Wang, X., Larsson, O., Selvaraj, A., Liu, Y., et al. (2010). mTORC1-mediated cell proliferation, but not cell growth, controlled by the 4E-BPs. *Science* 328, 1172–1176.
- Duran, A., Amanchy, R., Linares, J.F., Joshi, J., Abu-Baker, S., Porollo, A., Hansen, M., Moscat, J., and Diaz-Meco, M.T. (2011). p62 is a key regulator of nutrient sensing in the mTORC1 pathway. *Mol. Cell* 44, 134–146.
- Düvel, K., Yecies, J.L., Menon, S., Raman, P., Lipovsky, A.I., Souza, A.L., Triantafellow, E., Ma, Q., Gorski, R., Cleaver, S., et al. (2010). Activation of a metabolic gene regulatory network downstream of mTOR complex 1. *Mol. Cell* 39, 171–183.
- Easton, J.B., and Houghton, P.J. (2006). mTOR and cancer therapy. *Oncogene* 25, 6436–6446.
- Efeyan, A., Zoncu, R., and Sabatini, D.M. (2012). Amino acids and mTORC1: from lysosomes to disease. *Trends Mol Med.*
- Emsley, P., Lohkamp, B., Scott, W.G., and Cowtan, K. (2010). Features and development of Coot. *Acta Crystallogr. D Biol. Crystallogr.* 66, 486–501.
- Evans, D.S., Kapahi, P., Hsueh, W.-C., and Kockel, L. (2011). TOR signaling never gets old: aging, longevity and TORC1 activity. *Ageing Res. Rev.* 10, 225–237.
- Evans, P.R., and Murshudov, G.N. (2013). How good are my data and what is the resolution? *Acta Crystallogr. D Biol. Crystallogr.* 69, 1204–1214.

- Feldman, M.E., Apsel, B., Uotila, A., Loewith, R., Knight, Z.A., Ruggero, D., and Shokat, K.M. (2009). Active-site inhibitors of mTOR target rapamycin-resistant outputs of mTORC1 and mTORC2. *PLoS Biol.* *7*, e38.
- Forgac, M. (2007). Vacuolar ATPases: rotary proton pumps in physiology and pathophysiology. *Nat. Rev. Mol. Cell Biol.* *8*, 917–929.
- Franke, D., and Svergun, D.I. (2009). DAMMIF, a program for rapid ab-initio shape determination in small-angle scattering. *J Appl Crystallogr* *42*, 342–346.
- Frias, M.A., Thoreen, C.C., Jaffe, J.D., Schroder, W., Sculley, T., Carr, S.A., and Sabatini, D.M. (2006). mSin1 is necessary for Akt/PKB phosphorylation, and its isoforms define three distinct mTORC2s. *Curr. Biol.* *16*, 1865–1870.
- Ganley, I.G., Lam, D.H., Wang, J., Ding, X., Chen, S., and Jiang, X. (2009). ULK1.ATG13.FIP200 complex mediates mTOR signaling and is essential for autophagy. *J. Biol. Chem.* *284*, 12297–12305.
- Gao, X., Zhang, Y., Arrazola, P., Hino, O., Kobayashi, T., Yeung, R.S., Ru, B., and Pan, D. (2002). Tsc tumour suppressor proteins antagonize amino-acid-TOR signalling. *Nat. Cell Biol.* *4*, 699–704.
- Garami, A., Zwartkruis, F.J.T., Nobukuni, T., Joaquin, M., Rocco, M., Stocker, H., Kozma, S.C., Hafen, E., Bos, J.L., and Thomas, G. (2003). Insulin activation of Rheb, a mediator of mTOR/S6K/4E-BP signaling, is inhibited by TSC1 and 2. *Mol. Cell* *11*, 1457–1466.
- Garcia-Saez, I., Lacroix, F.B., Blot, D., Gabel, F., and Skoufias, D.A. (2011). Structural characterization of HBXIP: the protein that interacts with the anti-apoptotic protein survivin and the oncogenic viral protein HBx. *J. Mol. Biol.* *405*, 331–340.
- García-Martínez, J.M., Moran, J., Clarke, R.G., Gray, A., Cosulich, S.C., Chresta, C.M., and Alessi, D.R. (2009). Ku-0063794 is a specific inhibitor of the mammalian target of rapamycin (mTOR). *Biochemical Journal* *421*, 29–42.
- Gingras, A.C., Kennedy, S.G., O'Leary, M.A., Sonenberg, N., and Hay, N. (1998). 4E-BP1, a repressor of mRNA translation, is phosphorylated and inactivated by the Akt(PKB) signaling pathway. *Genes Dev* *12*, 502–513.
- Glaser, F., Pupko, T., Paz, I., Bell, R.E., Bechor-Shental, D., Martz, E., and Ben-Tal, N. (2003). ConSurf: identification of functional regions in proteins by surface-mapping of phylogenetic information. *Bioinformatics* *19*, 163–164.
- Gong, R., Li, L., Liu, Y., Wang, P., Yang, H., Wang, L., Cheng, J., Guan, K.-L., and Xu, Y. (2011). Crystal structure of the Gtr1p-Gtr2p complex reveals new insights into the amino acid-induced TORC1 activation. *Genes Dev.*

- Grabiner, B.C., Nardi, V., Birsoy, K., Possemato, R., Shen, K., Sinha, S., Jordan, A., Beck, A.H., and Sabatini, D.M. (2014). A diverse array of cancer-associated mTOR mutations are hyperactivating and can predict rapamycin sensitivity. *Cancer Discov* 4, 554–563.
- Guertin, D.A., and Sabatini, D.M. (2005). An expanding role for mTOR in cancer. *Trends Mol Med* 11, 353–361.
- Hammersley, A.P., Svensson, S.O., Hanfland, M., Fitch, A.N., and Hausermann, D. (1996). Two-dimensional detector software: From real detector to idealised image or two-theta scan. *High Pressure Research* 14, 235–248.
- Han, J.M., Jeong, S.J., Park, M.C., Kim, G., Kwon, N.H., Kim, H.K., Ha, S.H., Ryu, S.H., and Kim, S. (2012). Leucyl-tRNA synthetase is an intracellular leucine sensor for the mTORC1-signaling pathway. *Cell* 149, 410–424.
- Hara, K., Yonezawa, K., Weng, Q.P., Kozlowski, M.T., Belham, C., and Avruch, J. (1998). Amino acid sufficiency and mTOR regulate p70 S6 kinase and eIF-4E BP1 through a common effector mechanism. *J. Biol. Chem.* 273, 14484–14494.
- Hara, K., Maruki, Y., Long, X., Yoshino, K.-I., Oshiro, N., Hidayat, S., Tokunaga, C., Avruch, J., and Yonezawa, K. (2002). Raptor, a binding partner of target of rapamycin (TOR), mediates TOR action. *Cell* 110, 177–189.
- Harper, J.M., Leathers, C.W., and Austad, S.N. (2006). Does caloric restriction extend life in wild mice? *Aging Cell* 5, 441–449.
- Hartford, C.M., and Ratain, M.J. (2007). Rapamycin: something old, something new, sometimes borrowed and now renewed. *Clin. Pharmacol. Ther.* 82, 381–388.
- Hasty, P., Sharp, Z.D., Curiel, T.J., and Campisi, J. (2013). mTORC1 and p53: clash of the gods? *Cell Cycle* 12, 20–25.
- Haydon, M.S., Googe, J.D., Sorrells, D.S., Ghali, G.E., and Li, B.D. (2000). Progression of eIF4e gene amplification and overexpression in benign and malignant tumors of the head and neck. *Cancer* 88, 2803–2810.
- Hetz, C., Bernasconi, P., Fisher, J., Lee, A.-H., Bassik, M.C., Antonsson, B., Brandt, G.S., Iwakoshi, N.N., Schinzler, A., Glimcher, L.H., et al. (2006). Proapoptotic BAX and BAK modulate the unfolded protein response by a direct interaction with IRE1alpha. *Science* 312, 572–576.
- Horton, J.D., Goldstein, J.L., and Brown, M.S. (2002). SREBPs: activators of the complete program of cholesterol and fatty acid synthesis in the liver. *J. Clin. Invest.* 109, 1125–1131.
- Hosokawa, N., Hara, T., Kaizuka, T., Kishi, C., Takamura, A., Miura, Y., Iemura, S.-I., Natsume, T., Takehana, K., Yamada, N., et al. (2009). Nutrient-dependent mTORC1

- association with the ULK1-Atg13-FIP200 complex required for autophagy. *Mol. Biol. Cell* *20*, 1981–1991.
- Iglesias, A.H., Santos, L.F.A., and Gozzo, F.C. (2009). Collision-induced dissociation of Lys-Lys intramolecular crosslinked peptides. *J. Am. Soc. Mass Spectrom.* *20*, 557–566.
- Iglesias, A.H., Santos, L.F.A., and Gozzo, F.C. (2010). Identification of cross-linked peptides by high-resolution precursor ion scan. *Anal. Chem.* *82*, 909–916.
- Inoki, K., Corradetti, M.N., and Guan, K.-L. (2005). Dysregulation of the TSC-mTOR pathway in human disease. *Nat. Genet.* *37*, 19–24.
- Inoki, K., Li, Y., Xu, T., and Guan, K.-L. (2003). Rheb GTPase is a direct target of TSC2 GAP activity and regulates mTOR signaling. *Genes Dev* *17*, 1829–1834.
- Inoki, K., Li, Y., Zhu, T., Wu, J., and Guan, K.-L. (2002). TSC2 is phosphorylated and inhibited by Akt and suppresses mTOR signalling. *Nat. Cell Biol.* *4*, 648–657.
- Jacinto, E., Facchinetti, V., Liu, D., Soto, N., Wei, S., Jung, S.Y., Huang, Q., Qin, J., and Su, B. (2006). SIN1/MIP1 maintains rictor-mTOR complex integrity and regulates Akt phosphorylation and substrate specificity. *Cell* *127*, 125–137.
- Jacinto, E., Loewith, R., Schmidt, A., Lin, S., Ruegg, M.A., Hall, A., and Hall, M.N. (2004). Mammalian TOR complex 2 controls the actin cytoskeleton and is rapamycin insensitive. *Nat. Cell Biol.* *6*, 1122–1128.
- Jefferies, H.B., Fumagalli, S., Dennis, P.B., Reinhard, C., Pearson, R.B., and Thomas, G. (1997). Rapamycin suppresses 5'TOP mRNA translation through inhibition of p70s6k. *Embo J.* *16*, 3693–3704.
- Jefferies, H.B., Reinhard, C., Kozma, S.C., and Thomas, G. (1994). Rapamycin selectively represses translation of the “polypyrimidine tract” mRNA family. *Proc. Natl. Acad. Sci. U.S.A.* *91*, 4441–4445.
- Jeong, J.-H., Lee, K.-H., Kim, Y.-M., Kim, D.-H., Oh, B.-H., and Kim, Y.-G. (2012). Crystal structure of the Gtr1p(GTP)-Gtr2p(GDP) protein complex reveals large structural rearrangements triggered by GTP-to-GDP conversion. *Journal of Biological Chemistry* *287*, 29648–29653.
- Jewell, J.L., Russell, R.C., and Guan, K.-L. (2013). Amino acid signalling upstream of mTOR. *Nat. Rev. Mol. Cell Biol.* *14*, 133–139.
- Jiang, W., Zhu, Z., and Thompson, H.J. (2008). Dietary energy restriction modulates the activity of AMP-activated protein kinase, Akt, and mammalian target of rapamycin in mammary carcinomas, mammary gland, and liver. *Cancer Res.* *68*, 5492–5499.

- Joosten, R.P., Long, F., Murshudov, G.N., and Perrakis, A. (2014). The PDB_REDO server for macromolecular structure model optimization. *IUCrJ* *1*, 213–220.
- Jung, C.H., Jun, C.B., Ro, S.-H., Kim, Y.-M., Otto, N.M., Cao, J., Kundu, M., and Kim, D.-H. (2009). ULK-Atg13-FIP200 complexes mediate mTOR signaling to the autophagy machinery. *Mol. Biol. Cell* *20*, 1992–2003.
- Jung, J., Genau, H.M., and Behrends, C. (2015). Amino Acid-Dependent mTORC1 Regulation by the Lysosomal Membrane Protein SLC38A9. *Mol. Cell. Biol.* *35*, 2479–2494.
- Kaizuka, T., Hara, T., Oshiro, N., Kikkawa, U., Yonezawa, K., Takehana, K., Iemura, S.-I., Natsume, T., and Mizushima, N. (2010). Tti1 and Tel2 are critical factors in mammalian target of rapamycin complex assembly. *Journal of Biological Chemistry* *285*, 20109–20116.
- Kamada, Y., Funakoshi, T., Shintani, T., Nagano, K., Ohsumi, M., and Ohsumi, Y. (2000). Tor-mediated induction of autophagy via an Apg1 protein kinase complex. *J. Cell Biol.* *150*, 1507–1513.
- Kang, Seong A, Pacold, M.E., Cervantes, C.L., Lim, D., Lou, H.J., Ottina, K., Gray, N.S., Turk, B.E., Yaffe, M.B., and Sabatini, D.M. (2013). mTORC1 phosphorylation sites encode their sensitivity to starvation and rapamycin. *Science* *341*, 1236566.
- Kantidakis, T., Ramsbottom, B.A., Birch, J.L., Dowding, S.N., and White, R.J. (2010). mTOR associates with TFIIC, is found at tRNA and 5S rRNA genes, and targets their repressor Maf1. *Proceedings of the National Academy of Sciences* *107*, 11823–11828.
- Karplus, P.A., and Diederichs, K. (2012). Linking crystallographic model and data quality. *Science* *336*, 1030–1033.
- Keegan, R.M., and Winn, M.D. (2007). Automated search-model discovery and preparation for structure solution by molecular replacement. *Acta Crystallogr. D Biol. Crystallogr.* *63*, 447–457.
- Kelley, L.A., Mezulis, S., Yates, C.M., Wass, M.N., and Sternberg, M.J.E. (2015). The Phyre2 web portal for protein modeling, prediction and analysis. *Nat Protoc* *10*, 845–858.
- Kenyon, C.J. (2010). The genetics of ageing. *Nature* *464*, 504–512.
- Kim, D.-H., Sarbassov, D.D., Ali, S.M., King, J.E., Latek, R.R., Erdjument-Bromage, H., Tempst, P., and Sabatini, D.M. (2002). mTOR interacts with raptor to form a nutrient-sensitive complex that signals to the cell growth machinery. *Cell* *110*, 163–175.
- Kim, D.-H., Sarbassov, D.D., Ali, S.M., Latek, R.R., Guntur, K.V.P., Erdjument-Bromage, H., Tempst, P., and Sabatini, D.M. (2003). GbetaL, a positive regulator of the rapamycin-sensitive pathway required for the nutrient-sensitive interaction between raptor and mTOR. *Mol. Cell* *11*, 895–904.

- Kim, E., Goraksha-Hicks, P., Li, L., Neufeld, T.P., and Guan, K.-L. (2008). Regulation of TORC1 by Rag GTPases in nutrient response. *Nat. Cell Biol.* *10*, 935–945.
- Kim, J.E., and Chen, J. (2004). Regulation of peroxisome proliferator-activated receptor-gamma activity by mammalian target of rapamycin and amino acids in adipogenesis. *Diabetes* *53*, 2748–2756.
- Kim, Y.-M., Stone, M., Hwang, T.H., Kim, Y.-G., Dunlevy, J.R., Griffin, T.J., and Kim, D.-H. (2012). SH3BP4 is a negative regulator of amino acid-Rag GTPase-mTORC1 signaling. *Mol. Cell* *46*, 833–846.
- Kogan, K., Spear, E.D., Kaiser, C.A., and Fass, D. (2010). Structural conservation of components in the amino acid sensing branch of the TOR pathway in yeast and mammals. *J. Mol. Biol.* *402*, 388–398.
- Koonin, E.V., and Aravind, L. (2000). Dynein light chains of the Roadblock/LC7 group belong to an ancient protein superfamily implicated in NTPase. *Curr. Biol.* *10*, 774–776.
- Kozakov, D., Hall, D.R., Xia, B., Porter, K.A., Padhorny, D., Yueh, C., Beglov, D., and Vajda, S. (2017). The ClusPro web server for protein-protein docking. *Nat Protoc* *12*, 255–278.
- Kozin, M.B., and Svergun, D.I. (2001). Automated matching of high- and low-resolution structural models. *J Appl Crystallogr.*
- Kunz, J., Henriquez, R., Schneider, U., Deuter-Reinhard, M., Movva, N.R., and Hall, M.N. (1993). Target of rapamycin in yeast, TOR2, is an essential phosphatidylinositol kinase homolog required for G1 progression. *Cell* *73*, 585–596.
- Kurzbaue, R., Teis, D., de Araujo, M.E.G., Maurer-Stroh, S., Eisenhaber, F., Bourenkov, G.P., Bartunik, H.D., Hekman, M., Rapp, U.R., Huber, L.A., et al. (2004). Crystal structure of the p14/MP1 scaffolding complex: how a twin couple attaches mitogen-activated protein kinase signaling to late endosomes. *Proc. Natl. Acad. Sci. U.S.A.* *101*, 10984–10989.
- Kwiatkowski, D.J. (2003). Tuberous sclerosis: from tubers to mTOR. *Ann. Hum. Genet.* *67*, 87–96.
- Lackey, D.E., Lynch, C.J., Olson, K.C., Mostaedi, R., Ali, M., Smith, W.H., Karpe, F., Humphreys, S., Bedinger, D.H., Dunn, T.N., et al. (2013). Regulation of adipose branched-chain amino acid catabolism enzyme expression and cross-adipose amino acid flux in human obesity. *Am J Physiol Endocrinol Metab* *304*, E1175–E1187.
- Landau, M., Mayrose, I., Rosenberg, Y., Glaser, F., Martz, E., Pupko, T., and Ben-Tal, N. (2005). ConSurf 2005: the projection of evolutionary conservation scores of residues on protein structures. *Nucleic Acids Res.* *33*, W299–W302.

- Laplanche, M., and Sabatini, D.M. (2012). mTOR signaling in growth control and disease. *Cell* *149*, 274–293.
- Larkin, M.A., Blackshields, G., Brown, N.P., Chenna, R., McGettigan, P.A., McWilliam, H., Valentin, F., Wallace, I.M., Wilm, A., Lopez, R., et al. (2007). Clustal W and Clustal X version 2.0. *Bioinformatics* *23*, 2947–2948.
- Levine, T.P., Daniels, R.D., Wong, L.H., Gatta, A.T., Gerondopoulos, A., and Barr, F.A. (2013). Discovery of new Longin and Roadblock domains that form platforms for small GTPases in Ragulator and TRAPP-II. *Small GTPases* *4*, 62–69.
- Li, S., Ogawa, W., Emi, A., Hayashi, K., Senga, Y., Nomura, K., Hara, K., Yu, D., and Kasuga, M. (2011). Role of S6K1 in regulation of SREBP1c expression in the liver. *Biochem. Biophys. Res. Commun.* *412*, 197–202.
- Li, Y., Inoki, K., and Guan, K.-L. (2004). Biochemical and functional characterizations of small GTPase Rheb and TSC2 GAP activity. *Mol. Cell. Biol.* *24*, 7965–7975.
- Li, Y., Wang, Y., Kim, E., Beemiller, P., Wang, C.-Y., Swanson, J., You, M., and Guan, K.-L. (2007). Bnip3 mediates the hypoxia-induced inhibition on mammalian target of rapamycin by interacting with Rheb. *J. Biol. Chem.* *282*, 35803–35813.
- Liaw, D., Marsh, D.J., Li, J., Dahia, P.L., Wang, S.I., Zheng, Z., Bose, S., Call, K.M., Tsou, H.C., Peacocke, M., et al. (1997). Germline mutations of the PTEN gene in Cowden disease, an inherited breast and thyroid cancer syndrome. *Nat. Genet.* *16*, 64–67.
- Lim, C.Y., and Zoncu, R. (2016). The lysosome as a command-and-control center for cellular metabolism. *J Cell Biol.* *6*, 653-664
- Lima, D.B., de Lima, T.B., Balbuena, T.S., Neves-Ferreira, A.G.C., Barbosa, V.C., Gozzo, F.C., and Carvalho, P.C. (2015). SIM-XL: A powerful and user-friendly tool for peptide cross-linking analysis. *J Proteomics* *129*, 51–55.
- Loewith, R., Jacinto, E., Wullschleger, S., Lorberg, A., Crespo, J.L., Bonenfant, D., Oppliger, W., Jenoe, P., and Hall, M.N. (2002). Two TOR complexes, only one of which is rapamycin sensitive, have distinct roles in cell growth control. *Mol. Cell* *10*, 457–468.
- Long, X., Ortiz-Vega, S., Lin, Y., and Avruch, J. (2005). Rheb binding to mammalian target of rapamycin (mTOR) is regulated by amino acid sufficiency. *J. Biol. Chem.* *280*, 23433–23436.
- Lunin, V.V., Munger, C., Wagner, J., Ye, Z., Cygler, M., and Sacher, M. (2004). The structure of the MAPK scaffold, MP1, bound to its partner, p14. A complex with a critical role in endosomal map kinase signaling. *J. Biol. Chem.* *279*, 23422–23430.
- Ma, X.M., and Blenis, J. (2009). Molecular mechanisms of mTOR-mediated translational control. *Nat. Rev. Mol. Cell Biol.* *10*, 307–318.

- Magee, J., and Cygler, M. (2011). Interactions between kinase scaffold MP1/p14 and its endosomal anchoring protein p18. *Biochemistry* *50*, 3696–3705.
- Magnuson, B., Ekim, B., and Fingar, D.C. (2012). Regulation and function of ribosomal protein S6 kinase (S6K) within mTOR signalling networks. *Biochem. J.* *441*, 1–21.
- Manning, B.D., and Cantley, L.C. (2007). AKT/PKB signaling: navigating downstream. *Cell* *129*, 1261–1274.
- Manning, B.D., Tee, A.R., Logsdon, M.N., Blenis, J., and Cantley, L.C. (2002). Identification of the tuberous sclerosis complex-2 tumor suppressor gene product tuberin as a target of the phosphoinositide 3-kinase/akt pathway. *Mol. Cell* *10*, 151–162.
- Marat, A.L., Dokainish, H., and McPherson, P.S. (2011). DENN domain proteins: regulators of Rab GTPases. *J. Biol. Chem.* *286*, 13791–13800.
- Marusawa, H., Matsuzawa, S.-I., Welsh, K., Zou, H., Armstrong, R., Tamm, I., and Reed, J.C. (2003). HBXIP functions as a cofactor of survivin in apoptosis suppression. *Embo J.* *22*, 2729–2740.
- Mattison, J.A., Roth, G.S., Beasley, T.M., Tilmont, E.M., Handy, A.M., Herbert, R.L., Longo, D.L., Allison, D.B., Young, J.E., Bryant, M., et al. (2012). Impact of caloric restriction on health and survival in rhesus monkeys from the NIA study. *Nature* *489*, 318–321.
- McCoy, A.J., Grosse-Kunstleve, R.W., Adams, P.D., Winn, M.D., Storoni, L.C., and Read, R.J. (2007). Phaser crystallographic software. ... *Applied Crystallography* *40*, 658–674.
- Melegari, M., Scaglioni, P.P., and Wands, J.R. (1998). Cloning and characterization of a novel hepatitis B virus x binding protein that inhibits viral replication. *J. Virol.* *72*, 1737–1743.
- Murshudov, G.N., Skubák, P., Lebedev, A.A., Pannu, N.S., Steiner, R.A., Nicholls, R.A., Winn, M.D., Long, F., and Vagin, A.A. (2011). REFMAC5 for the refinement of macromolecular crystal structures. *Acta Crystallogr. D Biol. Crystallogr.* *67*, 355–367.
- Murzin, A.G., Brenner, S.E., Hubbard, T., and Chothia, C. (1995). SCOP: a structural classification of proteins database for the investigation of sequences and structures. *J. Mol. Biol.* *247*, 536–540.
- Mylonas, E., and Svergun, D.I. (2007). Accuracy of molecular mass determination of proteins in solution by small-angle X-ray scattering. *Journal of Applied Crystallography*.
- Nada, S., Hondo, A., Kasai, A., Koike, M., Saito, K., Uchiyama, Y., and Okada, M. (2009). The novel lipid raft adaptor p18 controls endosome dynamics by anchoring the MEK-ERK pathway to late endosomes. *Embo J.* *28*, 477–489.
- Newgard, C.B., An, J., Bain, J.R., Muehlbauer, M.J., Stevens, R.D., Lien, L.F., Haqq, A.M., Shah, S.H., Arlotto, M., Slentz, C.A., et al. (2009). A branched-chain amino acid-related

metabolic signature that differentiates obese and lean humans and contributes to insulin resistance. *Cell Metabolism* 9, 311–326.

O'Reilly, K.E., Rojo, F., She, Q.-B., Solit, D., Mills, G.B., Smith, D., Lane, H., Hofmann, F., Hicklin, D.J., Ludwig, D.L., et al. (2006). mTOR inhibition induces upstream receptor tyrosine kinase signaling and activates Akt. *Cancer Res.* 66, 1500–1508.

Olson, K.C., Chen, G., Xu, Y., Hajnal, A., and Lynch, C.J. (2014). Alloisoleucine differentiates the branched-chain aminoacidemia of Zucker and dietary obese rats. *Obesity (Silver Spring)* 22, 1212–1215.

Orthaber, D., Bergmann, A., and Glatter, O. (2000). SAXS experiments on absolute scale with Kratky systems using water as a secondary standard. *J. Appl. Cryst.* 33, 218–225

Parmigiani, A., Nourbakhsh, A., Ding, B., Wang, W., Kim, Y.C., Akopiants, K., Guan, K.-L., Karin, M., and Budanov, A.V. (2014). Sestrins inhibit mTORC1 kinase activation through the GATOR complex. *Cell Reports* 9, 1281–1291.

Pearce, L.R., Huang, X., Boudeau, J., Pawłowski, R., Wullschleger, S., Deak, M., Ibrahim, A.F.M., Gourlay, R., Magnuson, M.A., and Alessi, D.R. (2007). Identification of Protor as a novel Rictor-binding component of mTOR complex-2. *Biochemical Journal* 405, 513–522.

Pearce, L.R., Komander, D., and Alessi, D.R. (2010). The nuts and bolts of AGC protein kinases. *Nat. Rev. Mol. Cell Biol.* 11, 9–22.

Peng, M., Yin, N., and Li, M.O. (2014). Sestrins function as guanine nucleotide dissociation inhibitors for Rag GTPases to control mTORC1 signaling. *Cell* 159, 122–133.

Peterson, T.R., Laplante, M., Thoreen, C.C., Sancak, Y., Kang, Seong A, Kuehl, W.M., Gray, N.S., and Sabatini, D.M. (2009). DEPTOR is an mTOR inhibitor frequently overexpressed in multiple myeloma cells and required for their survival. *Cell* 137, 873–886.

Peterson, T.R., Sengupta, S.S., Harris, T.E., Carmack, A.E., Kang, Seong A, Balderas, E., Guertin, D.A., Madden, K.L., Carpenter, A.E., Finck, B.N., et al. (2011). mTOR Complex 1 Regulates Lipin 1 Localization to Control the SREBP Pathway. *Cell* 146, 408–420.

Petoukhov, M.V., Volkov, V.V., and Svergun, D.I. (2006). ATSAS 2.1, a program package for small-angle scattering data analysis. *J. Appl. Cryst.* 39, 277–286

Petoukhov, M.V., Franke, D., Shkumatov, A.V., Tria, G., Kikhney, A.G., Gajda, M., Gorba, C., Mertens, H.D.T., Konarev, P.V., and Svergun, D.I. (2012). New developments in the ATSAS program package for small-angle scattering data analysis. *J. Appl. Cryst.* 45, 342–350.

Porstmann, T., Santos, C.R., Griffiths, B., Cully, M., Wu, M., Leever, S., Griffiths, J.R., Chung, Y.-L., and Schulze, A. (2008). SREBP activity is regulated by mTORC1 and contributes to Akt-dependent cell growth. *Cell Metabolism* 8, 224–236.

- Potter, C.J., Pedraza, L.G., and Xu, T. (2002). Akt regulates growth by directly phosphorylating Tsc2. *Nat. Cell Biol.* 4, 658–665.
- Powis, K., Zhang, T., Panchaud, N., Wang, R., Virgilio, C.D., and Ding, J. (2015). Crystal structure of the Ego1-Ego2-Ego3 complex and its role in promoting Rag GTPase-dependent TORC1 signaling. *Cell Res.* 25, 1043–1059.
- Puente, C., Hendrickson, R.C., and Jiang, X. (2016). Nutrient-regulated Phosphorylation of ATG13 Inhibits Starvation-induced Autophagy. *Journal of Biological Chemistry* 291, 6026–6035.
- Rebsamen, M., Pochini, L., Stasyk, T., de Araujo, M.E.G., Galluccio, M., Kandasamy, R.K., Snijder, B., Fauster, A., Rudashevskaya, E.L., Bruckner, M., et al. (2015). SLC38A9 is a component of the lysosomal amino acid sensing machinery that controls mTORC1. *Nature.* 519, 477-481
- Reiling, J.H., and Hafen, E. (2004). The hypoxia-induced paralogs Scylla and Charybdis inhibit growth by down-regulating S6K activity upstream of TSC in *Drosophila*. *Genes Dev* 18, 2879–2892.
- Rodrik-Outmezguine, V.S., Okaniwa, M., Yao, Z., Novotny, C.J., McWhirter, C., Banaji, A., Won, H., Wong, W., Berger, M., de Stanchina, E., et al. (2016). Overcoming mTOR resistance mutations with a new-generation mTOR inhibitor. *Nature* 534, 272–276.
- Romero-Ramirez, L., Cao, H., Nelson, D., Hammond, E., Lee, A.-H., Yoshida, H., Mori, K., Glimcher, L.H., Denko, N.C., Giaccia, A.J., et al. (2004). XBP1 is essential for survival under hypoxic conditions and is required for tumor growth. *Cancer Res.* 64, 5943–5947.
- Sabatini, D.M., Erdjument-Bromage, H., Lui, M., Tempst, P., and Snyder, S.H. (1994). RAFT1: a mammalian protein that binds to FKBP12 in a rapamycin-dependent fashion and is homologous to yeast TORs. *Cell* 78, 35–43.
- Sabers, C.J., Martin, M.M., Brunn, G.J., Williams, J.M., Dumont, F.J., Wiederrecht, G., and Abraham, R.T. (1995). Isolation of a protein target of the FKBP12-rapamycin complex in mammalian cells. *J. Biol. Chem.* 270, 815–822.
- Sancak, Y., Bar-Peled, L., Zoncu, R., Markhard, A.L., Nada, S., and Sabatini, D.M. (2010). Ragulator-Rag complex targets mTORC1 to the lysosomal surface and is necessary for its activation by amino acids. *Cell* 141, 290–303.
- Sancak, Y., Peterson, T.R., Shaul, Y.D., Lindquist, R.A., Thoreen, C.C., Bar-Peled, L., and Sabatini, D.M. (2008). The Rag GTPases bind raptor and mediate amino acid signaling to mTORC1. *Science* 320, 1496–1501.
- Sancak, Y., Thoreen, C.C., Peterson, T.R., Lindquist, R.A., Kang, Seong A, Spooner, E., Carr,

- S.A., and Sabatini, D.M. (2007). PRAS40 is an insulin-regulated inhibitor of the mTORC1 protein kinase. *Mol. Cell* 25, 903–915.
- Sarbassov, D.D., Ali, S.M., Kim, D.-H., Guertin, D.A., Latek, R.R., Erdjument-Bromage, H., Tempst, P., and Sabatini, D.M. (2004). Rictor, a novel binding partner of mTOR, defines a rapamycin-insensitive and raptor-independent pathway that regulates the cytoskeleton. *Curr. Biol.* 14, 1296–1302.
- Sarbassov, D.D., Guertin, D.A., Ali, S.M., and Sabatini, D.M. (2005). Phosphorylation and regulation of Akt/PKB by the rictor-mTOR complex. *Science* 307, 1098–1101.
- Sarbassov, D.D., Ali, S.M., Sengupta, S.S., Sheen, J.-H., Hsu, P.P., Bagley, A.F., Markhard, A.L., and Sabatini, D.M. (2006). Prolonged rapamycin treatment inhibits mTORC2 assembly and Akt/PKB. *Mol. Cell* 22, 159–168.
- Saxton, R.A., Chantranupong, L., Knockenhauer, K.E., Schwartz, T.U., and Sabatini, D.M. (2016a). Mechanism of arginine sensing by CASTOR1 upstream of mTORC1. *Nature* 536, 229–233.
- Saxton, R.A., Knockenhauer, K.E., Schwartz, T.U., and Sabatini, D.M. (2016b). The apo-structure of the leucine sensor Sestrin2 is still elusive. *Sci Signal* 9, ra92.
- Saxton, R.A., Knockenhauer, K.E., Wolfson, R.L., Chantranupong, L., Pacold, M.E., Wang, T., Schwartz, T.U., and Sabatini, D.M. (2016c). Structural basis for leucine sensing by the Sestrin2-mTORC1 pathway. *Science* 351, 53–58.
- Schrödinger, L. (2016). The PyMOL Molecular Graphics System, Version 1.8 Schrödinger, LLC.
- Schrödinger, L. The PyMOL Molecular Graphics System. 1.4.: Schrödinger.
- Schweitzer, L.D., Comb, W.C., Bar-Peled, L., and Sabatini, D.M. (2015). Disruption of the Rag-Ragulator Complex by c17orf59 Inhibits mTORC1. *Cell Reports* 12, 1445–1455.
- Sekiguchi, T., Hirose, E., Nakashima, N., Ii, M., and Nishimoto, T. (2001). Novel G proteins, Rag C and Rag D, interact with GTP-binding proteins, Rag A and Rag B. *J. Biol. Chem.* 276, 7246–7257.
- Shaw, R.J., Bardeesy, N., Manning, B.D., Lopez, L., Kosmatka, M., DePinho, R.A., and Cantley, L.C. (2004a). The LKB1 tumor suppressor negatively regulates mTOR signaling. *Cancer Cell* 6, 91–99.
- Shaw, R.J., Kosmatka, M., Bardeesy, N., Hurley, R.L., Witters, L.A., DePinho, R.A., and Cantley, L.C. (2004b). The tumor suppressor LKB1 kinase directly activates AMP-activated kinase and regulates apoptosis in response to energy stress. *Proc. Natl. Acad. Sci. U.S.A.* 101, 3329–3335.

- Shimobayashi, M., and Hall, M.N. (2014). Making new contacts: the mTOR network in metabolism and signalling crosstalk. *Nat. Rev. Mol. Cell Biol.* *15*, 155–162.
- Shor, B., Zhang, W.-G., Toral-Barza, L., Lucas, J., Abraham, R.T., Gibbons, J.J., and Yu, K. (2008). A new pharmacologic action of CCI-779 involves FKBP12-independent inhibition of mTOR kinase activity and profound repression of global protein synthesis. *Cancer Res.* *68*, 2934–2943.
- Smith, E.M., Finn, S.G., Tee, A.R., Browne, G.J., and Proud, C.G. (2005). The Tuberous Sclerosis Protein TSC2 Is Not Required for the Regulation of the Mammalian Target of Rapamycin by Amino Acids and Certain Cellular Stresses. *Journal of Biological Chemistry* *280*, 18717–18727.
- Sonenberg, N., and Hinnebusch, A.G. (2009). Regulation of translation initiation in eukaryotes: mechanisms and biological targets. *Cell* *136*, 731–745.
- Stein, N. (2008). CHAINSAW: a program for mutating pdb files used as templates in molecular replacement. *J. Appl. Cryst.* *41*, 641-643
- Svergun, D.I. (1992). Determination of the regularization parameter in indirect-transform methods using perceptual criteria. *J. Appl. Cryst.* *25*, 495-503
- Tee, A.R., Fingar, D.C., Manning, B.D., Kwiatkowski, D.J., Cantley, L.C., and Blenis, J. (2002). Tuberous sclerosis complex-1 and -2 gene products function together to inhibit mammalian target of rapamycin (mTOR)-mediated downstream signaling. *Proc. Natl. Acad. Sci. U.S.A.* *99*, 13571–13576.
- Tee, A.R., Manning, B.D., Roux, P.P., Cantley, L.C., and Blenis, J. (2003). Tuberous sclerosis complex gene products, Tuberin and Hamartin, control mTOR signaling by acting as a GTPase-activating protein complex toward Rheb. *Curr. Biol.* *13*, 1259–1268.
- Thedieck, K., Polak, P., Kim, M.L., Molle, K.D., Cohen, A., Jenö, P., Arriemerlou, C., and Hall, M.N. (2007). PRAS40 and PRR5-like protein are new mTOR interactors that regulate apoptosis. *PLoS ONE* *2*, e1217.
- Thoreen, C.C., Kang, Seong A, Chang, J.W., Liu, Q., Zhang, J., Gao, Y., Reichling, L.J., Sim, T., Sabatini, D.M., and Gray, N.S. (2009). An ATP-competitive mammalian target of rapamycin inhibitor reveals rapamycin-resistant functions of mTORC1. *J. Biol. Chem.* *284*, 8023–8032.
- Tsun, Z.-Y., Bar-Peled, L., Chantranupong, L., Zoncu, R., Wang, T., Kim, C., Spooner, E., and Sabatini, D.M. (2013). The Folliculin Tumor Suppressor Is a GAP for the RagC/D GTPases That Signal Amino Acid Levels to mTORC1. *Mol. Cell.* *52*, 495-505

- Vagin, A., and Teplyakov, A. (1997). MOLREP: an automated program for molecular replacement. *J. Appl. Cryst.* *30*, 1022-1025
- Valbuena, N., Guan, K.-L., and Moreno, S. (2012). The Vam6 and Gtr1-Gtr2 pathway activates TORC1 in response to amino acids in fission yeast. *J. Cell. Sci.* *125*, 1920–1928.
- Vasudevan, K.M., Barbie, D.A., Davies, M.A., Rabinovsky, R., McNear, C.J., Kim, J.J., Hennessy, B.T., Tseng, H., Pochanard, P., Kim, S.Y., et al. (2009). AKT-independent signaling downstream of oncogenic PIK3CA mutations in human cancer. *Cancer Cell* *16*, 21–32.
- Wagle, N., Grabiner, B.C., Van Allen, E.M., Hodis, E., Jacobus, S., Supko, J.G., Stewart, M., Choueiri, T.K., Gandhi, L., Cleary, J.M., et al. (2014). Activating mTOR mutations in a patient with an extraordinary response on a phase I trial of everolimus and pazopanib. *Cancer Discov* *4*, 546–553.
- Wang, B.T., Ducker, G.S., Barczak, A.J., Barbeau, R., Erle, D.J., and Shokat, K.M. (2011). The mammalian target of rapamycin regulates cholesterol biosynthetic gene expression and exhibits a rapamycin-resistant transcriptional profile. *Proceedings of the National Academy of Sciences* *108*, 15201–15206.
- Wang, S., Lloyd, R.V., Hutzler, M.J., Rosenwald, I.B., Safran, M.S., Patwardhan, N.A., and Khan, A. (2001). Expression of eukaryotic translation initiation factors 4E and 2alpha correlates with the progression of thyroid carcinoma. *Thyroid* *11*, 1101–1107.
- Wang, S., Tsun, Z.-Y., Wolfson, R.L., Shen, K., Wyant, G.A., Plovanich, M.E., Yuan, E.D., Jones, T.D., Chantranupong, L., Comb, W., et al. (2015). Metabolism. Lysosomal amino acid transporter SLC38A9 signals arginine sufficiency to mTORC1. *Science* *347*, 188–194.
- Waterman, D.G., Winter, G., Gildea, R.J., Parkhurst, J.M., Brewster, A.S., Sauter, N.K., and Evans, G. (2016). Diffraction-geometry refinement in the DIALS framework. *Acta Crystallogr D Struct Biol* *72*, 558–575.
- Wendel, H.-G., de Stanchina, E., Fridman, J.S., Malina, A., Ray, S., Kogan, S., Cordon-Cardo, C., Pelletier, J., and Lowe, S.W. (2004). Survival signalling by Akt and eIF4E in oncogenesis and cancer therapy. *Nature* *428*, 332–337.
- Winn, M.D., Ballard, C.C., Cowtan, K.D., Dodson, E.J., Emsley, P., Evans, P.R., Keegan, R.M., Krissinel, E.B., Leslie, A.G.W., McCoy, A., et al. (2011). Overview of the CCP4 suite and current developments. *Acta Crystallogr. D Biol. Crystallogr.* *67*, 235–242.
- Winter, G. (2010). xia2: an expert system for macromolecular crystallography data reduction. *J Appl Cryst.* *43*, 186-190
- Wolfson, R.L., Chantranupong, L., Saxton, R.A., Shen, K., Scaria, S.M., Cantor, J.R., and Sabatini, D.M. (2016). Sestrin2 is a leucine sensor for the mTORC1 pathway. *Science* *351*, 43–

48.

Wong, Y.-H., Lee, T.-Y., Liang, H.-K., Huang, C.-M., Wang, T.-Y., Yang, Y.-H., Chu, C.-H., Huang, H.-D., Ko, M.-T., and Hwang, J.-K. (2007). KinasePhos 2.0: a web server for identifying protein kinase-specific phosphorylation sites based on sequences and coupling patterns. *Nucleic Acids Res.* *35*, W588–W594.

Wouters, B.G., and Koritzinsky, M. (2008). Hypoxia signalling through mTOR and the unfolded protein response in cancer. *Nat. Rev. Cancer* *8*, 851–864.

Xia, J., Wang, R., Zhang, T., and Ding, J. (2016). Structural insight into the arginine-binding specificity of CASTOR1 in amino acid-dependent mTORC1 signaling. *Cell Discov* *2*, 16035.

Xie, J., Ponuwei, G.A., Moore, C.E., Willars, G.B., Tee, A.R., and Herbert, T.P. (2011). cAMP inhibits mammalian target of rapamycin complex-1 and -2 (mTORC1 and 2) by promoting complex dissociation and inhibiting mTOR kinase activity. *Cell. Signal.* *23*, 1927–1935.

Yamamoto, T., Watanabe, K., Inoue, N., Nakagawa, Y., Ishigaki, N., Matsuzaka, T., Takeuchi, Y., Kobayashi, K., Yatoh, S., Takahashi, A., et al. (2010). Protein kinase C β mediates hepatic induction of sterol-regulatory element binding protein-1c by insulin. *J. Lipid Res.* *51*, 1859–1870.

Yan, L., Mieulet, V., Burgess, D., Findlay, G.M., Sully, K., Procter, J., Goris, J., Janssens, V., Morrice, N.A., and Lamb, R.F. (2010). PP2A T61 epsilon is an inhibitor of MAP4K3 in nutrient signaling to mTOR. *Mol. Cell* *37*, 633–642.

Yip, C.K., Murata, K., Walz, T., Sabatini, D.M., Kang, Seong A (2010). Structure of the human mTOR complex I and its implications for rapamycin inhibition. *Mol. Cell* *38*, 768–774.

Yoon, M.-S., and Choi, C.S. (2016). The role of amino acid-induced mammalian target of rapamycin complex 1(mTORC1) signaling in insulin resistance. *Exp. Mol. Med.* *48*, e201.

Yoon, S.-O., and Roux, P.P. (2013). Rapamycin resistance: mTORC1 substrates hold some of the answers. *Curr. Biol.* *23*, R880–R883.

Yu, K., Toral-Barza, L., Shi, C., Zhang, W.-G., Lucas, J., Shor, B., Kim, J., Verheijen, J., Curran, K., Malwitz, D.J., et al. (2009). Biochemical, cellular, and in vivo activity of novel ATP-competitive and selective inhibitors of the mammalian target of rapamycin. *Cancer Res.* *69*, 6232–6240.

Yu, Y., Yoon, S.-O., Poulgiannis, G., Yang, Q., Ma, X.M., Villén, J., Kubica, N., Hoffman, G.R., Cantley, L.C., Gygi, S.P., et al. (2011). Phosphoproteomic analysis identifies Grb10 as an mTORC1 substrate that negatively regulates insulin signaling. *Science* *332*, 1322–1326.

Zhang, D., Iyer, L.M., He, F., and Aravind, L. (2012). Discovery of Novel DENN Proteins: Implications for the Evolution of Eukaryotic Intracellular Membrane Structures and Human

Disease. *Front Genet* 3, 283.

Zhang, H.H., Huang, J., Düvel, K., Boback, B., Wu, S., Squillace, R.M., Wu, C.-L., and Manning, B.D. (2009). Insulin stimulates adipogenesis through the Akt-TSC2-mTORC1 pathway. *PLoS ONE* 4, e6189.

Zhang, Y., Gao, X., Saucedo, L.J., Ru, B., Edgar, B.A., and Pan, D. (2003). Rheb is a direct target of the tuberous sclerosis tumour suppressor proteins. *Nat. Cell Biol.* 5, 578–581.

Zoncu, R., Bar-Peled, L., Efeyan, A., Wang, S., Sancak, Y., and Sabatini, D.M. (2011a). mTORC1 senses lysosomal amino acids through an inside-out mechanism that requires the vacuolar H⁺-ATPase. *Science* 334, 678–683.

Zoncu, R., Efeyan, A., and Sabatini, D.M. (2011b). mTOR: from growth signal integration to cancer, diabetes and ageing. *Nat. Rev. Mol. Cell Biol.* 12, 21–35.

ANNEXES

Profa. Dra. Rachel Meneguello
Presidente
Comissão Central de Pós-Graduação
CCPG-PRPG
Declaração

As cópias de artigos de minha autoria ou de minha co-autoria, já publicados ou submetidos para publicação em revistas científicas ou anais de congressos sujeitos a arbitragem, que constam da minha Dissertação/Tese de Mestrado/Doutorado, intitulada "**Caracterização estrutural e funcional de subunidades do complexo Ragulator, um regulador da sinalização por aminoácidos na via mTORC1**", não infringem os dispositivos da Lei n.º 9.610/98, nem o direito autoral de qualquer editora.

Campinas, 25 de Abril de 2017

Assinatura: 
Nome do(a) Aluno(a): **Nadia Rasheed**
RNE n.º V898924-X

Assinatura: 
Nome do(a) Orientador(a): **Dra. Juliana Helena Costa Smetana**
RG n.º 32.221.649-7

Campinas, 25 de Abril de 2017

DECLARAÇÃO

Declaramos para os devidos fins que o projeto de tese de doutorado intitulado: “Estudos de interação do complexo Ragulator”: teve seu título alterado para: “Caracterização estrutural e funcional de subunidades do complexo Ragulator, um regulador da sinalização por aminoácidos na via mTORC1”; sendo este o título da Tese do doutorado da aluna Nadia Rasheed.



Nadia Rasheed

Aluna de doutorado do PPGGBM



Dra. Juliana Helena Costa Smetana

Orientador/Supervisor

Uso exclusivo da CIBio:

Número de projeto / processo: 2015-62

Formulário de encaminhamento de projetos de pesquisa para análise pela CIBio - Comissão Interna de Biossegurança do CNPEM – Centro Nacional de Pesquisa em Energia e Materiais

Título do projeto: Estudos de interações do complexo Ragulator

Pesquisador responsável: Juliana Helena Costa Smetana

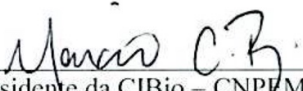
Experimentador: Nadia Rasheed

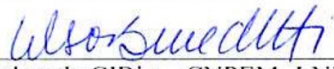
Classe de risco do OGM: Risco I Risco IINível do treinamento do experimentador: -Iniciação científica, -mestrado, -doutorado, -doutorado direto, -pós-doutorado, -nível técnico, -outro, especifique:

Resumo do projeto: As vias de sinalização comumente desreguladas no desenvolvimento do câncer envolvem, com muita frequência, alterações em proteínas da via PI3K-Akt-mTOR. A quinase mTOR, identificada como o alvo da droga imunossupressora rapamicina, desempenha um papel essencial na regulação do crescimento celular integrando sinais da concentração de nutrientes tanto local quanto sistêmica, sinalizada por fatores de crescimento, além de diversos tipos de estresse. Na resposta a nutrientes, destaca-se a regulação por aminoácidos como um componente conservado da via e ao mesmo tempo pouco compreendido. Estudos recentes têm demonstrado que a sinalização por aminoácidos é mediada pelas GTPases Rag e pelo complexo Ragulator, que ancora essas GTPases na superfície do lisossomo e também promove sua ativação mediante a troca de GDP por GTP. Neste projeto, buscamos validar um modelo estrutural do complexo Ragulator obtido previamente em nosso grupo. Serão construídos mutantes das subunidades do complexo, os quais serão transfectados em células HeLa ou HEK293 e analisados por imunofluorescência, para análises da distribuição subcelular, e imunoprecipitação para detecção de interações.

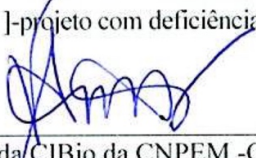
A CIBio analisou este projeto em reunião realizada no dia: 1/9/2015

Parecer final: -projeto aprovado, -projeto recusado, -projeto com deficiências, comentários anexo.

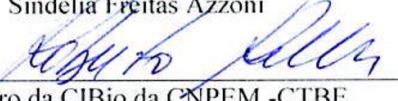

 Presidente da CIBio – CNPEM-LNBio
 Marcio Chaim Bajgelman


 Membro da CIBio – CNPEM -LNBio
 Celso Eduardo Benedetti

Membro da CIBio – CNPEM -LNBio
 Carolina Borsoi Moraes H. Freitas


 Membro da CIBio da CNPEM -CTBE
 Fabio Márcio Squina


 Membro da CIBio da CNPEM -CTBE
 Sindélia Freitas Azzoni


 Membro da CIBio da CNPEM -CTBE
 Roberto Ruller